



Politecnico di Milano

Doctorate in Geodetic and Surveying Sciences
Dottorato di Ricerca in Scienze Geodetiche e Topografiche
XII Course – 1996-1999

Doctorate Thesis

**A System for Automatic Aerotriangulation:
Concept, Implementation and Testing**

Author:

Marco Scaioni

Tutor:

Prof. Gianfranco Forlani

(Università degli Studi di Parma – Dip. di Ing. Civile)

Co-Tutor:

Ing. Livio Pinto

(Politecnico di Milano – Dip. I.I.A.R.)

Coordinator of the Doctorate:

Prof. Luigi Mussio (Politecnico di Milano - Dip. I.I.A.R.)

Contents

Contents	I
Introduction	V
1 Outlines of Automatic Aerial Triangulation	1
1.1 Introduction	1
1.2 Main tasks of Automatic Aerial Triangulation	3
1.3 Developments in Automatic Aerial Triangulation	6
1.4 Automation in ground control point measurement.....	8
1.5 Automatic interior orientation.....	11
1.6 The OEEPE-ISPRS test on tie point extraction.....	13
1.6.1 Test data set and goals	13
1.6.2 Test findings	15
1.7 Basic requirements of an automatic procedure for tie point extraction	16
1.7.1 Technical requirements.....	16
1.7.2 Operational requirements.....	17
2 The TRIADIGIT system for AAT	19
2.1 Genesis and goals.....	19
2.2 Framework of the whole system.....	20
2.3 Available a priori information.....	22
2.4 Strategy for tie point extraction.....	23
2.4.1 Improvement of the approximate exterior orientation.....	23
2.4.2 Tie point densification	24
2.4.3 Improving tie point accuracy and increasing the number of manifold points	24
2.5 Preliminary data setup.....	26
2.5.1 Selection of program control parameters	26
2.5.2 Approximate values of the exterior orientation.....	27
2.5.3 Image pyramids generation	27
2.5.4 Extraction of interest points.....	28
2.6 Gross error rejection.....	32
2.7 Implementation of the program TRIA_DIGIT	32
2.8 Measurements of ground control points	34

2.9	Block adjustment	36
3	Interior Orientation	37
3.1	Outlines of the procedure	37
3.2	Measurement of fiducial marks	38
3.3	Identification of fiducial marks.....	40
3.3.1	Searching for the mark position.....	43
3.3.2	Identification of digits.....	44
3.3.3	Identification of symbols.....	47
3.3.4	Consistency check for the symbol set.....	47
3.4	Transformation from pixel to image.....	48
3.5	Implementation of the program ORINT.....	48
3.6	Program tests.....	50
4	Tie points extraction	55
4.1	Matching algorithms.....	55
4.1.1	Normalized Cross Correlation.....	56
4.1.2	Least Squares Matching	58
4.1.2.1	2D-Least Squares Matching with affine model	59
4.1.2.2	Constraining the shaping parameters.....	61
4.1.2.3	Testing the determinability of the shaping parameters.....	61
4.2	Selection of candidate homologous points	64
4.2.1	Definition of the search window	65
4.2.2	Influence of EO parameter uncertainty on the search window shape	67
4.3	Outlier rejection in relative orientation.....	68
4.3.1	The “Longuet-Higgins” algorithm.....	70
4.3.2	Estimation of the fundamental matrix by Orthogonal Least Squares	72
4.3.3	Robust estimators for the fundamental matrix.....	75
4.3.4	Random Sampling Algorithms	75
4.3.5	Outlier rejection.....	77
5	Experimental results	79
5.1	Description of the tests.....	79
5.1.1	Test data sets	79
5.2	AAT of the blocks.....	82
5.2.1	AAT setup	82
5.2.1.1	Approximate exterior orientation.....	83
5.2.1.2	Ground model.....	83
5.2.1.3	Program control parameters	83
5.2.2	AAT strategy	84
5.2.3	AAT outcomes.....	85
5.2.3.1	Intermediate results	85
5.2.3.2	Outlier rejection	85
5.2.3.3	Tie point distribution.....	85
5.2.3.4	Outcomes of bundle adjustment	86
5.3	Independent accuracy check.....	92
6	Conclusions	95

6.1	TRIADIGIT system performance: status and prospects	95
6.1.1	Tie point extraction.....	95
6.1.2	Interior orientation.....	96
6.1.3	Ground Control Point Measurement.....	97
6.1.4	Miscellanea	97
6.2	What future for Automatic Aerotriangulation?.....	97
	References	99
	Acknowledgements	107

Introduction

Aerial triangulation (AT) has been leading development in photogrammetry in the last 30 years. The amount of experimental as well as theoretical researches witness its impact on the economy of map production. It has been capable of integrating the transitions from analog to analytical and then to digital which have marked fundamental steps, as well as the appearance of new technologies such as FMC devices, GPS, INS and the like.

With the transition from analytical to digital photogrammetry, the goal of finding automatic procedures capable to derive the exterior orientation of a block looked attainable, in the light of the growing success in DEM generation by image matching and in automatic relative orientation in aerial images. To the author's knowledge, the first paper depicting the concept and experimental results on *automatic aerial triangulation* (AAT) is due to Tsingas, in 1991.

In the last five years, AAT has been a topic of research and development in digital photogrammetry, by research institutes as well as by photogrammetric companies. A number of strategies and softwares have been presented, witnessing a true market interest on the subject. This arise from the far reaching changes digital photogrammetry is introducing in the way photogrammetry is understood and used: for instance, the widespread diffusion of digital orthophotos is giving a great impulse to AAT systems, because their production is purely based on digital imagery and largely automated.

AAT tries to reduce the AT problem to a batch process, with little or no help of a human operator; as for the analytical procedure, it is based on four main tasks:

1. Determination of the transformation between image and pixel coordinate systems (interior orientation).
2. Measurement of the ground control points.
3. Selection, transfer and measurement of a suitable number of tie points.
4. Computation of the bundle block adjustment.

The first task, namely the *interior orientation*, is a pre-requisite of any metric operation on digital imagery and has been successfully solved with different strategies.

Mensuration of *ground control points* is harder to automate: their identification (i.e. labelling) is a semantic task whose full automation cannot be achieved with the techniques available today. Besides, GCPs, either natural or signalized, are so small that they cannot be traced in an image pyramid and can hardly be automatically located and accurately collimated. The core of an AAT procedure is the selection and the measurement of tie points, which entail the choice of the *matching algorithm* and the *search for correspondencies*.

The success of an AAT procedure depends on its ability to extract a large number of tie points evenly distributed over the block and, most important, with a large percentage of manifold points in multiple-overlap areas (along as well as across strip). Test and experiences so far clearly point out that a smaller accuracy in point measurement by the matching algorithms may be compensated for by the larger redundancy.

As in analytical AT, the last step of AAT is the block adjustment, which is performed almost exclusively by bundles and, to cope with the amount of small and large outliers, by using robust methods.

Three years ago, we decide to took part in a test organized by the OEEPE and the ISPRS on tie point extraction. This led to the development, implementation and testing of a system for AAT, which is the subject of this thesis. The project has been carried out during the three years of the Doctorate Course on Surveying and Geodetic Sciences at the Dept. IAR, *Politecnico di Milano*.

The system, called TRIADIGIT, is made up of different modules which perform the automatic extraction of tie points and the interior orientation as well, and the measurement of ground control points by an interactive approach. After the description of concept and implementation of these procedures, some experimental tests on two aerial blocks with different scale, topography, image scene and resolution are presented. The results obtained are satisfactory, because a consistent set of tie points, homogeneously distributed and with many multi-ray points were found. With image resolutions varying from 20 to 30 μm , the sigma nought of the least squares bundle adjustment is in the range $0.3\div 0.5$ pixels, values in agreement with the results of other AAT programs reported in literature.

The first chapter deals with the fundamental aspects of AAT and the existing solutions to different tasks. Because of its relevance as a landmark in AAT and because of its specific relevance to this work, the test on tie point extraction organized by OEEPE and ISPRS in the years 1996-97 is described.

The second chapter, after an overview of the whole system TRIADIGIT, focuses on the strategy for tie point extraction, which relies on multi-resolution. Perhaps unlike most approaches, tie points are searched for in a block-like fashion, rather than by relative orientation, which is only used as consistency check. Three main stages are performed: improvement of the exterior orientation, tie point densification and refined measurement along the pyramids. Backprojection of the available tie points at a given level tries to increase multi-ray points. Robust relative orientation and bundle adjustment are used to remove the large percentage of outliers.

Chapter 3 describes the procedure for automatic interior orientation; again in a multi-resolution approach, fiducial marks are located and, if provided with identification symbols, are automatically labelled to their counterpart in the calibration file. The computation of the transformation between pixel and image coordinate system is carried out with a robust method.

In chapter 4 the main algorithms used in tie point extraction are presented, namely image matching techniques, computation of the approximate values for homologous tie points and their uncertainty, and a robust method for relative orientation applied to gross error rejection in tie point extraction.

Chapter 5 is devoted to the description of the two small aerial blocks the program has been tested. The results are discussed in terms of the bundle adjustment accuracy achieved for tie points as well as from an independent accuracy check. Merits and weaknesses of the

implementation are pointed out, stressing the need for a great amount of multi-ray points to control block deformations.

Chapter 6 draws a picture of the current status of the system, pointing to the perspectives for further developments of this project. The future of AAT in the light of the impressive progress of technologies for direct orientation of aerial images (INS/GPS) is addressed, showing how AAT is going to play a fundamental role in the mapping field for many years to come.

Chapter 1

Outlines of Automatic Aerial Triangulation

1. Introduction

The development of *aerial triangulation* (AT) during the last 30 years depicts very well the development of the entire field of photogrammetry. The transitions from analog to analytical and then to digital have marked fundamental steps, as well as the appearance of new technologies such FMC devices, GPS, INS, etc. An increase in accuracy from 25 μm to 5 μm , a tenfold increase in performance and reliability, and the widespread use of efficient block adjustment methods were achieved [SCHENK 1997]. However, the major impulse to the development of AT came from its really operational use for mapping. This practical interest has been pushing the advancement of experimental researches, by giving continuously new and new challenges.

The passage from analytical to digital photogrammetry introduced a new approach to AT, namely *digital aerial triangulation* [cf. FRITSCH 1995]. Two main methods can be told apart. The first one is *interactive* AT, which requires human operator guidance and softcopy *digital photogrammetric workstations* (DPWs). To capture the digital images, analog films are digitized by means of more and more accurate photogrammetric scanners [cf. BALTSAVIAS 1999]. The second approach is *automatic aerial triangulation* (AAT), which attempts to reduce the AT problem to a batch process, with little or no help of a human operator. Today's systems are close to meeting this challenge, but the identification and measurement of ground control points remain an interactive task, though studies have been carried out in order to increase the degree of automation. AAT systems perform operations such as tie points selection, determination of accurate initial values for the exterior orientation and match multiple images by means of the techniques of computer vision and image processing.

Especially in the last five years, AAT has been an increasingly interesting topic of research and development in digital photogrammetry; see [SCHENK 1997] for an excellent review of this subject. HEIPKE AND EDER (1998) report that a shift of focus concerning the objectives of AAT can be recently observed. While in earlier times point densification was the primary

goal, currently the orientation parameters themselves are of growing importance. Indeed automatically determined tie points are not really useful for point densification, since generally they do not fulfil the requirements set out in the point selection phase of analytical AT for the absolute orientation of the stereo-model. Besides, the orientation parameters themselves are increasingly used directly for subsequent tasks such as orthorectification, building extraction or vector data capture. By the way, it is the widespread diffusion of digital orthophotos which is giving a great impulse to AAT systems, because their production is purely based on digital imagery. On the contrary, map production is still more operational by analytical plotters and this puts AAT out of the traditional workflow.

For the sake of completeness it should be said that the exterior orientation parameters of an aerial image are being more and more measured directly using GPS and INS [cf. SKALLOUD AND SCHWARZ 1998; SKALLOUD 1999]. It could seem a paradox that the interest of the photogrammetric community is still aimed at AAT, when this practise will be dismissed in a close future. In reality, according to the results of OEEPE¹ test on the use of GPS in photogrammetry [ACKERMANN 1996], we might foresee that AT will remain in use for some time to come.

Nowadays several AAT software systems are available, either as stand-alone packages or as part of a digital photogrammetric workstation. Different research institutes have been developing their own systems for study purposes or for internal use. Several mapping agencies reported on the use of AAT in a production environment [DE VENECIA *et al.* 1996; KERSTEN AND O'SULLIVAN 1996; HARTFIEL 1997; KERSTEN AND HÄRING 1997; KERSTEN *et al.* 1998; KÖHLER 1998]. OEEPE organized common tests in order to evaluate the performance of digital AT and to compare different systems. The first one [JAAKOLA AND SARJAKOSKI 1996] was held in the period 1993-95 and focused on precision, performances and operational issues of both interactive and automatic digital systems. It gave an overview on the real possibilities of these procedures, so that it may be considered a starting point for the next developments. Many questions remained open, from the theoretical side (performances of different kinds of matching algorithms, influence of local image texture) as well as from the practical side (definition of an optimal pixel size, number of tie points per image, degree of automation and analysis of the factors affecting it, effect of image compression, quality check, etc.). In order to point out these problems, in 1996 OEEPE and ISPRS² launched a joint test on the performance of tie point extraction in AAT. This is the real kernel of AAT, because its success determines the quality of final results, i.e. the correct evaluation of the exterior orientation parameters. The test was aimed at the commercial software developers, the users of AAT systems and the research institutes as well. Outcomes of OEEPE-ISPRS test were published in [HEIPKE AND EDER 1998]. More details will be given in the sequel (see par. 1.6).

This first chapter reports about the fundamental aspects of AAT and the existing solutions to different tasks. This would like to give the readers a background before the description of the TRIADIGIT AAT system developed at Dept. IIAR (*Ingegneria Idraulica, Ambientale e del Rilevamento*) of *Politecnico di Milano*, being the subject of the present thesis.

¹ OEEPE stands for European Organization for Experimental Photogrammetric Research.

² ISPRS stands for International Society for Photogrammetry and Remote Sensing.

1.2 Main tasks of automatic aerotriangulation

The goal of AAT is to perform in an autonomous way all the tasks involved in analytical AT, where the term autonomous means that no interaction with the user is required, except the selection of initial parameters. More general aspects of AT such as those concerning bundle block adjustment techniques, flight planning and the like are not treated. These topics can be found exhaustively in literature [e.g. in KRAUS 1993, 1997].

A system for AAT is designed to carry out the following main tasks:

1. Establishing a relation between image and pixel coordinate systems (interior orientation).
2. Measuring ground control points.
3. Selecting and measuring a suitable number of tie points.
4. Computing a bundle block adjustment.

Other photogrammetric tasks such as orthorectification, DTM generation and map editing come afterwards, even though some systems yield a DTM as by-product of the tie point transfer phase.

The first task, namely the *interior orientation* (IO), is a pre-requisite of any metric operation on digital imagery. Different solutions to solve for it in automatic manner were proposed and implemented, whilst the interactive approach is operational since the appearance of the first DPWs. Details will be presented in literature survey (par. 1.5).

Mensuration of *ground control points* (GCPs) in digital aerotriangulation does not conceptually differ from the same task in analytical photogrammetry. The basic idea is that a suitable number of GCPs must be measured on the photographs in order to control block deformations. This number is bound to decrease, the more airborne GPS becomes commonplace, because the coordinates of perspective centers can be determined fairly accurate and provide better concordance with the flight plan due to the assisted guidance. The real problem affecting the GCPs' measurement in digital imagery arises from the fact that both natural and signalized points are so small that they cannot be traced in an image pyramid and can hardly be automatically located and accurately collimated. Furthermore their identification (i.e. labelling) is a semantic task whose full automation cannot be achieved with the techniques available today, as discussed in 1.4. On the other hand, interactive (and to some extent semi-automatic) mensuration is operational and does not entail much time.

The core of an AAT procedure is the selection and the measurement of tie points. Irrespective of the specific strategy, two important differences with analytical photogrammetry should be stressed. The first one concerns the workflow of tie point measurement, which at analytical plotter (and also at a DPW implementing an interactive procedure, barring artificially marked points) is the following:

1. *Preparation*: photographs are ordered according to the flight plan; camera data and ground control information are collected.
2. *Point selection*: on every photograph a suitable number of tie points are selected in the "von Grüber" positions.

3. *Point transfer*: selected points must be marked on every photographs, either directly by drilling a hole into the emulsion, or indirectly by the stereovision ability of a human operator.
4. *Point mensuration*: all selected points, including GCPs, are precisely measured at the analytical plotter (or DPW) by a trained operator, who plays the key-role in the good outcome of AT.

Apart from the preparation phase, which requires human knowledge and can be hardly automated, the last three steps are performed in autonomous way by AAT systems (except the measurement of GCPs). Although a point selection phase still exists, according to the particular matching strategy adopted, point transfer and mensuration are joined together. Starting from a point selected in an image of the block, its homologous are looked for in the other images and matched. If the result of matching is good enough, tie points found are considered as corresponding and are measured at the same time.

The second substantial difference between analytical and automatic AT concerns the number of tie points. In the traditional approach a minimum amount of tie points (usually 9 or 15 per photograph) is accurately measured in the “Von Grüber” positions, which in regular blocks correspond to forward and side overlap areas. The points selected in this way are manifold and guarantee reliability and stability to the block [FÖRSTNER 1985]; besides, a skilled operator may perform their mensuration with high precision (about $\sigma=5 \mu\text{m}$ in the image space). Due to these factors, the number of measurements usually is kept small in order to contain cost and time. In AAT the problem is reversed. On one hand, some matching techniques may perform the point measurement with the same precision, but are more error prone; this is due to occlusions, false candidates, repetitive patterns, lighting variations, moving objects, etc. On the other hand, a higher amount of tie points can be measured without any increase of cost while keeping processing time still short. Suppose that an AAT system could measure n_{AAT} tie points with an accuracy of σ_{AAT} smaller than the accuracy σ_{AT} obtainable by analytical AT. If the geometry and distribution of tie points are roughly constant, the same accuracy can be achieved by using n_{AT} points of accuracy σ_{AT} or

$$n_{\text{AAT}} = \left(\frac{\sigma_{\text{AT}}}{\sigma_{\text{AAT}}} \right)^2 n_{\text{AT}} \quad (1.1)$$

points of accuracy σ_{AAT} . Therefore, even though the accuracy of an individual point might be slightly worse, the final result will not, because the larger amount of tie points compensate for the less accuracy. Moreover, an improved reliability can be achieved.

Two aspects assume a key-role in tie point transfer: the *matching algorithm* and the *strategy to look for correspondencies*.

Concerning the *matching algorithm*, Table 1.1 reports some properties of the available techniques [FÖRSTNER 1995]. *Area-based* matching techniques are the most suitable to get accurate measurements, but require good starting points and are highly sensitive to occlusions. *Feature-based* techniques are more robust with respect to occlusions and to poor initial approximations, in spite of the minor accuracy. Points, edges or blobs can be used as entity to match. *Relational matching* makes use of a symbolic description of the image content. It is probably the most powerful technique to compute rough correspondencies between images in case no a priori information about approximate orientation is known. Unfortunately, so far relational matching had only few applications in AAT [see WANG 1996;

JACOBSEN AND WEGMANN 1998] because it is time-consuming. Some matching techniques have been modified to deal with more than two images contemporarily (*multi-image matching*), what can be exploited for the measurement of accurate multi-ray points.

Dependency on approximate values when looking for correspondencies, either in area-based or feature-based methods, can be made less critical in traducing *multi-resolution* techniques: images with lower resolution than the original (*image pyramids*) are generated. A first search for homologous points is performed by feature-based matching at the top level of the hierarchy, i.e. in the images at lower resolution. The points so found are used as initial values for more precise area-based matching which is applied to the next level.

type	cross correlation	least squares matching	feature-based matching			relational matching
			points	lines	blobs	
<i>pull in range</i>	large	3 [pel]	density	density	density	large
<i>scale/rotation sensitivity</i>	high	medium	medium/ low	medium/ low	medium/ low	medium/ low
<i>accuracy [pel]</i>	0.1	0.1	0.3÷0.5	0.1÷0.5	> 1	0.1÷1
<i>occlusion sensitivity</i>	high	high	medium	low	medium	low
<i>tool for image pairs</i>	yes	yes	yes	not possible	yes	yes
<i>tool for multi-image matching</i>	unknown	yes	yes	yes	yes	unknown

Table 1.1 – Properties of the available matching techniques (from [FÖRSTNER 1995]); for feature-based techniques, the term density refers to an average distance of features

In addition to the matching method, the success of an AAT procedure is related to its ability to extract homologous points homogeneously distributed over the block and, most important, with a large percentage of manifold points in all areas where models overlap (along as well as across strips). The correct transfer of a point from an image to another requires the knowledge of the approximate exterior orientation and a ground model with their uncertainties. The first one may be derived from the flight plan, from a map or by the use of airborne GPS. About the DTM, today every industrialized country has its own; if not available, a simplified model (e.g. a plan or a surface interpolating the GCPs) might be adopted. The first task of AAT is to improve these approximations through the measurement of a first set of tie points by a technique which does not need precise starting points. After, tie points can be found more accurately thanks to the improved exterior orientation and ground model.

As in analytical AT, the last step of AAT is the adjustment of the block based on measured tie points and ground control. The only difference with respect to the traditional approach is the widespread use of *bundles* instead of *independent models* approach [KRAUS 1993], because the photogrammetric observations directly refer to images and no more to stereoscopic models.

1.3 Developments in Automatic Aerial Triangulation

As the 80s have been the era of the development of fundamental measurement tools (matching techniques) for digital photogrammetry, during the 90s the orientation procedures

(relative orientation, AAT, etc.) have become to be implemented by digital techniques.

The first who carried out investigations to automate AT and set up a program was V. Tsingas at the University of Stuttgart, showing that image matching methods can be applied to solve the automated identification of tie points and to derive their image coordinates [TSINGAS 1991]. The approach of Tsingas is based on four main steps:

1. Feature extraction in every image.
2. Preliminary pairwise feature matching.
3. Outlier rejection by use of an affine transformation as functional model.
4. Multi-image matching of incidence matrices in a graph-theoretical model [TSINGAS 1994].

This scheme is repeated along a three-level image pyramid. In [TSINGAS 1995; FRITSCH 1995] more details about latest developments of this method are reported and results on the OEEPE test's block "Forssa" are presented.

Building on Tsingas' approach, HONKAVAARA AND HØGHOLEN (1996) developed their AAT system, including also the possibility of selecting tie points in different configurations as well as to re-extract points in those areas poorly covered at the end of the processing. Furthermore, they carried out an interesting analysis of different aspects of tie point distribution. Also the solution developed at Technical University of Munich [HEIPKE *et al.* 1997; BRAND AND HEIPKE 1998] is based on the graph-theoretical approach of TSINGAS (1994), whilst initial pairwise extraction of tie points is carried out by a method for automatic relative orientation [TANG AND HEIPKE 1996]. The core of the procedure consists of a strategy to increase the number of manifold conjugate point tuples based on RANSAC algorithm [FISCHLER AND BOLLES 1981].

The work of T. Schenk and his group at the Ohio State University [SCHENK 1995] is based on a multi-image version of the l.s. matching approach in object space [AGOURIS AND SCHENK 1996]. Their strategy starts from the sequential formation of the block by relative orientations within the strips [SCHENK *et al.* 1991], scale transfer and strip connection using a polynomial fit. Then the ground coverage of every image of the block is found, defining those areas where manifold tie points might be extracted [TOTH AND KRUPNIK 1996].

The method proposed by ACKERMANN (1995) is based on image pyramids and makes use of a DTM during the procedure. It is further assumed that all GCPs have been measured interactively on the original images. The proposed system applies feature-based matching in all overlap combinations and then tries to identify mismatches by a robust bundle block adjustment after each pyramid level. This approach has been implemented into the commercial software MATCH AT by Inpho, Germany [ACKERMANN AND KRZYSZEK 1997].

The three systems of Tsingas, Schenk and Ackermann can be considered as the fundamental starting points in the historical evolution of AAT; see [FÖRSTNER 1995] for a further comparative analysis of these methods. Other approaches have been investigated and implemented, either for experimental [JACOBSEN AND WEGMANN 1998] and commercial use.

A clear signal that AAT was leaving the academy for the market came with the announcement of the first commercial packages. This gave further momentum to the research on the topic, either because of growing competition between companies as well as from the response of the everyday practice in photogrammetric production. Compare to systems developed by research teams, commercial packages feature a sophisticated GUI, improved user-friendliness

and capability of dealing with large blocks, which enable their use in operational aerotriangulation. We quote in the following some of the most widespread.

In the United States, since the 1980s HELAVA Systems implemented automated digital triangulation procedures, which at the beginning were based on hardware devices such as the “Digital Comparator Correlator System” [HELAVA 1987]. Later on, products for digital AT become mainly software-based. Recently, HELAVA and Leica Systems (Switzerland) established a joint company, named LH Systems, which sells the AAT package HATS [MILLER *et al.* 1996; DE VENECIA *et al.* 1997], whose main features are reported in Table 1.4.

Autometric Inc. (USA) has developed its own AAT package, integrated into the the digital photogrammetric system SoftPlotterTM [LUE 1996; AUTOMETRIC 1999].

A very popular product is PHODISTM AT by Z/I Imaging, the new brand for digital photogrammetry which came up from the joint venture of Carl Zeiss (Germany) and Intergraph Inc. (USA). The strategy adopted for tie point extraction [Tang *et al.* 1997] is based on a multi-resolution approach, starting from approximate values for the exterior orientation parameters and then improving them by feature-based matching at the highest pyramid level. A number of tie points is selected which guarantees the geometric stability of the block and traced through all the pyramid levels. Particular care is put in the selection of multi-ray points, especially in the latest software release [DÖRSTEL 1999].

1.4 Automation in Ground Control Point Measurement

Ground control in AT refers to establish a correspondence between a given object coordinate system and the intrinsic reference system of the photogrammetric block as well as controlling block deformations. Although GPS and INS technologies nowadays permit direct measurement of position and attitude parameters, their reliability don't fulfil yet the demand for direct restitution [ACKERMANN 1997]. The traditional indirect determination of exterior orientation (EO) is still the most suitable approach and control information must be provided externally by measuring a consistent number of GCPs. However, INS improving steadily, this issue is one of the hottest topic in the photogrammetric community [COLOMINA 1999].

In analog and analytical photogrammetry *signalized points* (round, square targets, crosses) allow to obtain the highest precisions because they can be easily located and measured; besides misidentification errors are strongly reduced. Unlike other countries in Europe, signalized GCPs are not used in Italy except for a few experimental tests. Photogrammetric blocks are registered by using natural features as GCPs, e.g. corners of buildings, fields, stones, etc. A sketch or a terrestrial photograph helps to identify the point in the image.

In recent years researchers have made many efforts in order to automate this task but, with respect to other photogrammetric procedures such as tie-point transfer, relative and interior orientation, DTM and orthophoto generation, here studies are halted to experimentations and only applications tailored for specific cases were developed. A complete review of this subject can be found in [GÜLCH 1995b; HAHN 1997; HEIPKE 1997].

The main difficulty in detection and measurement of GCPs is designing or selecting suitable

models, even for signalized points, that allow homogeneously good recognition over a whole block. This is obvious if natural points are selected, as virtually for each point a different model has to be provided. Conventional signalized points are not designed to fulfil the needs of image analysis with respect to size, shape and background of signals. They appear too small in aerial images and this makes almost impossible their automatic detection in a large image patch; in Figure 1.2 some examples of signalized GCPs from 15 μm to 30 μm imagery are depicted.

Besides these technical considerations, another factor reducing the interest in automating GCPs' measurement is that the interactive method is still the most precise, quick and reliable, considering that the growing use of GPS-AT is going to dramatically reduce the amount of GCPs needed.

Semi-automatic measurement procedures are currently the best deal (see e.g. [HAHN *et al.* 1996]). If airborne GPS has been used, a good approximation for the EO of the block is known; otherwise it can be computed by manually measuring a least number of control points. This EO is used to assist the mensuration of other GCPs, starting from the interactive localization of a point in an image, which then can be projected onto the other images of the block. By means of multi-image matching including a coarse-to-fine strategy, the point may be automatically measured overall the block. Such a method might be optimized by using signalized GCPs and a database of templates representing different kinds of signals.

In an early study [MALMSTRÖM 1986], image patches with GCPs taken from old aerial photographs or orthophotos were used for automatic registration of satellite imagery. Obviously, this method suffers from temporal variations between images and is most suited for periodic survey and stable monumentation. Also the approach of HÖHLE (1998) is based on extracting GCPs from older orthophotos, together with height data.

The concept of extracting ground information from existing maps or GIS data is exploited by different approaches [VOSSELMANN AND HAALA 1992; HEIKKINEN 1994; CHRISTMAS *et al.* 1995; DOWMAN *et al.* 1995, 1996; HOLM *et al.* 1995, HILD AND FRITSCH 1998]. Feature and relational matching are used to compare the image and the model description on a symbolic representation level. However, extracting a useful symbolic image description to an acceptable level of confidence and reliability is difficult, so that these methods have found merely experimental application for the registration of small scale imagery. The work of PEDERSEN (1996) relates to large scale aerial photographs and makes use of data derived from a digital map, but the quality of the results falls down with high resolution images (less than 60 μm), when the influence of shadows, vegetation, dirt, people and vehicles on the roads cannot be neglected.

The increasing availability of *3-D city models* is raising the interest for the approach of SCHICKLER (1993, 1996), based upon prior studies by FÖRSTNER (1988) and SESTER AND FÖRSTNER (1989). Three dimensional wire frame models of houses are used as control information.

Another approach is based on the use of a DTM as control information for a photogrammetric block adjustment [EBNER AND STRUNZ 1988]. In a further development of this method [EBNER AND OHLHOF 1994] 3-D control points are used without the need for their direct identification in the image, under the hypothesis that each GCP lies on a planar area.

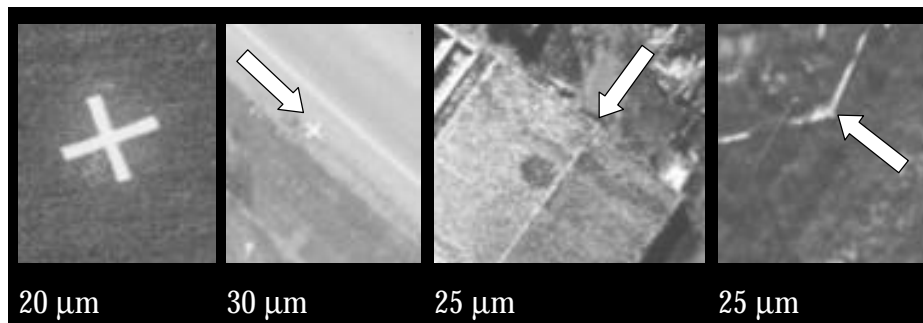


Fig. 1.2 – Some examples of signaled and natural GCPs (at different resolutions)

Coming back to methods based on point-like GCPs, GÜLCH (1994, 1995a) performs the mensuration of signaled points by means of *active contour models*, i.e. a feature extraction technique [GÜLCH 1996]. DREWNIOK AND ROHR (1997) proposed the extraction of manhole covers from images in urban area, to be used as GCPs since their coordinates are available in a sewage cadastre. Localization and mensuration of manhole is carried out by *model-fitting* to a parametric description of these objects. Identification is then performed by relational technique considering mutual distances between the located manholes and those in the database. Other references on point-like GCPs' measurement can be found in [HÄDEN 1994; FORLANI *et al.* 1995; HAHN 1997].

Summarizing automation of GCPs' measurement works well only in special applications. Among the methods proposed, some were applied to register single images and then the correspondence between more images were not examined. Hierarchical approaches did not help as in other tasks of digital photogrammetry. The same applies to area-based matching techniques, which seem to suffer from different illumination and other disturbances. On the contrary, feature-based and relational matching can reliably detect large control structures in aerial imagery with coarse or no approximations. Unfortunately their application is restricted to large scale imagery and high precision cannot be reached.

Today interactive measurement is still the more operational method to measure GCPs, but semi-automatic methods can be a realistic improvement. The measurement itself might become automatic, while the identification and the rough localization require a support by a human operator.

1.5 Automatic Interior Orientation

Any photogrammetric evaluation process requires the relation between the measurement system and the camera body. The determination of this relation is called the reconstruction of the *interior orientation* (IO), while the other parameters such as focal length, location of principal point (PP), and lens distortion are known from the calibration of the camera.

In aerial images the fiducial marks (FMs) define the image coordinate system. On a classical analytical plotter the measuring system is represented by the machine coordinate system, while on a DPW is the pixel coordinate system. After localization of the FMs within the digital image, a two dimensional transformation (usually an *affine* or a *bilinear*) between pixel and image system can be easily calculated. The main effort to automate the reconstruction of the IO is therefore the automatic and reliable location of the fiducials within the digital image.

The FMs (see some examples in Figure 3.2) usually are impressed into the image, with well defined shapes and colors resulting in well defined objects to be located, even though in real imagery several problems may occur. Often the contrast between the fiducial and its background is rather poor (e.g. in old cameras the fiducial center might not be as bright as expected). Dust and scratches near the FMs are a common source of disturbance, while scanning without proper parameter settings may prevent recognition as well.

HEIPKE (1997) gives a list of fundamental requirements for automatic computation of the IO. The procedure should be fast, accurate, robust, reliable and capable to deal with different camera types, image resolution, kind of image (positive/diapositive, B/W or color), varying number of FMs, unknown pose. The last point refers to the fact that there are eight basic ways of placing an analog image onto a scanner: emulsion up or down and, in both cases, four different orientations (see Fig. 3.4). An automatic reconstruction of the IO should be able to detect this and take it into account when estimating the transformation between pixel and image system. The sequence is the following:

1. Approximate localization of FMs.
2. Subpixel measurement of fiducial centers.
3. Mark number identification.
4. Computation of the transformation parameters.

Different methods have been studied and implemented in order to solve for these tasks in automatic manner. Table 1.3 summarizes the main features of a few published approaches; one more entry (the last) has been added, which reports the capabilities of the program ORINT, presented in chapter 3. The existing methods may be shared into two categories. The first one groups strategies based on hierarchical image correlation [SCHICKLER AND POTH 1996; LUE 1997]. The second one collects two procedures based on a rough localization of the FMs' position by means of image processing techniques, while the subsequent precise measurement is performed by image correlation algorithms [STRACKBEIN AND HENZE 1995; KERSTEN AND HÄRING 1997].

The procedure devised by SCHICKLER AND POTH (1996) of the Institute of Photogrammetry of Bonn University is implemented in the Digital Stereoplotter PHODISTM ST by Z/I Imaging. It performs the localization of FMs with an accuracy of better than 1/10th of a pixel without using any approximate values. After image binarization, an efficient localization is

carried out by binary correlation using hierarchical image pyramids. The pose of the image onto the scanner can be determined taking into account the asymmetric shape of the film border.

At the Surveying and Mapping Agency of Northrhine-Westfalia in Bonn, a program for automatic IO has been developed for the IS 200 image processing system of Signum Company (Germany) [STRACKBEIN AND HENZE 1995]. The localization and measurement of the FMs is based on the binary image analysis. The FM detection is performed by comparing all labelled objects in the image to the characteristics of a real FM, while the exact position of the fiducial center is derived with subpixel accuracy by a polynomial estimation in the original g.v. image [KNABENSCHUH 1995].

LUE (1997) introduced a fully automatic digital interior orientation based on hierarchical template matching techniques using a database containing fiducials of widely distributed aerial cameras. The operational software is the SoftPlotter™ product from Autometric Inc.

reference	approximate FM positioning	use of hierarchy	accurate FM measurement	pose estimation	availability	automatic pos./neg. recognition
KERSTEN AND HÄRING	Modified Hough transform	not	l.s. matching	only for Wild RC20, RC30	internal use at. Swissair Photo + Surveys Ltd.	not
LUE	g.v. correlation	yes	l.s. matching	manual	implemented in the SoftPlotter™ from Autometric Inc.	not
SCHICKLER AND POTH	Binary Correlation	yes	g.v. correlation	automatic	implemented in PHODIST™ ST from Z/I Imaging	yes
STRACKBEIN AND HENZE	Binary image analysis	not	fitting of parabolas to g.v. function (?)	manual (?)	internal use at the LVA Nordrhein-Westfalen	not
ORINT	g.v. correlation	yes	l.s. matching	automatic	internal use at Dept. IAR, Politecnico di Milano	not

Table1.3 - Approaches to automatic interior orientation (from [HEIPKE 1997]); the last row concerns the program ORINT which will be presented in chapter 3

At Swissair Photo+Surveys Ltd., a software for automatic IO was developed for internal use [HÄRING 1995; KERSTEN AND HÄRING 1997] and implemented on the LH DPW770. A rough localization of FMs is performed by means of a *modified Hough Transform* [HOUGH 1962; ILLINGWORTH AND KITTER 1988] while precise measurement is carried out by l.s. template matching. To avoid storing the image patch of templates for each camera type and for different resolutions, each template is described with a combination of three elements (circle, cross and dot) which is codified in a file. From this description, templates are dynamically built up at the desired resolution, after suitable filtering. The program can also recognize the pose of the image in case of cameras equipped with bars as symbols (Wild RC20 and RC30).

1.6 The OEEPE-ISPRS test on tie point extraction

As mentioned in 1.1, a test was launched in 1997 by OEEPE and ISPRS on the “Performance of tie point extraction in automatic aerial triangulation.” The test goal was to assess and compare existing AAT algorithms and strategies in terms of achievable accuracy for the tie points and for the orientation parameters. Operational aspects (dealing with large blocks, influence of GCP distribution) as well as topics related to the implementation of the procedures (GUI, program stability, computing time, etc.) were not investigated.

Apart from its relevance in AAT, there is a second reason, peculiar to this work, to introduce this test. The Dept. IIAR of *Politecnico di Milano* was invited to participate in the test, triggering the interest in this subject. A system for AAT was quickly designed and implemented in order to process the data of the test. The first release of the program named TRIADIGIT [FORLANI *et al.* 1998] was presented at the final Workshop of the test in Cambridge (July 1998). Later the main program was further developed and new modules for automatic IO and for interactive GCPs’ measurement were added to the system. Concept and implementation of the final version of TRIADIGIT will be illustrated in the next chapters.

1.6.1 Test data set and goals

The test was addressed to commercial photogrammetric software developers, mapping agencies, private companies and research institutes, employing commercial or experimental AAT programs. In Table 1.4 the systems used by different test participants are reported.

Each of the 21 participants was asked to perform the extraction of tie points from a set of 5 small blocks covering different scales, scene contents, topography, photographic materials and block configurations. The task had to be carried out in a totally autonomous manner, without user interaction. Only outlier rejection by an external program was allowed after automatic extraction of tie points. This strict condition was applied in order to separate the basic aspects of AT (influence of GCP distribution, block geometry, accuracy propagation, etc.) from the new topic of digital methods, namely automation. In particular the aim of the test was to investigate:

- The geometric stability of the block.
- The accuracy of the image coordinates of tie points.
- The limitations of existing commercial and experimental AAT systems.

Participants received a detailed description of the test, the digital imagery, the camera calibration certificates, together with a priori information on the blocks (rough EO, average terrain height). No GCPs were delivered, except if specifically required. Each participant could carry out the mensuration of fiducial marks by whatever method. The extracted sets of conjugate points were sent back to the pilot center. A detailed report about the procedure used was asked as well.

	matching entities	matching method for accuracy refinement	no. of images during matching refinement	image pyramids	DTM as input (optional)	use of "von Grüber" positions	automatic blunder elimination	integration of block adjustment	need for GCPs	autonomous system design	parameter file
HATS (LH Systems)	points	subpixel cross correlation	2	×	—	×	—	(×)	—	(×)	×
Match AT (Inpho)	points	l.s. matching	all overlapping	×	×	(×)	×	×	×	×	×
Phodis AT (Z/I Imaging)	points	l.s. matching	2	×	—	—	—	—	—	×	—
Finnish Geodetic Inst., Masala	points	l.s. matching	2	×	—	×	(×)	(×)	×	×	×
Inst. of Phot. & Eng. Surveys, Hannover	points/structures	l.s. matching	2	×	—	—	—	—	—	×	×
TU, Munich	points	—	2	×	—	—	×	×	—	×	×
Dept. IAR, Politecnico di Milano	points	l.s. matching	2	×	—	—	—	—	—	×	×
Univ. of Agricultural Tech., Olsztyn	points	cross correlation	2	×	—	—	—	—	—	×	×

Table 1.4 – Main features of the different AAT systems used in the OEEPE-ISPRS test (from [HEIPKE AND EDER 1998])

1.6.2 Test findings

The pilot center at Munich Technical University carried out the analysis on the data sets coming from each group. The procedure adopted to assess the results is presented in the final report [HEIPKE AND EDER 1998]. It consisted of two main stages:

1. A robust bundle adjustment of each block was performed to remove inconsistencies and to check the accuracy of EO parameters.
2. A set of image coordinates of check points, which were manually measured and adjusted for each block, where computed by space intersection on the basis of each EO, to investigate the accuracy of tie points extracted by AAT.

In the final report the following conclusions are stressed, according to three main items:

1. Geometric block stability:

- A large number of tie points per image (100÷300) is strictly required in order to guarantee a sufficient geometric block stability. This is due to the unavoidable presence of blunders in the set of automatically extracted tie points, whose influence can only be reliably eliminated if their percentage is relatively small.
- Although the distribution of GCPs and/or GPS-INS measurements was not investigated, it may greatly affect the stability of the blocks, especially in large blocks.
- A large number of multi-ray points should be guaranteed, otherwise severe block deformations are introduced.

2. Accuracy of tie point coordinates:

- A global evaluation of tie point accuracy is given by the sigma nought of the bundle adjustment, which under favourable conditions (open and flat ground, good texture of the images) and using l.s. matching can reach a value of 0.15÷0.2 pixels (3÷4 μm).
- A more realistic value for σ_0 lies in the range of 0.2÷0.3 pixels (4÷9 μm), in case of images digitalized at 20÷30 μm . According to [ACKERMANN AND KRZYSZEK 1997], pixel sizes smaller than about 20 μm will not improve the accuracy of tie points.

3. Limitations of existing systems:

- In mountain and forest area some AAT systems fail, especially in strip connections.
- Most systems are not provided with internal self control to check the quality of AAT's results. A small value for σ_0 of bundle adjustment, even if a robust procedure is implemented, does not rule out errors or deformations within the block. The *reliability analysis* seems to be the only way to introduce into AAT systems an automatic mechanism of self control.

- Graphic representation of point distribution in image and object space helps to assess the quality of the results.
- Performance of AAT systems strictly depends on the correct input of a set of control parameters. This task requires AAT operators to be enough experienced in handle the program set up.

Even though some aspects of AAT were neglected in OEEPE-ISPRS test, the outcomes show that in many cases a fully autonomous extraction of tie points is feasible, but verification and editing stage must be carried out by a human operator. In a recent workshop of the ISPRS (Munich, September 1999), the term AAT has been “downgraded” to AAAT (i.e. assisted AAT) [COLOMINA, 1999], pointing out that editing and revision of the results is necessary. Further developments on this subject are expected, even though on the basis of current researches they are foreseeable.

1.7 Basic requirements of an automatic procedure for tie point extraction

In the light of the OEEPE-ISPRS test’s results, we would try to stress what really matters in an AAT program, especially as far as tie point extraction is concerned. We have *technical* and *operational* requirements. The first aims to reach a precise, reliable and stable aerotriangulation of a photogrammetric block, encompassing issues such as number, distribution and local redundancy of tie points, accuracy of initial values of the exterior orientation, data necessary to start up the search for homologous points, analysis of the quality of the outcomes. Operational requirements concern the practical use of the AAT, i.e. user-friendliness, limitations in block size and shape, computing time, hardware aspects, capability to deal with different data format.

1.7.1 Technical requirements

The way by which the technical requirements are fulfilled characterizes each AAT system, especially when speaking about experimental systems, whereby a good quality aerotriangulation of the block is the main goal. On the contrary, the evaluation of a commercial system must take into account practical aspects as well. For instance, a system could give very good results in term of precision and block stability but its use may be too cumbersome or the outcome presentation and editing tool may be poor.

The main technical requirements of a program for tie point extraction may be expressed as follows:

- The method to search for homologous points should not strongly depend on the quality of the approximate values for the exterior orientation of the block.
- The number of tie points per image should feature sufficiently high, according to relation

(1.1) showing that the less accuracy achievable in point measurement by image matching may be compensated for by a higher number of observations.

- Tie points should be homogeneously distributed all over the block to guarantee enough stability; in particular the number of multi-ray points is expected to be high.
- A procedure to check the quality of intermediate and final results should be implemented into the system, with particular emphasis to the internal reliability analysis.
- A consistent part (about 20÷30%) of the tie points found by image matching are outliers, requiring a robust procedure to reject them within the AAT process.
- The set of input control parameters should be as small as possible.

1.7.2 Operational requirements

Everyday use of an AAT system demands the following requirements to be satisfied:

- The system should be user-friendly, i.e. equipped by a GUI and by visualization tools to display images, block structure, in project setup as well as in editing.
- Every geometric configuration for the photogrammetric block should be dealt with, including different overlaps, cross-strips, different flight elevations; also very large blocks should be accepted, possibly by splitting them into smaller sub-blocks.
- Different image data formats should be accepted, at least the most widespread.
- The system should output the computed EO parameters and tie point object coordinates in a format readable by digital and analytical plotters.
- An interface to the most popular bundle adjustment packages should be provided.
- The minimum hardware configuration may be a significant part of the cost. Today the implementations under operating systems running on a PC are to be preferred, due to the large diffusion of this platform and its relatively low cost.

Perhaps most important is the time required to complete a project, involving both technical and operational aspects: if AAT is to be used in practical applications, an automatic procedure must be as precise as an operator at the analytical plotter and cannot take longer to complete, including the final editing. Therefore the technical solutions have to compromise between computationally expensive but accurate algorithms and faster but less accurate strategies. Programming efficiency and hardware characteristics are crucial in this respect.

Chapter 2

The TRIADIGIT system for AAT

2.1 Genesis and goals

In this chapter we report about the TRIADIGIT system for AAT developed during the last three years at Dept. IIAR of *Politecnico di Milano* in collaboration with the Dept. of Civil Engineering of *Università degli Studi di Parma*. The package is made up of different modules, each performing a basic task of AAT, as measurement of fiducial marks, tie point extraction, measurement of GCPs and bundle adjustment.

The idea of implementing an AAT system arose in the years 1994-95 for the first time, when the OEEPE test on digital aerotriangulation was launched [JAAKOLA AND SARJAKOSKI 1996]. Since the beginning of the 90s digital photogrammetry has been gaining more and more the interest of Dept. IIAR. In the occasion of the test, matching techniques and algorithms implemented at that time were applied into a first program for AAT. Unfortunately, the hardware available at the Department did not allow to deal effectively with the large amount of data which a digitalized photogrammetric block requires.

Two years later, when the OEEPE-ISPRS test on “Performance of tie point extraction in AAT” was proposed (see 1.6), the situation has changed dramatically. Thanks to a very quick improvement in computer technology, large storage capacity and fast processors became available at a low cost. At the same time, the experience on digital photogrammetry increased, enabling the implementation of the first release of the program TRIADIGIT for automatic tie point extraction [FORLANI *et al.* 1998], applied to the blocks of the OEEPE-ISPRS test [HEIPKE AND EDER 1998]. A new module for automatic interior orientation was designed and implemented [FORLANI *et al.* 1999], as well as another for interactive measurement of GCPs. Based on the analysis of the test results, the strategy for tie point extraction was improved, reaching eventually the actual state.

Nevertheless, the availability at Dept. IIAR of a software for automatic aerotriangulation could be exploited in the future for other researches or applications, as well as for teaching purposes.

Because so far usage of TRIADIGIT system has been only internal, a user-friendly GUI has not been implemented yet.

This chapter will present the whole system TRIADIGIT, including the strategy for tie point transfer, its implementation and some other subsidiary modules; besides, the program for the measurement of GCPs and that for the bundle adjustment will be illustrated. On the contrary, the automatic interior orientation will be the subject of chapter 3.

2.2 Framework of the whole system

Automatic aerotriangulation is a complex task involving different basic procedures, as shown in 1.2. The existing systems for AAT are structured in modules, each of them performing a single stage, and TRIADIGIT is not exception. We have 4 main components, which execute the fundamental tasks:

1. Automatic interior orientation (module ORINT).
2. Automatic tie point extraction (module TRIA_DIGIT).
3. Interactive measurement of GCPs (module APPBLOCK).
4. Bundle adjustment and data snooping package (REJECT, based on the bundle adjustment program CALGE).

Each of this modules may exist as stand-alone program, allowing its use in other packages, provided that the input/output files are formatted in a suitable way.

Furthermore, the automatic tie point extraction, which is the core of the whole process, requires some other subsidiary modules to generate image pyramids, to extract interest points and to display the results.

Before analyzing each single step, we want to give an overview of the strategy for AAT implemented in TRIADIGIT. In Figure 2.1 is reported a general scheme illustrating how the main tasks are structured.

The first stage which is performed is the automatic computation of the interior orientation of every image of the block, pre-requisite of every metric operation on the imagery.

The second operation is the measurement of a minimum set of GCPs, carried out interactively by the module APPBLOCK, to define the photogrammetric block datum, which is used throughout the tie point extraction stage and to compute intermediate bundle adjustments. In fact, this GCPs' measurement could be avoided if a program able to compute a *free network adjustment* is available [KRAUS 1997]. Otherwise, a minimum constraint can be defined as well by fixing 7 exterior orientation parameters (for example, 6 parameters of an image and one baseline). The last preparation stage is the image pyramids generation and the interest points extraction from the images.

Tie points are selected and matched in automatic way through a hierarchical procedure from coarse-to-fine. Besides, a robust procedure to discard gross errors is carried out at the end of each level. Between different levels, a bundle adjustment is computed in order to reject those outliers which have still survived and to update the EO of the block. The bundle adjustment requires a check of the results by the user, because if the geometry of tie/ground control points is weak, the solution may be not stable, causing the subsequent failure of the whole AAT. At the end of this stage, the remaining GCPs may be measured faster, because the improved EO of the block is exploited by the program APPBLOCK to assist the user.

A final bundle adjustment ends the AAT.

In the following paragraphs the core of the AAT procedure, i.e. tie point extraction, will be analyzed in detail.

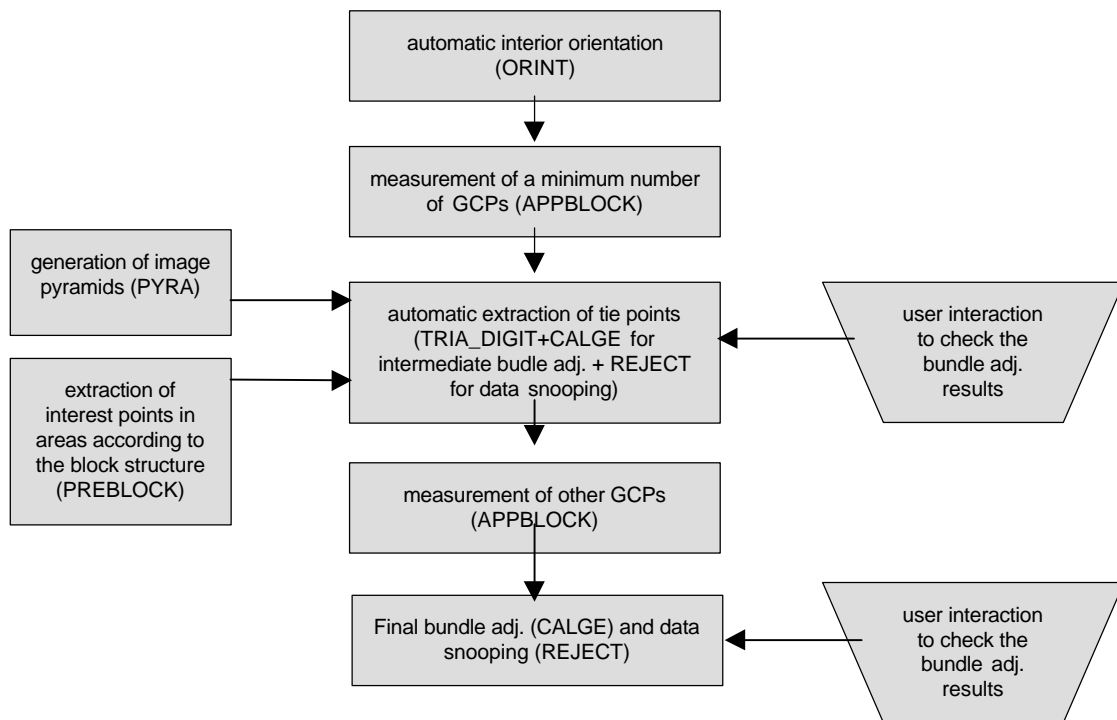


Fig. 2.1 – Workflow of the procedure for AAT in TRIADIGIT

2.3 Available a priori information

The dream of an AAT program only requiring to supply the images into the storage unit, to push a button, to have lunch and then to enjoy the results of aerotriangulation is still utopian. Data preparation is always required also by the best commercial packages and the knowledge of some a priori information about the photogrammetric block is necessary.

Broadly speaking, feature-based matching techniques are less dependent on a priori information; for precise point transfer, the following data are anyway mandatory:

- Image resolution, camera model and sizes of the images.
- Interior orientation elements and camera calibration data.
- Block structure, defined implicitly by the approximate projection center coordinates or simply by giving the image sequence, the strip sequence and forward/side lap. Complex blocks, with cross or oblique strips may require additional specifications.

Since TRIADIGIT relies on area-based methods, additional information is required on EO parameters and the ground shape. An EO orientation of the block may be always derived. Considering that pitch and roll angles may be neglected and assumed equal to zero, the remaining parameters, i.e. yaw and photo centers, may be derived by different approaches. The simplest and also most precise manner to compute approximate perspective centers is the use of GPS during the flight (precision of about 1÷2 m). The drift angle may then be derived from the flight line projected over a map or orthophoto. If the flight was not assisted by GPS, X_0 and Y_0 may be inferred from the flight plan, while Z_0 can be assumed equal to the instrumental flight height. An accuracy ranging from 10 to 100 m is achievable for the perspective centers and of about $1^g\div 2^g$ for the κ angles, depending on the scale of the map (or orthophoto) and of the photographs. Another way to proceed is the interactive computation of a minimum number of parallaxes inside and across the strips; in this case, the results is highly sensitive to the determination of the scales, for which the knowledge of the instrumental flight heights may not be enough. If possible, it's better to recognize on an image (or more) of the block two GCPs and then to compute the mean scale of the photograph as ratio between their mutual planar distances in image and object space.

An approximate value for the end and side overlap is usually known, because after the flight the design values are verified and, if not satisfied, the block is refused. By the way, the use of GPS to assist the airborne guidance contributes to obtain blocks having a more regular shape.

- A very rough model for the ground is always available, at least in developed countries. We report about three different solutions for the ground model, from the simplest to the more accurate:
 1. a horizontal plane passing through the average ground height, which can be derived from the existing cartography; also the maximum height difference with respect to this plan may be achieved in this way, otherwise it may be guessed;
 2. the GCPs allow to define a rough DTM by interpolating a surface through them;
 3. a DTM of the block' s area is available.

2.4 Strategy for tie point extraction

The AAT program TRIADIGIT performs tie point selection, measurement and transfer within a photogrammetric block, based on some a priori information. This consists mainly of a rough EO and of a ground model. Apart from blocks in mountainous zones, where a DTM is strictly necessary, elsewhere a horizontal plane and the maximum height difference in the area is enough.

The strategy for tie point transfer is based on a *multi-resolution* approach, starting from a pixel size of about 0.8 mm and using all the levels of the image pyramids (see par. 2.4.1). This reduces the risk of ambiguities in the image matching, because only the main features appear in the top of the pyramids¹. Besides, the influence of terrain shape as well as of radiometric and perspective differences between the images are less important.

The workflow of the process is made up of three main stages, each of them absolving one of the following functions:

1. Improvement of the approximate exterior orientation of the block.
2. Tie point densification.
3. Improvement of tie point accuracy and of the number of multi-ray points.

The first stage can be skipped if a set of accurate values for the EO parameters is available (e.g. if GPS has been used during the flight). In this case the procedure may start from stage 2.

In the next paragraphs the three main stages of tie point transfer are illustrated, while more details about data pre-processing (par. 2.5) and about the algorithms used will be given later (in 2.6 and in chapter 4).

2.4.1 Improvement of the approximate exterior orientation

This stage is carried out in one or two levels at the top of the image pyramids, depending on the resolution of the original images. As a rule of thumb, with imagery having a pixel size less than 20 μm two levels are necessary, otherwise one is enough.

A set of *interest points* is extracted by means of *Förstner operator* (see 2.5.4) on every image at the lowest resolution and is stored in a file; in the sequel we will refer to these points as *secondary points*. For each image, a sub-set of points is derived from the set of secondary points in areas dependent on the geometry of the block; the strategy for this selection will be reported in 2.5.4. These new points are labelled according to the image where they lie, hereafter referred to as *primary points*. The primary points act as templates in the image matching, while the secondary points as slaves. When a matching is accepted, the two points become conjugates and take the label of the primary point.

¹ Usually an image pyramid starts from the original resolution and reaches the n -th level with the lowest resolution (termed *top of the pyramid*).

The search for homologous points is built up on two nested loops. The external loop runs on all images of the block, which become in turn *primary images*. The inner loop runs on all the remaining images, which become *secondary images*.

When an image is primary, around each of its primary points is extracted a template and its homologous point is looked for on the secondary image. Searching is carried out in two steps. The first one defines a rectangular window on the secondary image (see 4.2.1). The template point is projected from the primary image down to the DEM and then backprojected onto the secondary image. Around the point is extracted a rectangular window whose size depends on the uncertainty of EO parameters of both images and on the uncertainty of the ground model.

All secondary points falling in the search window are selected as candidates and matched one at a time by *l.s. template matching* (see 4.1.2). The homologous point is selected on the basis of the highest *correlation coefficient*, given however a minimum threshold (usually $\rho_{\min}=0.70$). By this procedure, the conjugate points of each primary point are looked for on the whole block, so that multi-ray points might be found.

When all points of a primary image have been tried, the external loop moves to the next image until the block is completed.

Hopefully, a first set of tie points has now been found. Unfortunately, as many as 30÷40% of them are outliers: due to wrong EO the conjugate points were searched for also in areas far from the correct position. To cope effectively with the large number of mismatches, a robust procedure for *gross error rejection* is implemented. Every feasible pair of images is considered and the set of common points is checked against outliers by means of two possible methods: *robust relative orientation* or *parallax analysis*; using the former or the latter depends on the number of points in the pair (see 2.6).

TRIA_DIGIT is now stopped and the set of “clean” tie points is adjusted by the bundle program CALGE to further remove outliers by *data snooping* and to improve the initial EO parameters. The top level of the image pyramids usually gives tie points with an accuracy of about 0.25÷0.30 pixels.

Optionally, a DTM is computed from the object coordinates of tie points to reduce the search window in the next level.

2.4.2 Tie point densification

Experience showed that the number of tie points found in the first stage is not enough to get in the end a strong photogrammetric block. Transfer through all the remaining levels of the image pyramids shrinks the set of about 10÷20% of the total amount in each level. Then a point densification procedure is carried out, involving the $n-1$ (or the $n-2$) level. Thanks to the larger size of the images more interest points can be extracted and by exploiting the improved EO, homologous points are expected to be found more easily.

From an operational point of view, the procedure for point transfer is the same as in the first stage, but the goal is different. The improvement of the EO is now less important, while seeking more tie points is crucial to give stability to the block. At the end of this stage the tie points found are transferred “vertically” to the next level after the bundle adjustment.

Moreover, the object coordinates of tie points are *backprojected* from the ground onto all the images of the block giving raise to new secondary points, so that the number of rays per

point should increase wherever it is possible. All the tie points found (directly and by the backprojection) are then transferred to the following level.

2.4.3 Improving tie point accuracy and increasing the number of manifold points

Two tasks are executed in the third stage: first, since tie points have been measured at a coarse resolution (some hundreds micrometers) the accuracy of their measurement must be improved; second, the number of manifold points should be increased as much as possible.

Every primary point has now assigned its corresponding tie points on the other images and these don't have to be looked for any more.

Interest points extracted at the top level of the image pyramids are located on well contrasted features, allowing a good determinability of the geometric parameters of l.s. matching. Transferred points to the next level should keep this peculiarity, but this is not possible by direct transfer (simply multiplying the image coordinates of the point by a factor 2). The coordinates of each primary point are therefore redefined on the new level by applying the Förstner operator on a window centered on the point obtained from the direct transfer. The best point is selected according to the highest value of the *interest parameter* w (see 2.5.4). For secondary points, a similar procedure is followed, this time by considering the best n_s positions ranked according to w (usually $n_s=12$). In Figure 2.2 a six-ray point transferred through all the image pyramids levels is shown.

The loops on the primary and secondary images are repeated as in the initial level, trying the redefined primary point with all new secondary points.

Obviously, the measurement at current level may improve the precision, but may also fail, due to the appearance of new details which cause mismatches or to inaccurate backprojection.

After the measurement stage the outlier rejection is performed again and then tie points are used to compute a bundle adjustment. The remaining points are backprojected on every image of the block and then transferred to the next level. This scheme is repeated until the level 0 of the image pyramids is reached. To save time, the adjustment and the backprojection are carried out only after the levels 4 and 2, whilst after the other levels all the points found by image matching are transferred without any further processing.

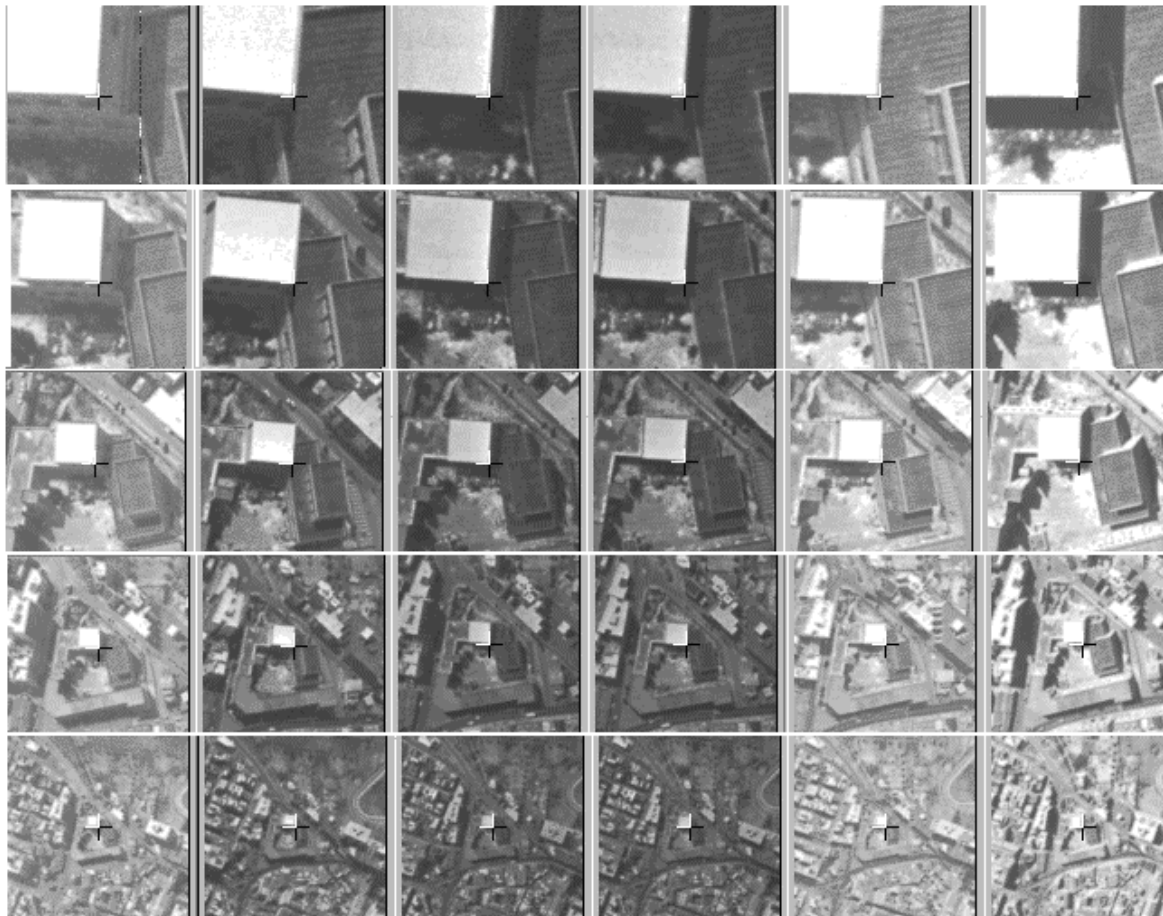


Fig. 2.2 – Example of a 6-ray tie point traced along 5 level image pyramids

2.5 Preliminary data setup

Prior the automatic tie point extraction a pre-processing stage builds up the image pyramids, extracts the initial interest points, forming the primary and secondary data sets. These data are prepared by specific programs. Furthermore, some control parameters must be setup: information on the photogrammetric block (number of images, pixel size, etc.), specific image characteristics (number of image pyramids levels, l.s. matching parameters, etc.). Finally the approximate exterior orientation of the block must be defined.

2.5.1 Selection of program control parameters

The program may work on the whole block or in sub-areas, defined by the image numbers, and with any number of levels in the pyramids. Standard corrections to image coordinates (distortion, refraction, Earth curvature) may be applied. To control the matching process, the window size of the l.s. matching is specified, together with the threshold for the correlation coefficient. The size of the window may be the same in all levels or may be increased from a level to another. Usually a window size of 9-11 pixels is used in the level 5 of the hierarchy, which is the initial level for resolutions ranging from 20 to 30 μm .

Furthermore a model for the ground must be given, although a simple horizontal plane is enough for most blocks. In this case a mean height of the block area has to be provided as well as the maximum height difference.

2.5.2 Approximate values of the exterior orientation

The search for homologous points is directly performed on the whole block, using a bundle approach. Therefore, good initial values are necessary to limit the search area and to ensure a certain likelihood that tie points can be found in more than a pair of images. The program accepts as reference system that given by the control points or a conventional reference system. In the former case, projection centers and strip directions (given by the k angle, drift is neglected) are derived by GPS or from the flight plan, while w and f are taken to be zero. In the latter case the system is parallel to the image coordinate system of an arbitrarily chosen reference image, under the assumption of nadir images. The image reference systems of the other photographs are tied to the first by computing simple shifts or plane Helmert transformations based on the interactive measurement of one or two pairs of image points. This approach has worked reasonably on the small blocks we have dealt with in the test phase, but may become impractical on larger blocks.

Moreover, the uncertainty of the approximate EO parameters must be estimated, according to the way they have been computed.

2.5.3 Image pyramids generation

Pixels in a neighbourhood are highly correlated. *Image pyramids* provide a means to speed up processing and increase reliability using only relevant information. A pyramid is a generalized image structure consisting of several successively increased levels of resolution of one image (see an example in Fig. 2.3). Practical applications of image pyramids in digital photogrammetry may be found in [ACKERMANN AND HAHN 1991].

Image pyramids generation is made up of two steps: *image filtering* to avoid aliasing, *image resampling* with a decimation step of two. Both tasks may be arranged together as suggested by BURT AND ADELSON (1983), which use a separable 5×5 Gaussian mask. The mask is applied only to the pixels to pick up, saving about 75% of the computation time.

The number of levels in the pyramid depends on the texture content and on the geometric resolution of the images. Our experience agrees with the literature: 5 levels are adequate for pixel size around $20 \div 30 \mu\text{m}$, given a top level of the pyramids with a pixel size of about $0.6 \div 1 \text{ mm}$.

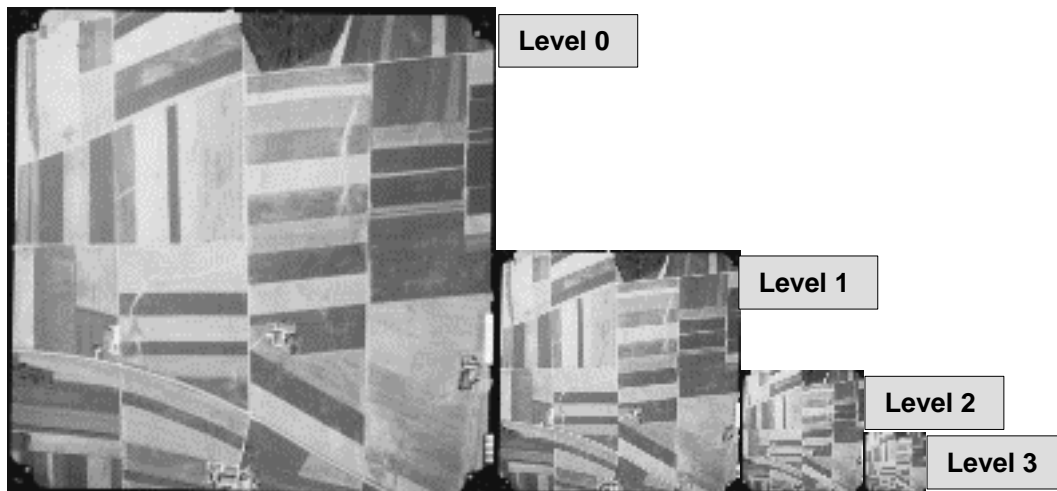


Fig. 2.3 – Example of an image pyramid



Fig. 2.4 – An aerial image with all the interest points extracted (secondary points, on the left) and with the primary points (on the right)

2.5.4 Extraction of interest points

Templates for tie points are selected by the *Förstner operator* [FÖRSTNER 1986] applied to the images at the highest level of the image pyramids.

Pixels are discriminated based on the *roundness* q (which must be greater than 0.5) and on the local maxima of the *interest value* w . We remind the definition for q and w :

$$w = \frac{\det \mathbf{N}}{\text{tr} \mathbf{N}} = \frac{\lambda_1 \lambda_2}{\lambda_1 + \lambda_2} \quad (2.1)$$

$$q = \frac{4 \det \mathbf{N}}{(\text{tr} \mathbf{N})^2} = 1 - \left(\frac{\lambda_1 - \lambda_2}{\lambda_1 + \lambda_2} \right)^2 \quad (2.2)$$

where \mathbf{N} is *normal equation matrix* of the shift parameters of the l.s. matching:

$$\mathbf{N} = \begin{bmatrix} \sum g_r^2 & \sum g_r g_c \\ \sum g_r g_c & \sum g_c^2 \end{bmatrix} \quad (2.3)$$

g_r and g_c are the row and column derivatives of the g.v.s; λ_1 and λ_2 are the eigen-values of the inverse of the normal matrix \mathbf{N} . Förstner operator is applied with a 5×5 window.

The program PREBLOCK performs the extraction of interest points on every image of the block, storing them in files. As illustrated in 2.4.1, a sub-set of these points is extracted to form the primary points, which will serve as templates (see Fig. 2.4). If there is no a priori knowledge about the geometry of the block, a case however seldom happening, the primary points are selected all over the images, by taking the first n_p points ranking with the highest interest value w . The upper limit n_p (usually setup as 1000) is adopted to avoid too many computations.

If on the contrary the geometry of the block is approximately known, the primary areas are selected to avoid overlaps among them. Besides, areas where only twofold points might be found are neglected, apart from the border images. The scheme for the distribution of primary areas for blocks with standard overlaps (i.e. 60÷65% end and 20÷25% side) is reported in Figure 2.5, while Figure 2.6 depicts the same for blocks with 60÷65% end and 60÷65% side overlap. Obviously, the scheme of the block structure has to be provided in input.

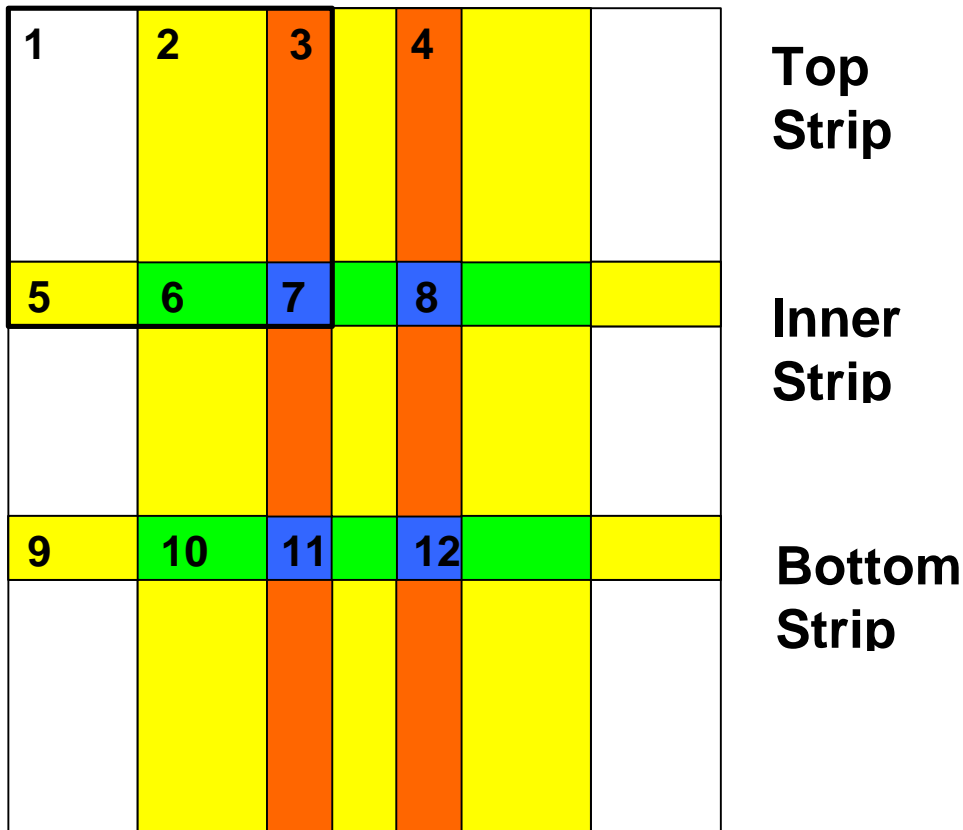
With this partitioning of the tie point set:

- Tie points may be found all over the block, covering all the manifold areas and neglecting twofold areas which do not contribute to the stability of the block.
- Every point in object space plays as primary point in only one image, so that reducing the computation time.

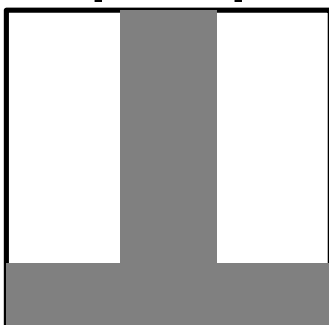
Indeed, the EO is still rough at these stage and some overlaps are present. Moreover, the ground height variation cannot be kept into account when planning the primary areas. However the use of these primary areas has given very good results in experimental tests, either in time-saving and in improving the selection of tie points.

Block 60% end 20% side

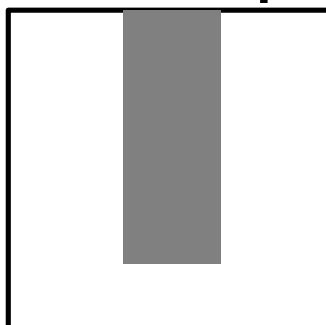
images



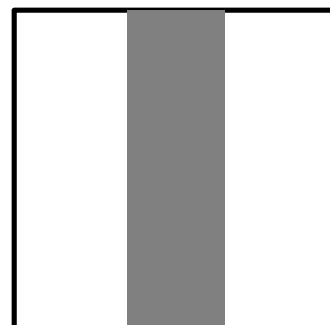
Top Strip



Inner Strip



Bottom Strip



Number of overlapping images

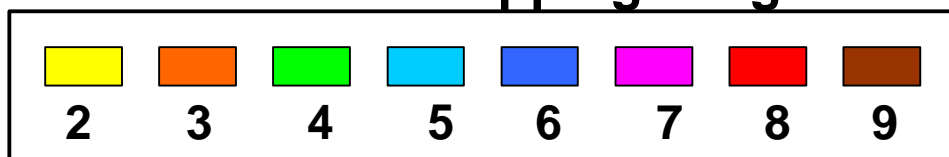
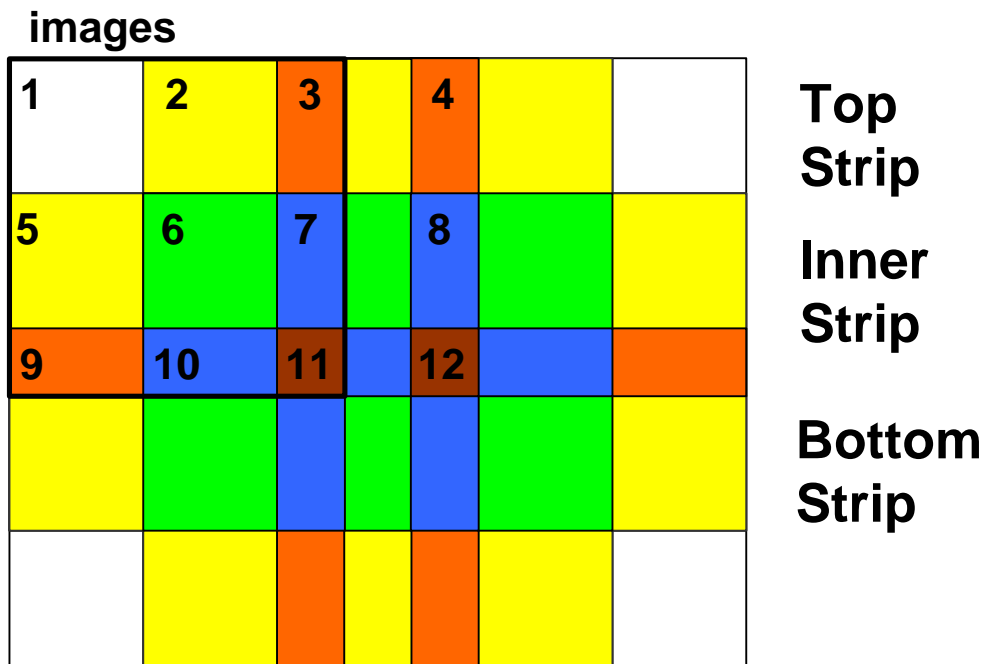
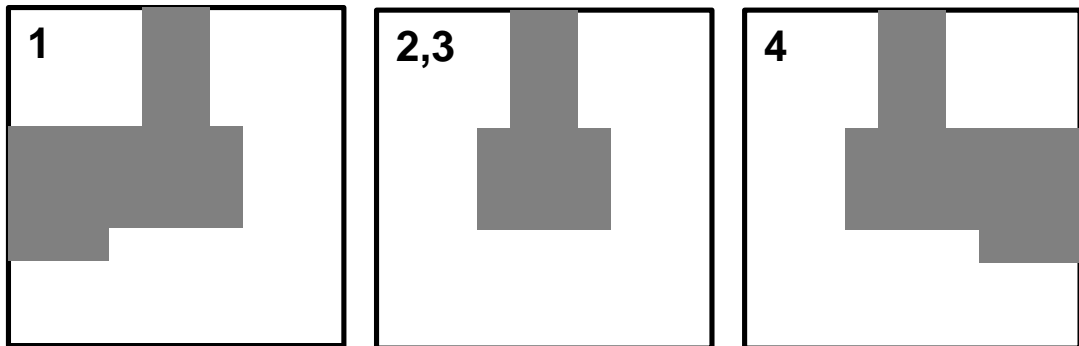


Fig. 2.5 – Scheme of the distribution of primary areas for a standard block. In the middle of the figure, the resulting areas are depicted, according to the position of the photo in the block

Block 60% end 60% side



Top Strip



Inner Strip

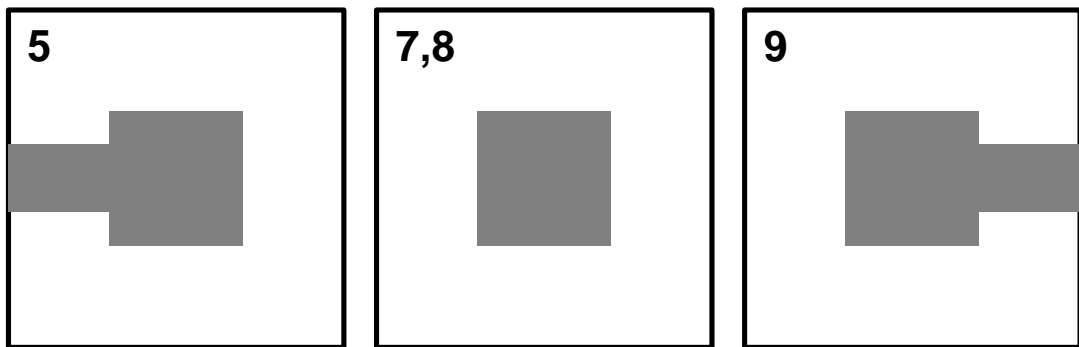


Fig. 2.6 – Scheme of the distribution of primary areas for a block with overlap 60% side-60% end. In the middle of the figure, the resulting areas are depicted, according to the position of the photo in the block; the bottom strip is symmetric with respect to the top strip

2.6 Gross error rejection

The search for conjugate points by stereo image correlation does not include geometric constraints, since information on the exterior orientation is too weak. In order to identify inconsistencies among tie points, a robust procedure is adopted. Some examples of wrong conjugate points are shown in Figure 2.7. Every feasible pair of images is considered and the outlier rejection is performed according to the number n_p of common points in the pair:

- If $n_p < 3$: no reliable algorithm can be applied.
- If $3 \leq n_p < 20$: x and y parallaxes are computed, under the hypothesis of quasi nadir images, approximately flat terrain and negligible relative k rotation between the pair. Two robust location and dispersion measures are computed: the *median* of the parallaxes (me) and the *median of the absolute values* (mav) of the residuals with respect to me . If the measured parallaxes are outside a symmetric acceptance interval centered on me , the coordinate pair is rejected. The endpoints of the interval are given by:

$$me \pm \alpha mav \quad (2.4)$$

where the coefficient α is usually set to 2. It is apparent that the discrimination power of the test is maximum in flat terrain, while it sharply decreases with terrain roughness (as it happens not only in mountain areas, but in large scale images of downtowns). Even in flat terrain, if there is a significant relative k rotation between the images, as it happens especially between adjacent strips, the test is not much worth. However, it is used when no other method can be called on due to the small number of points.

- If $n_p \geq 20$: in this case, after a further check on point distribution, a *robust relative orientation* is computed and the points which would not fit in the estimated model discarded. This approach needs no restrictive assumption for the ground, but works well only if a consistent overlap area exists between the images of the pair. The algorithm adopted to compute the robust relative orientation (presented in 4.3) may cope effectively with a percentage of 50% of outliers in the data set.

2.7 Implementation of the program TRIA_DIGIT

The program TRIA_DIGIT has been implemented in FORTRAN77, running under the operating system LINUX. Just a PC, possibly with a large capacity of storing and well equipped by RAM memory, is required. This choice has been made in order to run AAT on a widespread and quite economic system.

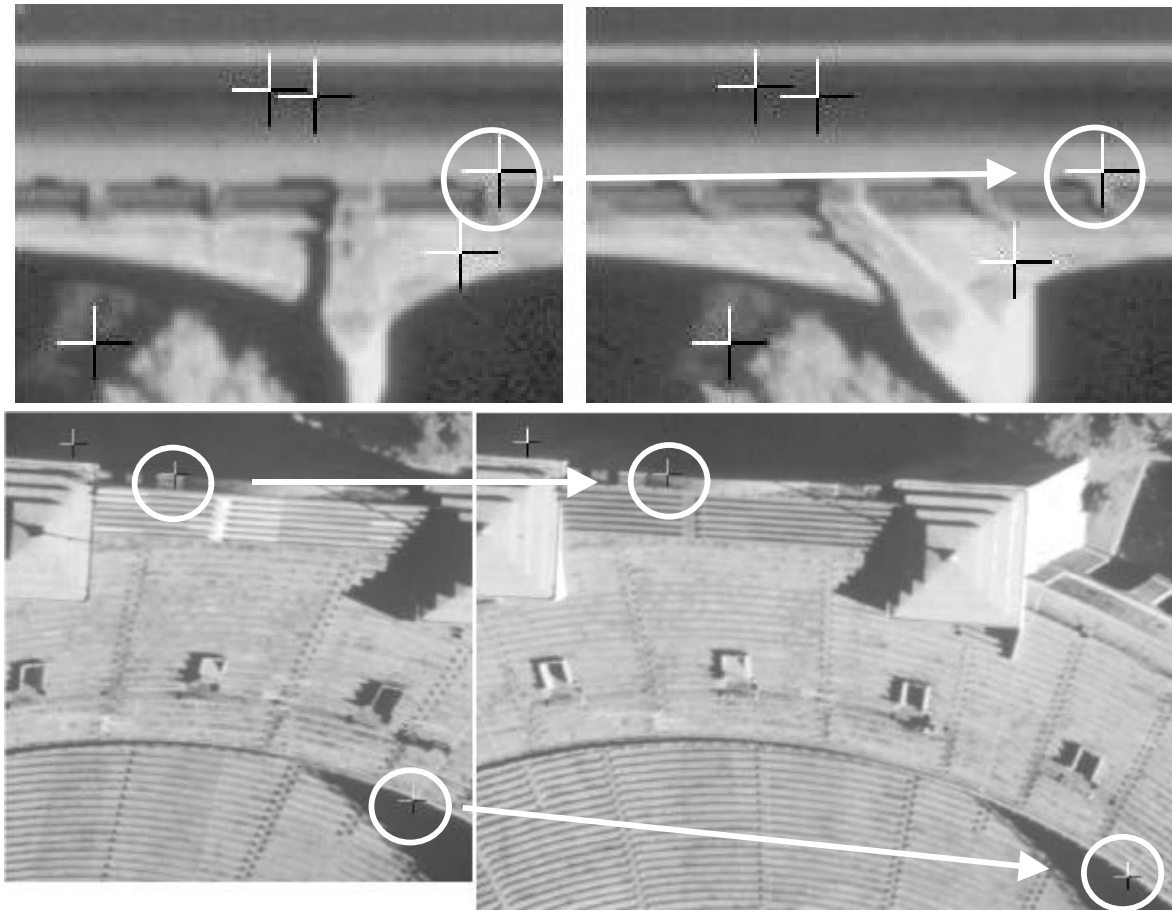


Fig. 2.7 – Examples of outliers

Automatic aerotriangulation is implemented as a batch process, starting from an input file where all the control parameters must be supplied by the user. Original images must be converted to BMP, that is the only format accepted by the actual release of the system. Image pyramids are generated by the module PYRA, as well as the extraction of interest points. The interior orientation of each image is computed in advance by the program ORINT, yielding a file containing the 6 parameters of the affine transformation.

The intervention of the user is required at the end of every level on which the bundle adjustment has to be computed.

The output is made up of:

- A detailed report file illustrating any single step of the process.
- Tie points found at each level of the image pyramid.
- Image coordinates of tie points in format readable by the bundle program CALGE (this requires also a file with the approximate object coordinates of tie points).

The tie points extracted on the block may be converted into a format readable by a CAD commercial software and then visualized.

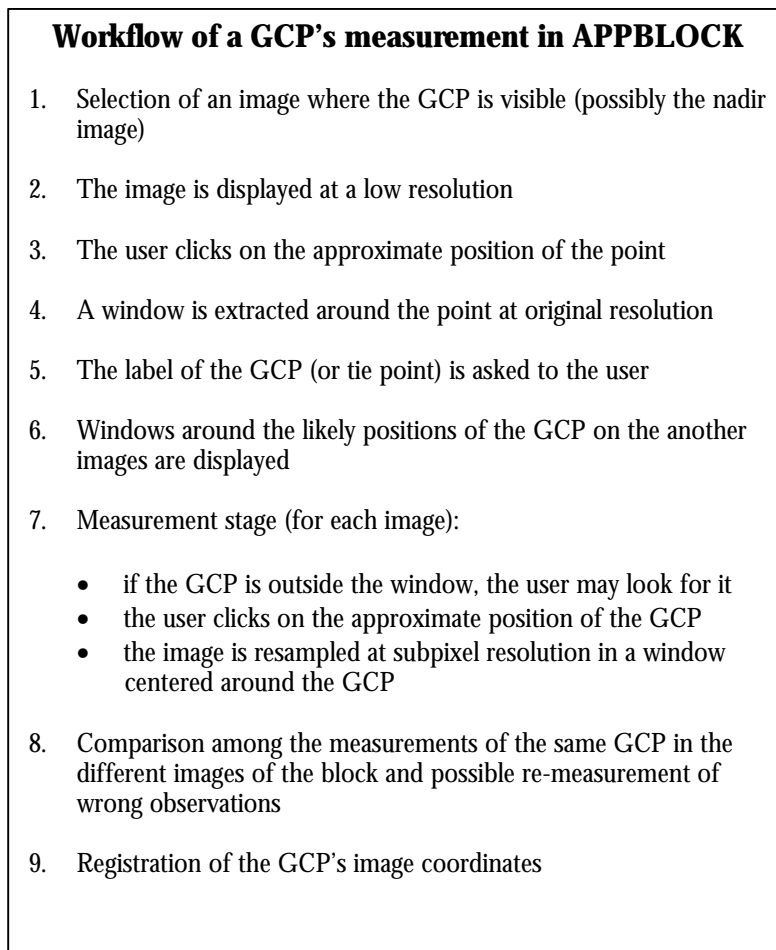


Fig. 2.8 – Workflow of GCPs' measurement by APPBLOCK

2.8 Measurement of ground control points

In 1.4 we have already pointed out that the measurement of GCPs is the most difficult task to automate in digital aerotriangulation, yet it is strictly necessary even with the use of GPS. The program APPBLOCK in TRIADIGIT system performs the interactive measurement of GCPs with subpixel accuracy, thanks to image resampling. This solution is the best suited to natural GCPs, which are widely used in Italy. In Figure 1.2 some examples of this kind of points are depicted, showing how it's difficult to recognize them.

Apart from the measurement in strict sense, the program APPBLOCK assists the user in the following tasks:

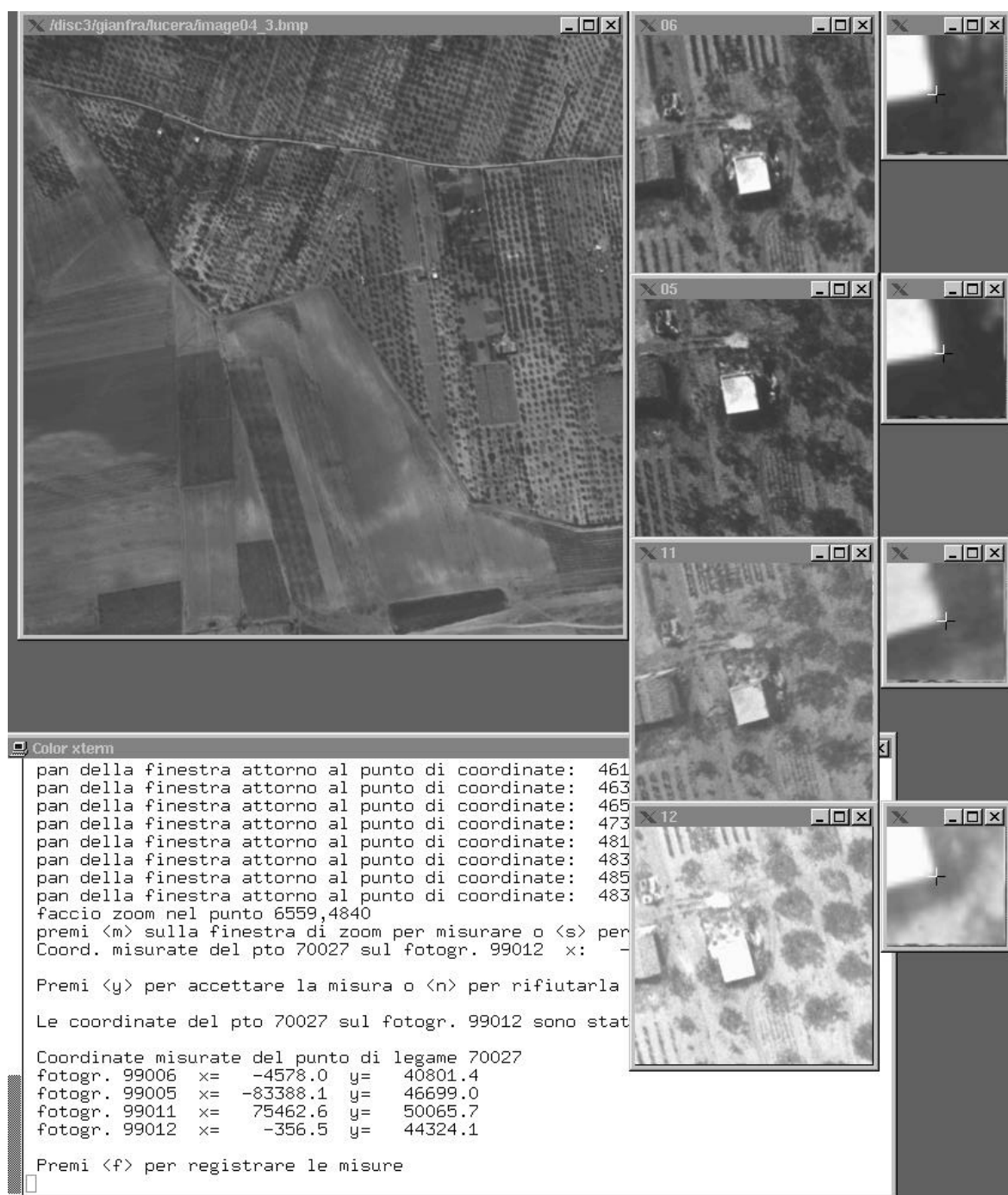


Fig. 2.9 – The measurement of a GCP by APPBLOCK

- Management of photogrammetric observation files.
- Display of windows where the GCPs are likely to be in the different images of the block, based on the available exterior orientation and DEM. As shown in Figure 2.1, initially a minimum number of GCPs may be measured in order to constrain the photogrammetric block during the intermediate bundle adjustments; this task is performed with only a rough

information about the block orientation. After tie point extraction, other GCPs may be added up, this time by using a more accurate exterior orientation.

- In the measurement stage, GCPs are contemporarily displayed in the different images to facilitate their correct collimation.
- Resampling the patch around the GCP allows a subpixel measurement.

This procedure may be applied also to the measurement of tie points in interactive aerotriangulation, or to introduce additional observations in areas of the block where the automatic extraction failed. In this case the localization of approximate positions may be performed by the same strategy adopted in 2.4.1.

In Figure 2.8 is reported the workflow of APPBLOCK, while Figure 2.9 depicts a phase of the measurement of a GCP on the screen.

2.9 Block adjustment

The l.s. bundle block adjustment is performed by the program CALGE [FORLANI 1986], developed at Dept. IIAR.

The high sensitivity of the l.s. to outliers may lead to a completely wrong solution. Moreover, without check points, the accuracy parameters (sigma nought, covariance matrix) given by the l.s. estimate are not enough to verify the results. In this direction, a *reliability analysis* is the only tool which may give an evaluation of the consistency of the tie point data set, but currently is not yet implemented. On the other hand, the tie point extraction software implements also a procedure to carry out the outlier rejection in a robust manner (see 2.6) so that the tie points provided to CALGE contain only a small percentage of outliers (<5÷10%), which do not compromise the correct convergency. Nevertheless, a robust solution for the bundle adjustment would be better.

Furthermore, the approximate values for all the unknowns are mandatory. For exterior orientation parameters the values adopted to start the search for homologous points are good, while for tie points the object coordinates computed during the definition of the search window (see par. 4.2.1) may be enough accurate.

A batch procedure (REJECT) has been written to run automatically the *data snooping* [BAARDA 1968], that is needed to recognize and to discard the outliers which could be in the set of tie points yielded by AAT.

Chapter 3

Interior Orientation

3.1 Outlines of the procedure

Computing the transformation between the pixel coordinate system and the image coordinate system defined by the fiducial marks (FMs) is conventionally referred to as the determination of the *interior orientation* (IO) of a digital aerial image. Usually the transformation adopted is an *affine*, but also other are used (e.g. a *bilinear* [KRAUS 1993]). The knowledge of this transformation is a pre-requisite of any metric evaluation process on the digital image itself.

In TRIADIGIT system this task is performed by a module called ORINT, which operates on every image of the block before running AAT. The procedure adopted by ORINT will be thoroughly discussed in this chapter. Here we would like to point out some important requirements which have been considered in the design and the implementation of this procedure.

First of all, the *flexibility*. A software for computing the IO should work with different camera types at different image resolutions and accommodate new camera models which may become available. Aerial photographs can be laid down on the plate of a photogrammetric scanner in 8 different positions, 4 of these due to rotations and emulsion up or down (see Fig. 3.4). These should be automatically discriminated by the IO software, to assign the correct identification number to each fiducial mark (at least when these are provided by symbols or figures) and to spot image pose errors. Automatic recognition of whether an image is diapositive or negative has not been considered so important, though some softwares do [SCHICKLER AND POTH 1996], this information being unique for the whole block and then always easily known a priori.

The *robustness* in the estimation of the affine (or another) transformation and in measurement of fiducials is a further important requirement, because a mark may appear deteriorated or can be cut out from the digitalized image.

As far as software implementation is concerned, a graphical user-interface and the visualization of the diverse phases of image matching is not to be underrated, especially if the software is used for teaching purposes.

In Figure 3.1 the general scheme of the procedure implemented in ORINT is depicted. The first operation executed is the measurement of the fiducials, whose approximate location is

found by a multi-resolution approach and checked against gross errors by a preliminary transformation from image to pixel system. Then follows the identification of the mark's symbols (if any) to associate the measured pixel location to its counterpart in image system. Finally the computation of the parameters is carried out.

In the sequel every step of the outlined procedure is presented and analyzed. At the end of the chapter some results of experimental tests made to check the behaviour of the software and the robustness against gross errors are presented.

3.2 Measurement of fiducial marks

It is assumed that the photograph has been laid down on the scanner with an average degree of care, that is, that image and pixel coordinate systems are rotated one with respect to the other by integer multiples of $\pi/2$, but for a few degrees of misalignment.

The measurement is carried out in two stages, first by looking for the approximate position of the fiducials, then by improving these coordinates to subpixel accuracy.

The procedure adopted for approximate localization is based on *hierarchical correlation* [HANNAH 1974] starting from an a priori knowledge of very rough positions of the fiducial marks, according to the above mentioned assumption that images have been scanned on regular positions.

Depending on camera type, 4 or 8 windows are extracted from the 0 level of the pyramid at the image corners and/or along the image borders; the window size may be freely selected, based on the dimension of fiducials as well as the accuracy of the image positioning over the photostage. In all experiences up today a 15 mm square on the image has been found large enough, barring images acquired with Zeiss RMKA, where only with a larger window (25×25 mm) our method had no failures. These windows are resampled in order to obtain a coarse image of the area surrounding the fiducial marks. Obviously in this task the problem of aliasing must be kept into account and solved by a low-pass filtering; because the ratio between original and resampled windows may assume a large range of values, the mask is designed case by case using the *window method* [LIM 1990].

Then, the approximate position of each fiducial is found by computing the *normalized cross-correlation* between the resampled window and a synthetic template read from a library. The use of this algorithm during the localization stage is justified by the fact that translations are the only parameters to be really computed: image rotations are very small and however widely under $\pm 20^\circ$, which is considered a limit for applying cross-correlation in a successful way [FÖRSTNER 1984]; the scale factor between patch and template is approximately unitary, while affinity is not present because the image of the fiducial is impressed by contact. For each window the approximate mark position is defined at the pixel having maximum value of the correlation coefficient. Coordinates estimated in this way are integer values and this is considered enough for intermediate steps in the hierarchical localization.

Dimension and resolution of extracted windows depend on the shape of fiducial marks to be looked for. As you can see in Figure 3.2, fiducials in the most widely used aerial cameras (Leica and Zeiss) are made up by a small dot (diameter about $40\div 50\ \mu\text{m}$) surrounded by a cross and a circle to help the operator in the collimation. The image border, black or white according to whether the image is positive or diapositive, is larger than along the edges and

rounded where it encloses the fiducials. Rough localization of the FMs may be approached in two ways:

- By looking for the coarse shape of the symbol (usually a circle, as in Figure 3.3) on a homogeneous background.
- By looking for the border's part around the fiducial against the image background.

The first situation, typical of more recent cameras, can be dealt with in a straightforward way, because you have to look for a well defined symbol on a homogeneous background. Patches are first resampled to a 200 μm resolution, obtaining a search area which is approximately 75 \times 75 pixels. Templates of size 16 \times 16 pixels are used, resulting in a cross-correlation matrix of size 59 \times 59 pixels.

The second case, typical of Zeiss RMKA camera, presents one more difficulty due to the fact that the shape to be found is surrounded by the image content, which may assume all values in the range 0-255. On the contrary, template background has unique average intensity leading poor correlation values. In literature a solution to this problem can be found in [SCHICKLER AND POTH 1996], who make use of *binary cross correlation* and of the so called "*don't care area*". Here a different approach has been adopted, which can be summarised by the following items:

- Use of rectangular instead of square windows; in this way, only a small portion of the effective image area will show up when template and patch actually correspond, so the correlation coefficient is less biased.
- By histogram equalization [PRATT 1991] the contrast between the border and the image is increased.

In this second case patches are resampled at a resolution of 400 μm , twice that used for the first case. The size of the patches is 50 \times 50 and the rectangular shaped templates are 25 \times 9 large, giving a cross-correlation matrix of size 25 \times 41 pixels.

At the first level of the hierarchy the whole set of fiducials is looked for and then, thanks to the symmetry of the image format, a preliminary approximate transformation (an affine if more than two marks were successfully located, a conformal one if only two were detected) from pixel to image system is carried out. To this aim, the pairs of pixel coordinates are arbitrarily assigned (on the basis of their sequence in the image format and of the calibration values) to the image coordinates of the fiducials. The labelling is likely to be incorrect (chances are 8 to 1) and in principle all permissible associations may be computed to find the best agreement; this is not so important at this stage, since the primary objective here is to highlight gross errors (if enough marks have been measured) and to predict the position of those marks where the cross-correlation didn't yield a reliable (larger than a given threshold) outcome. This may be worth where noise sources may have changed significantly the radiometry in a (relatively large) neighbourhood of the mark: the computed position will be used in the lower level of the pyramid, in the hope that noise didn't affect the surroundings of the dot.

The next level of the pyramid is set to 100 μm (or 200 μm for Zeiss RMKA); a new set of templates (see Fig. 3.3) is again employed to find the position yielding the maximum correlation. This time the window size L is much smaller than the previous one and is

obtained by increasing the template size L_T by an amount related to the uncertainty of the estimate for sigma naught of the approximate affine transformation just computed:

$$L = L_T + 6 \sigma_0 \quad (3.1)$$

As before, a new affine transformation is performed and the coordinates of the fiducials are predicted, with an accuracy, based on the tests carried out, in the range 1÷3 pixels, a reasonable starting point for refining the position by l.s. template matching (cfr. 4.1.2). For Zeiss RMKA one more intermediate level at resolution 100 μm is considered.

The precise measurement is carried out by resampling an original template, built up at a 10 μm resolution, to the actual image resolution.

At the end of measurement, the affine transformation is computed to check against gross errors and to predict again the positions of marks possibly not yet identified. On the basis of the coordinates predicted in this way, now the missing or rejected FMs are measured again. Remember that at this stage the association between measured and actual marks is very likely incorrect, therefore a new computation will be executed later.

3.3 Identification of fiducial marks

This section applies only to images with identification symbols: if they are not available (and if for any reason the procedure failed) the program asks the user to provide the correct numbering. If the previous assumption about handling the images during scanning holds, they can be laid down on the scanner very close to eight basic poses, corresponding to values of 0°, 90°, 180° and 270° of the angle between pixel and image system and to emulsion up or down for diapositive or negative images. In Figure 3.4 is shown an image in all the positions it might be scanned. For a given camera model the clockwise sequence of mark numbering is fixed: therefore, once just a symbol is identified, the whole sequence may be recovered. As a tradeoff between reliability and speed, we identify the four symbols at the corners.

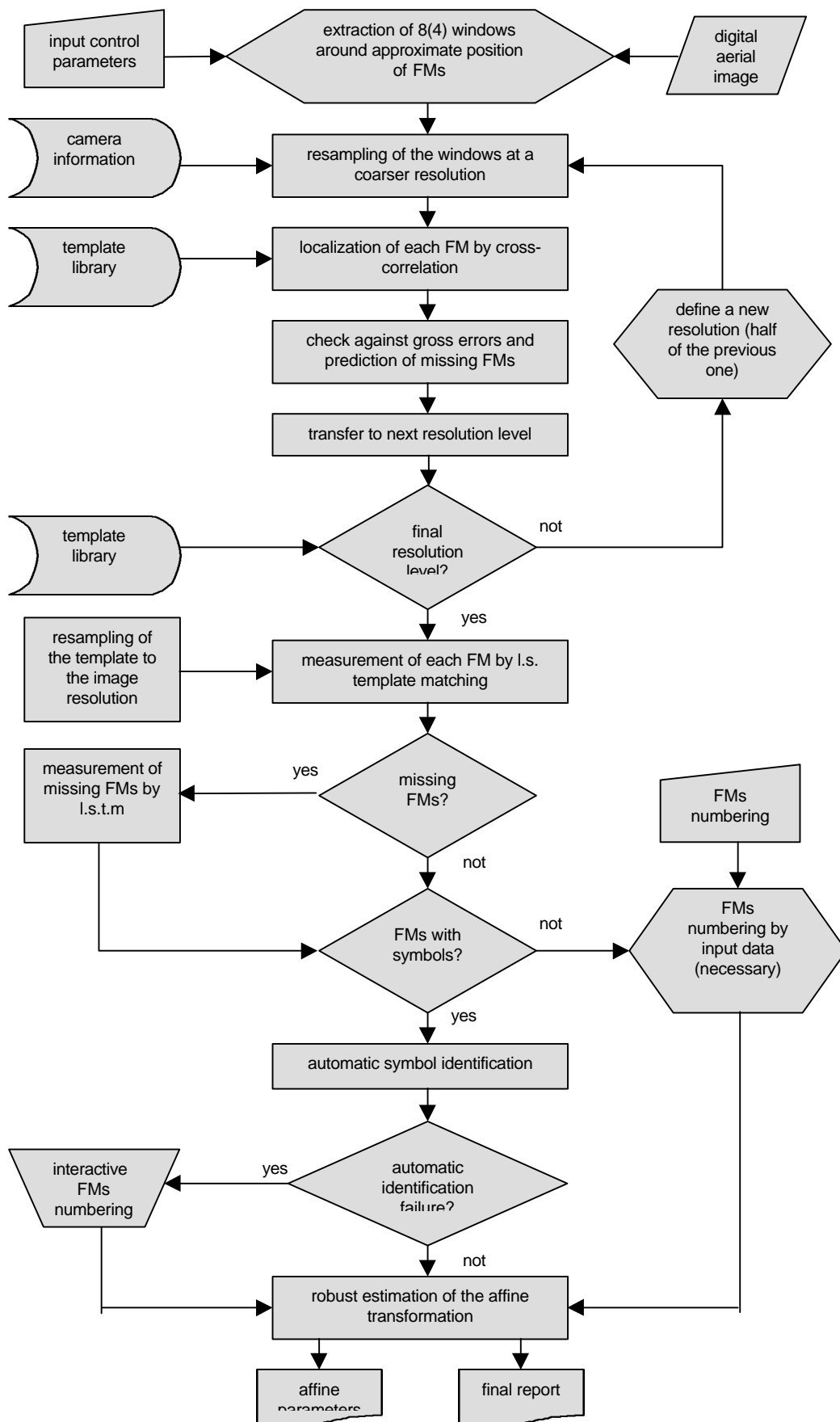


Figure 3.1 – Workflow of the program ORINT

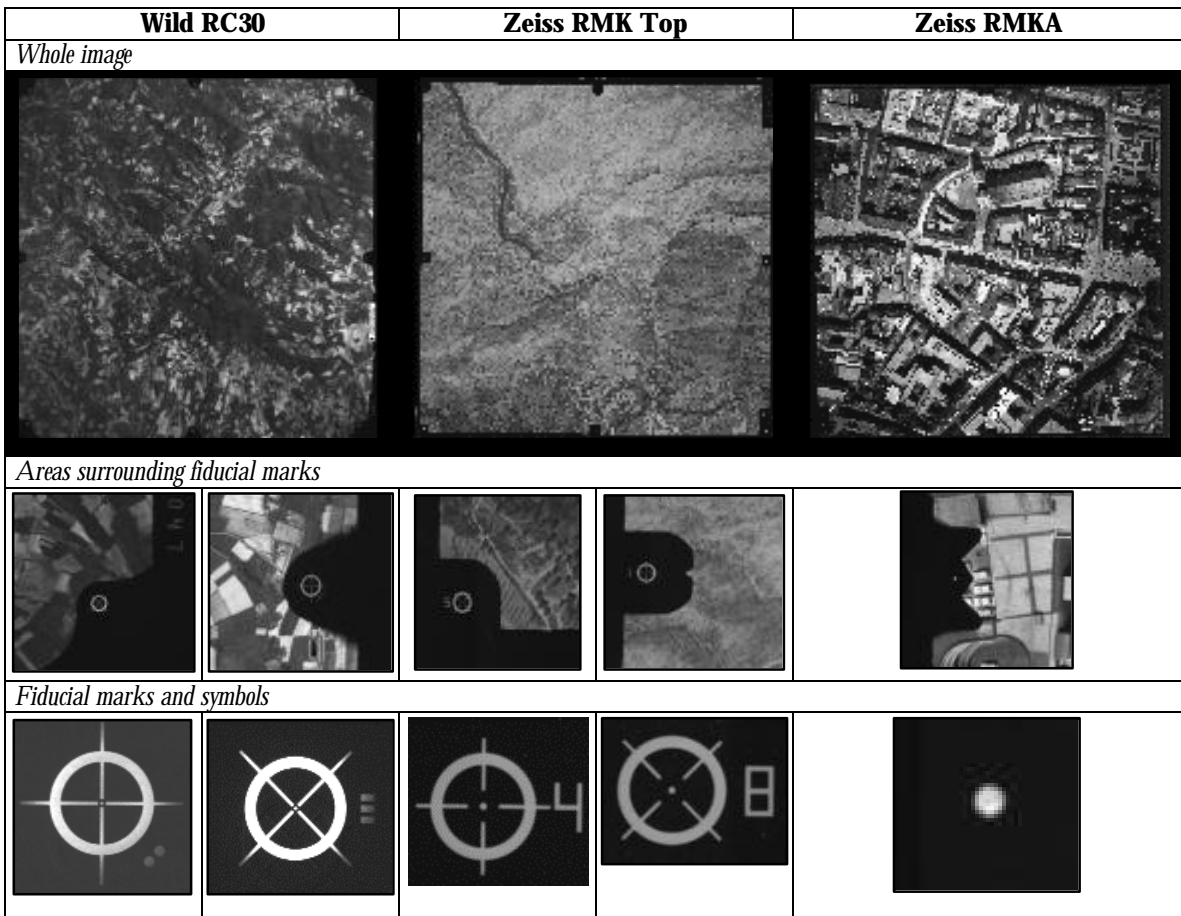


Figure 3.2 – Fiducial marks of the most popular aerial cameras

	Wild RC30	Zeiss RMK Top	Zeiss RMKA
400 μm			
<i>template size</i>			25×9
200 μm			
<i>template size</i>	16×16	16×16	23×17
100 μm			
<i>template size</i>	32×32	32×32	21×21

Figure 3.3 – Template of FMs at different resolutions

Identification of fiducials is performed in three steps:

1. Looking for the position of the symbol with respect to the mark (above, below, right or left).
2. Identification of the mark number, following a different procedure in case of digits or symbols.
3. Checking for mis-identification errors and, if necessary, trying to correct them.

	<i>Angles between pixel and image system</i>											
	0°			90°			180°			270°		
emulsion up	1	2	3	7	8	1	5	6	7	3	4	5
	8		4	6		2	4		8	2		6
	7	6	5	5	4	3	3	2	1	1	8	7
emulsion down	3	2	1	5	4	3	7	6	5	1	8	7
	4		8	6		2	8		4	2		6
	5	6	7	7	8	1	1	2	3	3	4	5

Figure 3.4 - The 8 different positions in which an image may be scanned

3.3.1 Searching for the mark position

Because of the unknown pose on the scanner stage, the symbol may appear in any of the four positions, symmetrically with respect to the fiducial, whose coordinates are now known. Since the size and the relative position of symbol and mark can be measured in the image system, a window enclosing the symbol can easily be extracted in all the four positions, at any given resolution. The most likely to contain the symbol is selected by simply looking at the average value of the g.v. distribution within each window. This approach may be error prone, in case scratches or other disturbances appear in the selected areas, but since the symbol locations must be in agreement, the findings can be cross-checked against mis-identification errors. To perform this a numeric value is given to each of the four positions a symbol may stay in, and the median of all the results is computed. If more than one result differs from this solution, the identification is labelled as unreliable¹. In this case, the automatic procedure for identifying symbols fails and the user is asked to insert interactively the true fiducial mark label.

The procedure now changes according to the characteristics of the symbols used by the camera manufacturer and therefore any new type of symbol may require a tailored approach: up today, we have available images containing digits (as of the Zeiss RMK Top) or bars (as of the Wild RC20 and RC30). In figure 3.5 are depicted the two sets of symbols that can be identified by the procedure described in the following paragraphs.

¹ The median may cope effectively with a maximum of $(N/2)-1$ errors in a data set adding up to N . In this case, one error may be tolerated without affecting the result.

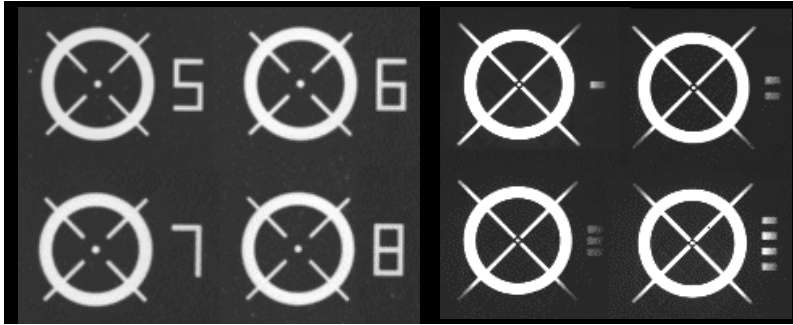


Figure 3.5 – The symbol sets of the camera Zeiss RMKTop (on the left) and of cameras RC20 and RC30 (on the right)

3.3.2 Identification of digits

Digits are identified, after image binarization, by the analysis of the *principal moments of inertia* within the extracted window [PRATT 1991].

To find the threshold value for the binarization, the average value of the ratio R_d of each digit area to the window area has been computed for the digits 5, 6, 7, 8 appearing on the image corners: ideally, the threshold is the g.v. in the distribution function corresponding to that ratio (more exactly, to its complement to unity). Though R_d is different for each digit, the histogram is always clearly bimodal, therefore an average value of R_d is good enough.

After binarization the procedure runs as follows:

1. The centre of gravity G of the binarized image (from here on, the term image refers to each of the extracted window around the figure to be identified), is computed through the ratios of the first-order to the zero-order spatial moments:

$$x_G = \frac{M(1,0)}{M(0,0)} \quad y_G = \frac{M(0,1)}{M(0,0)} \quad (3.2a-b)$$

The centroid evaluated in this way is the gravity center of the image function $F(i,j)$ and the *discrete spatial moments of order (m,n)th* are defined as follows:

$$M(m,n) = \sum_{j=1}^J \sum_{k=1}^K (x_k)^m (y_j)^n F(j,k) \quad (3.3)$$

where the scaled x_k and y_k coordinates are:

$$x_k = k - 0.5 \quad y_j = J + 0.5 - j \quad (3.4a-b)$$

and the origin of the coordinate system is the lower left corner of the image.

2. With the center of gravity established, it is possible to define the unscaled spatial central moments of the image, defined as follows:

$$U(m,n) = \sum_{j=1}^J \sum_{k=1}^K (x_k - x_G)^m (y_j - y_G)^n F(j,k) \quad (3.5)$$

The three second-order unscaled moments are the *row moment of inertia*:

$$U(2,0) = \sum_{j=1}^J \sum_{k=1}^K (x_k - x_G)^2 F(j,k) \quad (3.6)$$

the *column moment of inertia*:

$$U(0,2) = \sum_{j=1}^J \sum_{k=1}^K (y_j - y_G)^2 F(j,k) \quad (3.7)$$

and the *row-column cross moment of inertia*:

$$U(1,1) = \sum_{j=1}^J \sum_{k=1}^K (x_k - x_G) (y_j - y_G) F(j,k) \quad (3.8)$$

The three second-order moments define the *moment of inertia covariance matrix* for the thresholded image:

$$U = \begin{vmatrix} U(2,0) & U(1,1) \\ U(1,1) & U(0,2) \end{vmatrix} \quad (3.9)$$

- Let λ_M and λ_N be respectively the largest and the smallest eigenvalues of \mathbf{U} ; it can be shown that the orientation angle θ , i.e. the angle the semimajor axis is tilted with respect to the horizontal axis (see Fig. 3.6), can be computed as:

$$\theta = \tan^{-1} \left\{ \frac{\lambda_M - U(0,2)}{U(1,1)} \right\} \quad (3.10)$$

The eigenvalues and the orientation angle define an ellipse whose major axis is λ_M and whose minor axis is λ_N . This elliptically-shaped object has the same moments of inertia along the horizontal and vertical axes and the same moments of inertia along the principal axes as does an actual object in an image. The ratio of the minor-to-major axes is a useful shape feature:

$$R_A = \frac{\lambda_N}{\lambda_M} \quad (3.11)$$

The pair of parameters just defined are used to recognize the figure in the extracted window, by the comparison between their computed values to a set of reference values evaluated a priori. Both parameters are independent of shifts and scale (R_A also of rotation); the angle θ must in principle be corrected taking into account the pose of the photograph on the scanner (multiple of $\pi/2$), which has been already evaluated in 3.3.1. According to these considerations, the parameters used for figure identification are the ratio R_A and the corrected angle θ' :

$$\theta' = \theta + n \frac{\pi}{2} \quad n \in \{1,2,3,4\} \quad (3.12)$$

The computed values are checked against the reference values of “ideal” digits R_{0i} and θ_{0i} ; let R and θ' be the computed values, the digit k is identified if:

$$|R - R_{0k}| = \min_i \{ |R - R_{0i}| \} \quad \text{and} \quad |\theta - \theta_{0k}| = \min_i \{ |\theta - \theta_{0i}| \} \quad i=1 \div 4 \quad (3.13)$$

After completing the identification of the 4 digits, the consistency of the symbols sequence is checked.

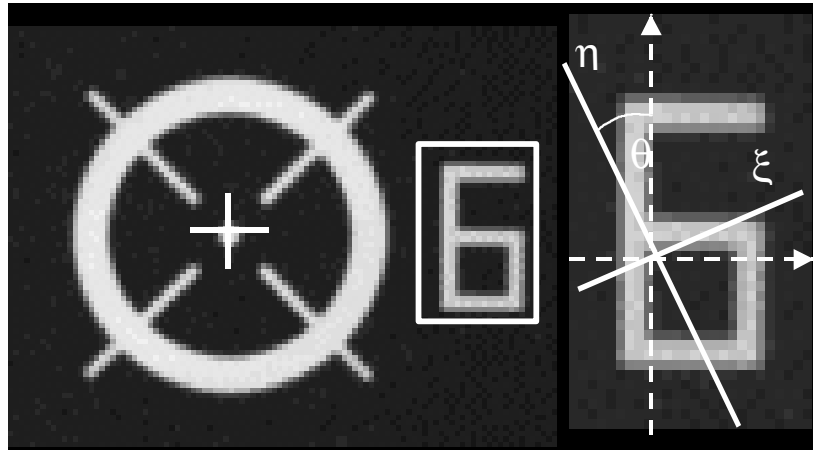


Fig. 3.6 – Identification of digits

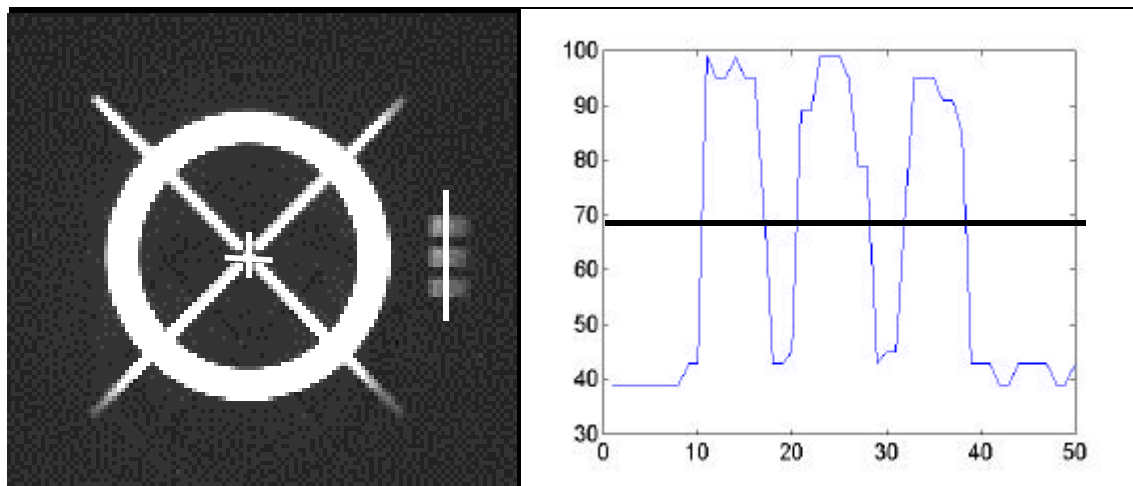


Fig. 3.7 - Identification of symbols

3.3.3 Identification of symbols

As stated earlier, the program currently handles the Wild RC30 and RC20 symbols, simply by counting the number of bars [SCHICKLER ADN POTH 1996]. To this aim, a g.v. profile is extracted along the main side of the search window and its intersections with a threshold are computed (see Fig. 3.7). By counting the number of intersection points the number of bars can be easily derived. The value for the horizontal threshold is evaluated as the mean between maximum and minimum g.v.s in the extracted window.

3.3.4 Consistency check for the symbol set

After the numbers at the image corners have been identified, their mutual consistency is checked to evaluate the correctness of the solution.

The fiducials may appear in 8 different configurations arising from the pose of the photograph on the scanner plate (4 rotations and 2 sides are possible, as depicted in figure 3.4). At the current step of the procedure four degrees of freedom have already been fixed when the symbol position has been established. The two remaining may be discriminated by assigning the correct label to one fiducial: the results coming from others marks are redundant and can be used to check the correctness of the solution.

The solution found is compared to the 8 possible ones. The following scores are assigned in the evaluation:

- for each correct identification: 1
- for each mark not identified: 0
- for each wrong identification: -1

According to the total score, the identification is classified into one out of the following three classes:

1. Correct identification: all the fiducials have been well labelled (score 4).
2. Identification with errors which can be corrected (score 2 or 3) because the identified fiducials lead to a unique solution; then even wrong or missing marks can be labelled.
3. Uncorrect identification (score less than 2).

If the result is in the first or in the second class, the consistency test is passed and the final solution for the affine transformation is computed (see next paragraph). In the third case automatic labelling cannot be performed and the user is asked to do it interactively.

3.4 Transformation from pixel to image

After measurement and identification of the FMs, an affine transformation from pixel to image system is computed by least squares; given the expected accuracy (we assume usually 1/3 of pixel size) if the test on sigma naught fails, a *L1-norm* solution [BARRODALE AND ROBERTS 1973] is computed and the observation with the largest residual is proposed to be discarded. At this point three tests are performed in order to verify whether this mark is to be really discarded:

1. *Test of the area* A_{int} of the polygon enclosed by the FMs considered as inliers, which must be larger than a minimum value A_{min} depending on the camera type, chosen to avoid a weak geometric configuration for the remaining marks.
2. *Test of the ratio*: values of sigma naught of the affine transformations before and after discarding the mark with the largest residual are computed. The test is passed if their ratio is larger than 2, that is, if the rejection of the mark results in a large improvement of the solution.
3. *Test only for cameras with 4 fiducials*: a mark is discarded only if $\hat{\sigma}_0 > 3\sigma_0$. This condition is expected to allow the elimination of the fourth mark only in case it effectively worsens the solution.

In case at least one of these tests is not passed, the discarded mark is recovered and the final solution is computed. On the contrary, a new solution for the affine transformation is estimated and the sequence is repeated, until all the tests are satisfied, if enough redundancy is provided.

As already mentioned in 3.2, the estimation of the affine transformation is carried out also during the localization of fiducials when moving from a resolution level to another, to spot outliers and to predict the position of FMs which have not been localized. The a priori sigma naught of l.s. estimation equals the pixel size at the current resolution.

3.5 Implementation of the program ORINT

The program ORINT has been designed for the automatic measurement and identification of the fiducials, including the computation of the transformation parameters. It may run interactively or completely automatically, depending on camera characteristics: if the fiducials are provided with identification symbols, ORINT performs all the required steps; otherwise some interaction is necessary, to associate the measured fiducials with their identification numbers.

The program input parameters for each image to be processed are the following ones:

- camera type

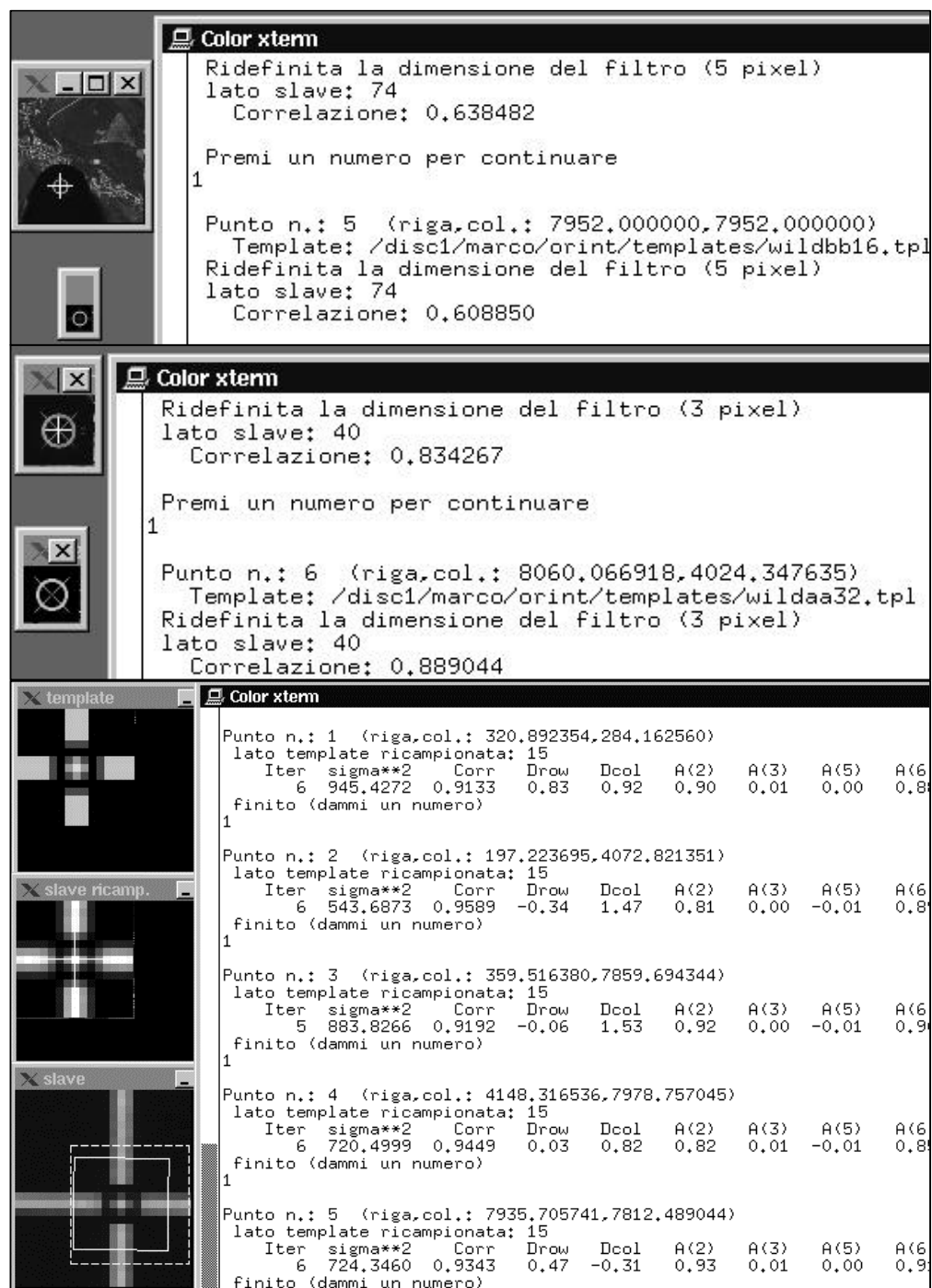


Fig. 3.8 - Execution of program ORINT in graphic mode; from top to bottom: approximate localization of a FM at resolution of 200 μm, at 100 μm and precise measurement at the original resolution

- fiducial coordinates from the calibration certificate
- identification number of each FM (only in case of camera without symbols)
- image type (diapositive, negative)

- pixel size

Thanks to a modular structure, new cameras and camera types may be easily introduced: camera data are read by configuration files, where the geometric characteristics of fiducials have been recorded; templates specific to each kind of fiducial have been generated at different resolution, based on measurement at an analytical plotter of their shape parameters. Currently all camera types reported in Table 3.9 can be dealt with.

The program output consists of a file containing the 6 parameters of the affine transformation, to input later to other modules of TRIADIGIT system. Furthermore, a report giving detailed information on program execution is provided.

ORINT has been written in C and FORTRAN77 and runs in X-Windows graphic environment; the current release has been implemented on a Linux platform.

ORINT can run both in batch and in graphic mode. This second option allows to visually inspect the different steps of FMs' measurement, so that problems concerning specific images can be easily understood. The helpfulness of this option will be better appreciated after illustration of the experimental tests of the software, which are discussed in the next paragraph. In figure 3.8 some steps of the execution of program ORINT in graphic mode are depicted.

3.6 Program tests

Program testing has been executed on the images of several small blocks with different cameras with the photographic material available at Dept. IIAR (images of OEEPE-ISPRS tests² and of other blocks flown in Italy). Up today the program has been tested with about a hundred images taken with 6 diverse cameras.

The quality of the used images was generally good, without noise or disturbances close to the marks. Both the measurement and the identification procedure run without user interaction. Table 3.9 summarizes the results for some of the blocks with computing time referring to a P200 PC.

The sigma naught of the affine transformations is the unique parameter that may be analyzed in order to assess the quality of FMs' measurement. Unfortunately, the precision of l.s. matching is not the only factor which affects this parameter, because the affine transformation is computed to compensate for film deformations as well. Experimental tests have resulted in a mean estimated value of σ_0 of about 0.4 the pixel size. The maximum value of σ_0 never exceeded the pixel size. Converting in micrometers give a mean value of σ_0 of about 10 μm , which is practically the result obtainable at the analytical plotter. Besides, images used in these tests come from blocks flown some years ago and then deformations might have appeared, as the IO performed at the analytical plotter has shown for some images.

For all images provided with symbols, the identification has been correctly performed.

In order to test the program behaviour against poor image quality, disturbances were artificially introduced in some images, both for measurement and symbol identification.

² Here we refer to blocks delivered to participants at OEEPE Test on "Digital Aerial Triangulation" [JAAKOLA AND SARJAKOSKI 1996] and OEEPE-ISPRS Test on "Performance of tie point extraction in AAT" [HEIPKE AND EDER 1998].

Results are shown in Table 3.10 for the camera Wild RC30 and in Table 3.11 for Zeiss RMK Top.

The first kind of errors which have been introduced are small disturbances near the dot (cases A and B in Table 3.11). These errors result in a reduction of the measurement precision, as the values of sigma naught show. Even larger disturbances on the whole fiducial do not cause a failure of measurement process (case A in Table 3.10 and cases C and D in Table 3.11). Though the cross correlation algorithm is very robust respect to marks somehow “occluded”, if a corrupted mark is not located on the first level, the remaining measured fiducials allow to predict its approximate position so that it may be then recovered.

Case B in Table 3.10 and cases C, E and G in Table 3.11 refer to errors which prevent mark identification. The findings of this group of tests can be summarized by concluding that if the identification failed for only one symbol, then the procedure described in 3.3.4 allows to recover it. If more than one mark is corrupted by errors, then the automatic procedure halts and the user is asked to input the correct number of the two fiducials at the image top. To make easier this task, images of these marks are shown on the screen, so that the user may interactively identify the symbol. When the identification has been solved for, eventually the measurement ended without problems concerning FMs' measurement.

The last test has been carried out by rotating an image of 5° , to mimic that may happen when the photograph has not correctly laid down on the scanner plate (Table 3.11). Also this test gave a positive outcome, because the only two marks located at the initial level allow to predict the positions of the others and then to complete the measurement.




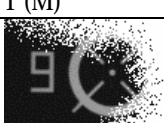
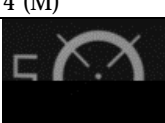




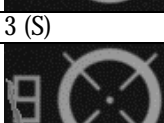

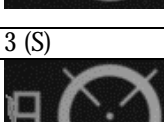

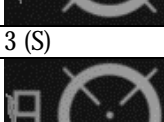
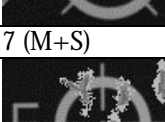

				<i>a priori</i>	<i>estimated</i>	2	1	0		
A				0.20	0.42	0	0	0	0	automatic
	1 (M)									
B				0.20	0.45	0	0	0	0	automatic
	1 (M)	4 (M)								
C				0.20	0.34	2	1	0	1	automatic
	3 (M)	7 (M+S)								
D				0.20	0.31	0	0	0	0	automatic
	3 (M)	4 (M)	5 (M)							
E				0.20	0.29	0	0	0	1	automatic
	3 (S)									
F				0.20	0.32	0	0	1	1	automatic
	3 (S)	8 (M)								
G				0.20	0.29	0	0	0	2	interactive
	3 (S)	7 (M+S)								
J				0.20	0.32	0	0	0	2	interactive
	3 (S)	4 (M)	7 (M+S)							
image tilted of 5°				0.20	0.31	6	0	0	0	automatic
reference image (not corrupted)				0.20	0.29	0	0	0	0	automatic

Table 3.11 - Results of tests on an image with artificially corrupted fiducials (Zeiss RMK Top)

Chapter 4

Some aspects of tie-point extraction

4.1 Matching algorithms

In this paragraph we will not discuss different matching algorithms, but rather describe the topic aspects of those algorithms which have been implemented in the TRIADIGIT AAT system. An exhaustive overview of existing methods may be found in literature [BALTSAVIAS 1991; LANG AND FÖRSTNER 1998].

Matching techniques that will be presented in the sequel are *normalized cross correlation* and *least squares matching*, belonging to the class of the so called *area-based matching* algorithms. Starting from two descriptions of the images, the basic idea is to shift and possibly to warp one of the images – the *slave* – such that its intensities best fit the intensities of the other image – the *template* (see Fig. 4.1). The best fit can be achieved using either a similarity or a distance measure.

Before describing the algorithms, let us have a quick look to the model used in the sequel to describe the transformation between template and slave. Considering single channel or gray value (g.v.) images, we may write the following image model:

$$g_1(r_i, c_i) = f(r_i, c_i) + n_1(r_i, c_i) \quad (4.1)$$

$$g_2(p_i, q_i) = h(f(r_i, c_i, p_C); p_i) + n_2(p_i, q_i) \quad (4.2)$$

The model contains the following components:

$f(r_i, c_i)$	the ideal image
$g_1(r_i, c_i)$	the first image (slave)
$n_1(r_i, c_i)$	the noise of the slave
$g_2(p_i, q_i)$	the second image (template)
$n_2(p_i, q_i)$	the noise of the template
$T_G = f : \mathfrak{R}^2 \rightarrow \mathfrak{R}^2$	a geometric transformation from the (r,c)-coordinate system of g_1 to the (p,q) coordinate system of g_2

- p_G the parameters of T_G
- $T_I = h : \mathfrak{R} \rightarrow \mathfrak{R}$ an intensity transformation
- p_I the parameters of T_I

Figure 4.2 shows the generation process of images g_1 and g_2 . The original image f is observed leading to a noise version g_1 ; f is now warped, pointwise transformed and observed independently leading to g_2 . The general image matching problem such as in tie points extraction is to find an estimate for p_G and p_I . In the case of localization and measurement of fiducial marks, the second image g_2 is substituted for an artificial model representing the ideal image f ($n_2=0$).

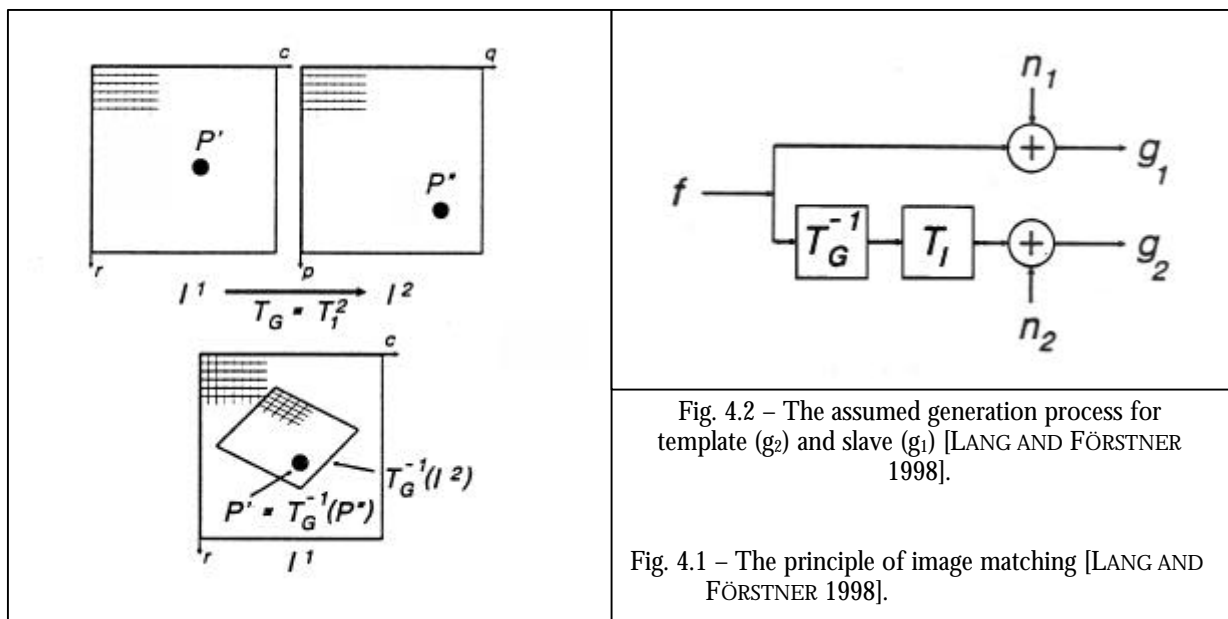


Fig. 4.2 – The assumed generation process for template (g_2) and slave (g_1) [LANG AND FÖRSTNER 1998].

Fig. 4.1 – The principle of image matching [LANG AND FÖRSTNER 1998].

4.1.1 Normalized Cross Correlation

Cross correlation is a powerful method to find the correspondence between digital images [JÄHNE 1989; HARALICK AND SHAPIRO 1993]. Its applications are manifold: point transfer in AAT, registration of satellite images, fiducial mark or signalized GCP location, generation of DEMs, character recognition, object tracking in image sequences [HAHN 1994].

It assumes that the two images differ only by a shift in geometry and only by brightness and contrast in radiometry. Thus the geometric transformation:

$$T_G : \begin{pmatrix} p \\ q \end{pmatrix}_i = \begin{pmatrix} r \\ c \end{pmatrix}_i - \begin{pmatrix} u \\ v \end{pmatrix} \tag{4.3}$$

only contains two unknown shift parameters $p_G = (u,v)^T$. The radiometric transformation:

$$T_I : h(f) = a + bf \tag{4.4}$$

is linear with the parameters $p_1 = (a,b)^T$.

In cross correlation a moving template is shifted row-wise and column-wise within the (larger) search window and the cross correlation coefficient is computed for each position of the template. The center of the window with associated the maximum correlation value is assumed as the resulting point. The dimension of the slave may be selected as large as you need, so that no good approximate coordinates of the point to find are strictly required. However by limiting the search window you can reduce the risk of mismatches. Disadvantages of cross correlation consist mainly on a sharp decrease of precision when the geometric model is violated. Rotations greater than 20° and scale differences greater than 30% should be avoided [FÖRSTNER 1984].

Considering the scheme shown in Figure 4.3, the estimate may be obtained by maximizing the correlation coefficient ρ into the slave:

$$(\hat{u}, \hat{v}) = \max_{u,v} \rho_{12}(u, v) \quad (4.5)$$

with

$$\rho_{12}(u, v) = \frac{\sigma_{g_1 g_2}(u, v)}{\sigma_{g_1}(u, v) \sigma_{g_2}} \quad (4.6)$$

$$\sigma_{g_1 g_2}(u, v) = \frac{1}{m} \sum_{i=1}^m g_1(r_i - u, c_i - v) g_2(p_i, q_i) - \frac{1}{m} \sum_{i=1}^m g_1(r_i - u, c_i - v) \frac{1}{m} \sum_{i=1}^m g_2(p_i, q_i) \quad (4.7)$$

$$\sigma_{g_1}^2(u, v) = \frac{1}{m} \sum_{i=1}^m g_1^2(r_i - u, c_i - v) - \left[\frac{1}{m} \sum_{i=1}^m g_1(r_i - u, c_i - v) \right]^2 \quad (4.8)$$

$$\sigma_{g_2}^2(u, v) = \frac{1}{m} \sum_{i=1}^m g_2^2(p_i, q_i) - \left[\frac{1}{m} \sum_{i=1}^m g_2(p_i, q_i) \right]^2 \quad (4.9)$$

In these expressions the index 1 refers to the slave, which varies for each position, as the index 2 indicates the parameters computed for the template, which on the contrary is unique; m refers to the number of pixels of the template. The estimate is independent on differences in brightness and contrast due to normalization with respect to mean and standard deviation.

Obviously, this method cannot give a subpixel precision directly from eq. (4.5). This is sufficient for the intermediate steps in the hierarchy, because any position found is used as starting point for the search in the next finer level. At the final level of the image pyramid, cross correlation leaves the place to more accurate *least squares matching*, which will be focused in the next paragraph. When necessary, a subpixel estimate can be however obtained from cross correlation by approximating the two dimensional correlation function $\rho_{12}(u,v)$ in the vicinity of the estimate obtained from eq. (4.5), by using a second order polynomial and determining its local maximum analytically [KRAUS 1997; LANG AND FÖRSTNER 1998].

To speed up the computation of the cross correlation between two windows, several tricks may be used. The mean and the variance of the template are constant and thus they can be evaluated only one time at the beginning. The corresponding values in the search image vary from one position to the next. Nevertheless, many of the terms of the summation remain constant between two neighbouring positions (see Fig. 4.4). Only the summations $\sum g_1$ e $\sum g_1^2$ of the new rows or

columns must be added each time and the no longer covered rows or columns in the reference image subtracted. Thus, instead of $I \cdot J$ operations (I = number of rows, J = number of columns), only $2 \cdot I$ or $2 \cdot J$ operations are necessary [KRAUS 1997]. The sum of the products $\sum g_1 g_2$ must be fully recomputed for every new position of the new reference image, however. This saves about a half of the time spent in applying the first formulation of the algorithm.

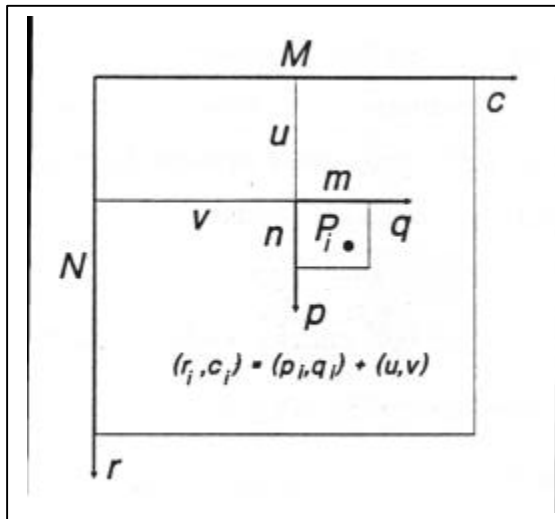


Fig. 4.3 – The principle of cross correlation [LANG AND FÖRSTNER 1998].

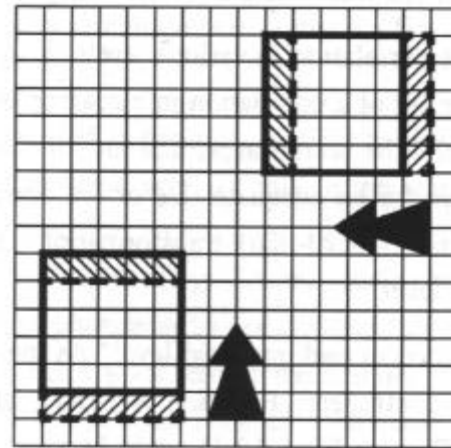


Fig. 4.4 – Efficient computation of the correlation coefficients from one position to the next. Hatched areas: rows or columns whose densities must be added or subtracted from the sums when the reference image is moved [KRAUS 1997].

4.1.2 Least Squares Matching

Least squares matching [FÖRSTNER 1982; ACKERMANN 1984; GRÜN 1985] is a generalization of cross correlation, including any parametric type of mapping function and not only shifts, as well as any parametric type of radiometric relation between the two images. It takes all the advantages of l.s. estimation, such as the efficiency of the estimation process, the evaluation tools and the optimized computational methods.

Here we present the implementation of least squares matching (LSM) algorithm in TRIADIGIT system, where it is used for different tasks. In the module ORINT it is applied to precise measurement of fiducial marks; in tie-points transfer it is adopted as criterium to discriminate homologous points and to measure them.

First of all the choice of the geometric and radiometric model to be implemented in LSM is fundamental, according to the goal the algorithm is applied. The geometric model assumed for resampling within the search window is an *affine transformation*, where any of the parameter may be constrained, adjusting the model to a simpler one (shift only, conformal transformation, etc.) based on the image content. The first three iterations are performed by using only shifts, in order to get a rough localization of the shape to match and to avoid an over-parametrization, which may converge to a false position. From a large number of experimental tests we observed that a LSM algorithm implementing an affine might easily resample the template to fit also a quite

different slave. This leads to mismatches, more likely to happen when the initial matching position is far from the true point. The use during the initial iterations of a simpler model permits to robustify the procedure, because the computation is halted if a sufficient value for the correlation coefficient (let say 0.5) is not reached. When the affine model turns over the shift model automatic testing of parameters' significance is performed in the iteration process to update the model. To stop the iterations, the relative change of sigma nought, of the correlation coefficient and of the shifts are used; furthermore, an upper bound for the number of iterations is adopted.

To improve the fitting between template and search window, a radiometric transformation is introduced, which should partly compensate for differences in illumination, reflectivity and the like. The parameters of the transformation are not included in the l.s. adjustment, but are computed prior to the matching: we use the *Wallis filter* [WALLIS 1976], forcing the equalization of the mean and the variance of the g.v. between the two windows [FORLANI *et al.* 1996]. Excluding the radiometric model from the LSM avoids the possibility of over-parametrizing the model.

In the next sub-paragraphs (4.1.2.1-2) a LSM algorithm implementing a controlled affine transformation is described, while in 4.1.2.3 the tests for the determinability of the shape parameters are presented.

4.1.2.1 2D-Least Squares Matching with affine model

We want now to explicitly give the linearized observation equations for the case of affine transformation as geometric model, neglecting the radiometric model.

The geometric model (T_G) expressing the relation between slave and template is as follows:

$$T_G : \begin{pmatrix} p \\ q \end{pmatrix}_i = \begin{pmatrix} a_1 & a_2 \\ a_4 & a_5 \end{pmatrix} \begin{pmatrix} r \\ c \end{pmatrix}_i + \begin{pmatrix} a_3 \\ a_6 \end{pmatrix} \quad (4.10)$$

The geometric interpretation of the affine parameters is important for the analysis of their determinability. The coefficients a_3 and a_6 represent respectively shifts in row and column direction. Scales are given by a_1 and a_5 , while the two shears by a_2 and a_4 .

Assuming that no a priori information on the geometric transformation is given (e.g. approximation of the parameters of the affine), initial values may be assumed as:

$$\begin{aligned} a_{0k} &= 1 & k &= 1; 5 \\ a_{0k} &= 0 & k &= 2; 3; 4; 6 \end{aligned} \quad (4.11)$$

Considering a square template of n^2 pixels, we can write $m=n^2$ observation equations such the following:

$$\Delta g_i = f_{p_i} \cdot r_i \hat{d}_1 + f_{p_i} \cdot c_i \hat{d}_2 + f_{p_i} \cdot \hat{d}_3 + f_{q_i} \cdot r_i \hat{d}_4 + f_{q_i} \cdot c_i \hat{d}_5 + f_{q_i} \cdot \hat{d}_6 + \bar{n}_i \quad (4.12)$$

where $\hat{d}_k = \hat{a}_k - a_{0k}$ are the corrections to the affine parameters, $\Delta g_i = g_2(r_i, c_i) - g_1(p_{0i}, q_{0i})$ is the known term and $\bar{n}_i = n_2(r_i, c_i) - n_1(p_{0i}, q_{0i})$ is the difference between the noise of the template and the slave. The row and column derivatives f_{p_i} and f_{q_i} are computed with equal contribution of template and slave in order to reduce the noise and to make easier the convergence [BALTSAVIAS 1991]. The initial transferred coordinates (p_{0i}, q_{0i}) are given by:

$$\begin{pmatrix} p \\ q \end{pmatrix}_{0i} = \begin{pmatrix} a_{01} & a_{02} \\ a_{04} & a_{05} \end{pmatrix} \begin{pmatrix} r \\ c \end{pmatrix}_i + \begin{pmatrix} a_{03} \\ a_{06} \end{pmatrix} \quad (4.13)$$

According to these equations, coordinates (p_{0i}, q_{0i}) are not integer values which therefore requires resampling when calculating the derivatives, e.g. by means of bilinear interpolation.

The observations equations (4.12) lead to a 6×6 normal system:

$$\mathbf{N}\hat{\boldsymbol{\beta}} = \mathbf{h} \quad (4.14)$$

whose solution $\hat{\boldsymbol{\beta}} = (d\hat{a}_k)$ yields the 6 corrections to the approximate values of the affine transformation at iteration v , which at their turn may be used as new approximate values in the further iteration $v+1$. The normal matrix \mathbf{N} contains the average $\overline{\Gamma\mathbf{f}}$ of the squared gradient $\Gamma\mathbf{f} = \nabla\mathbf{f}\nabla\mathbf{f}^T$, with $\nabla\mathbf{f} = [\partial f/\partial p \quad \partial f/\partial q]^T$. The estimated noise variance:

$$\sigma_{\bar{n}}^2 = \frac{1}{m-6} \sum_i \bar{n}_i^2 \quad (4.15)$$

measures the average noise difference between the two windows. In case the variances of g.v.s are similar and radiometric difference is due to shift only, the estimate of the image noise variance can be assumed as:

$$\hat{\sigma}_n = \hat{\sigma}_{\bar{n}} / \sqrt{2} \quad (4.16)$$

The covariance matrix of the unknowns then can be derived from:

$$\mathbf{C}_{\hat{a}\hat{a}} = \hat{\sigma}_n^2 \mathbf{N}^{-1} \quad (4.17)$$

The estimated accuracy of the transferred point (p_0, q_0) may be derived from the diagonal elements of the covariance matrix (4.17) corresponding to the shifts $(a_3$ and $a_6)$. This accuracy depends on the number of pixels used (i.e. the window size), the noise variance and the average squared gradient which set up the normal matrix. The local texture of the image to be matched decides the well-determinability of the geometric transformation parameters. In case the window contains an irregular texture, a corner or a distinct point, $\overline{\Gamma\mathbf{f}}$ will be large with the diagonal elements being small and approximately equal. All the affine parameters are determinable with accuracy. In case the window contains an edge or oriented texture, the elements of $\overline{\Gamma\mathbf{f}}$ will be large, but $\overline{\Gamma\mathbf{f}}$ will be nearly singular. This indicates that the estimation of the parameters controlling the affine in the direction of the edge or the texture is uncertain. On the contrary, estimates of the parameters across the edge may be very precise. Finally, if the window contains no or only weak information, $\overline{\Gamma\mathbf{f}}$ will be small, leading to a widely uncertain estimation of the shape parameters.

This discussion makes it clear that precise point measurement by LSM is possible only if the matching window contains well defined texture, motivating the use of *interest operators* designed to this aim [LUHMANN AND ALTROGGE 1986; BALTSAVIAS 1991; FUCHS AND HEUEL 1998]. When only some parameters may be precisely determined, weak parameters might be constrained, reducing the transformation to a simpler one. Selecting the parameters to fix may be done interactively, but in automatic procedure this operation has to be controlled by suitable tests. The two next paragraphs will just deal with this two aspects.

4.1.2.2 Constraining the shaping parameters

A priori knowledge about the transformation may be introduced in a Bayesian manner by using additional observations (possibly fictitious ones):

$$da_k = d\hat{a}_k + n_{ak} \quad w_{ak} = \frac{\sigma_n^2}{\sigma_{a_k}^2} \quad k = 1, \dots, 6 \quad (4.18)$$

with individual weights depending on the standard deviations of the corrections to the a priori values da_k . This leads to the modified and stabilized normal equation system:

$$[\mathbf{N} + \text{diag}(w_{a_k})] \cdot \hat{\beta} = \mathbf{h} \quad (4.19)$$

The right hand side \mathbf{h} remains unchanged, because of the corrections assumed to be $da_k=0$. According to the ranges proposed by LANG AND FÖRSTNER (1998), for scales and shears standard deviations $\sigma_{a_k}=0.2$ ($k=1,2,4,5$), whereas for shifts $\sigma_{a_k}=4$ ($k=3,6$) have been assumed. The noise standard deviation σ_n should be estimated; however, the result is not too sensitive to errors (up to a factor 2) in this assumed standard deviation. We adopted an a priori value $\sigma_n=1$ [g.v].

4.1.2.3 Testing the determinability of the shaping parameters

The decision of constraining one or more shaping parameters can be rarely left only to the human interaction: LSM is mostly applied in automatic procedures, and the bad determinability is often not easily understandable by simply looking at the image. Many statistical methods have been applied to this aim. BALTSAVIAS (1991) gives a complete overview on these techniques, which may be collected into the following categories:

- Significance and determinability tests using data snooping.
- A priori test of the shaping parameters using the shift error ellipse.
- Test of the correlations of the shaping parameters.
- Test of the alterations the of the shaping parameters.
- Test of the eigenvalues of the inverse of the normal matrix.
- Test of the trace of the inverse of the normal matrix.

In theory the application of these tests should give sufficient information about whether or not constraining a shape parameter. In practice most of them test should be calibrated for a limited range of image textures, due to the sensitivity of thresholds used to discriminate whether the initial hypothesis is satisfied or not. In AAT the content of the matching windows may widely vary, so that a test on the determinability of the shape parameters should be as general as possible.

On the basis of these considerations, we adopted the following procedure to detect the parameters to be constrained. Two tests are applied just after the normal matrix of LSM has been built. On the basis of tests' results, one or more shaping parameters might be constrained by summing the contribution of the corresponding pseudo-observation equation to the normal matrix. Then the l.s. problem is solved for and, if necessary, further iterations are carried out.

The first test gives information about the determinability of the shifts. Scales and shears will be then more accurately analyzed by the second test. The analysis of shifts can be done by evaluating the shape of their error ellipse. BALTSAVIS (1991) suggests a test based on a set of thresholds for the error ellipse's parameters and for the standard deviations of the shifts. The same author reports about another similar, computationally less intensive but coarser approach which makes use of only the relative size and ratio of standard deviations. Furthermore, these are approximated fairly well by the following simpler quantities:

$$\text{ratio} = \sqrt{\frac{\max(n_{rr}, n_{cc})}{\min(n_{rr}, n_{cc})}} \quad (4.20)$$

$$G_r = \sqrt{\frac{n_{rr}}{m}} \quad G_c = \sqrt{\frac{n_{cc}}{m}} \quad (4.21a-b)$$

whereby n_{rr} and n_{cc} are the diagonal elements of the normal matrix pertaining to the shifts and m the pixel number of the window.

The test adopted is that of BALTSAVIAS (1991), barring the last part which gives information about the weakness of the signal content in row and column directions but may not be directly used for constraining any parameters. Two thresholds are needed: t_1 is the upper limit for the ratio (4.20), while t_3 is the lower limit for G_r and G_c . The scheme of the test is:

```

if(ratio ≥ t1) then
  if(nrr > ncc) then
    constrain column shaping parameters
  else
    constrain column shaping parameters
  end if
if(min(Gr, Gc) ≤ t3/2) then
  constrain all the shaping parameters
end if

```

After several empirical trials, the two thresholds have been fixed as $t_1=1.2$ and $t_3=8.0$ [g.v.].

A further (but not implemented) possibility of this test would be to adapt the slave size to the signal content.

The second test deals with the analysis of the shaping parameters' correlations. High correlations between each parameter of the affine and the others might mean its non-determinability. Of great importance are correlations of each of the shaping parameters with the shifts, between similar shaping parameters (two scales, two shears), and between shaping parameters in the same direction. If the correlation exceeds an a priori fixed threshold (e.g. 0.9), one of the correlating parameter must be excluded and the test is repeated until all the correlations are below the threshold. Naturally, the shifts can never be excluded. In [BALTSAVIAS 1991] is observed that in case a parameter has high correlation with a shift, it must be checked whether this happens because that parameter has high correlation with another one which also highly correlates with that shift. More practical seems to be the criterion to exclude the parameter having the larger variance.

When a parameter is excluded, the correlation matrix \mathbf{Q}_{xx} must be recomputed since it changes. The generic element (l,m) of \mathbf{Q}_{xx} is reduced by [GRÜN 1985]:

$$\Delta Q_{x_l x_m} = \frac{q_{x_l x_l} q_{x_l x_m}}{q_{x_l x_l}} \quad (4.22)$$

and the new correlation coefficient between the parameters l and m is given by:

$$\tilde{\rho}_{l,m} = \frac{(\rho_{l,m} - \rho_{i,l} \rho_{i,m})}{\sqrt{(1 - \rho_{i,l}^2)(1 - \rho_{i,m}^2)}} \quad (4.23)$$

An alternative way to deal with the determination of high correlations are statistical test [BALTSAVIAS 1991].

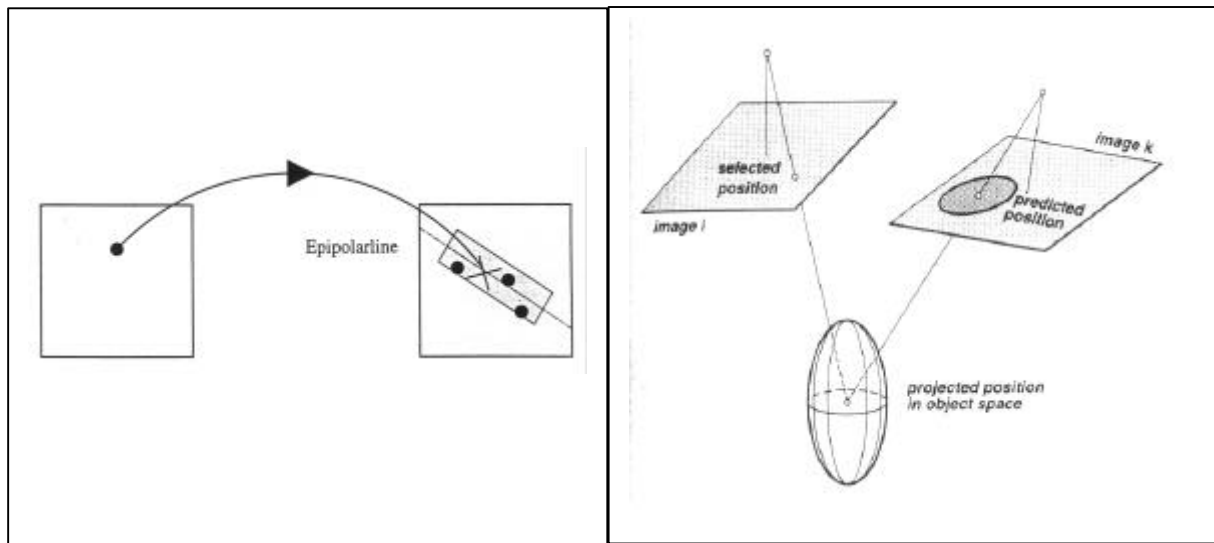


Fig. 4.5 – Search area defined by epipolar geometry [WOLFF 1998].

Fig. 4.6 – Schematic diagram of predicting conjugate locations [SCHENK 1997].

4.2 Selection of candidate homologous points

Reducing the search space for the homologous of a point in the images of a photogrammetric block can be achieved using the *epipolar geometry constraint* and using an *approximate ground model*. If only the first constraint is applied, as you may observe in Figure 4.5, the homologous of a point in another image lie on a strip around the epipolar line, whose width depends on the uncertainty of EO parameters. To put bounds to the strip length the ground information can be used, combining both information in a double projection: of a ray from the first image to the ground model, and from the ground onto the second image. By applying covariance propagation, the uncertainties of this double projection may be computed, defining the search area as the error ellipse of the projected point at a fixed probability (Fig. 4.6). The error ellipse is computed from the covariance matrix of the point in the second image, which depends on all the parameters involved and their standard deviations. Therefore this method requires approximate values for the EO and a model of the ground as well as their uncertainties. In order to simplify the screening of points which are inside the search area, the ellipse may be substituted by the rectangle enveloping it.

4.2.1 Definition of the search window

The computation of the search window is performed through two steps:

1. Projecting the point P from the first image to the ground to find the point P_G and its covariance matrix (\mathbf{C}_G).
2. Computing the coordinates and the covariance matrix (\mathbf{C}') of the point P' by projecting P_G onto the second image.

The first step can be performed by the collinearity equations:

$$X_G = X_0 + (Z_G - Z_0) \frac{r_{11}(x - x_0) + r_{21}(y - y_0) + r_{31}c}{r_{13}(x - x_0) + r_{23}(y - y_0) + r_{33}c} \quad (4.24a)$$

$$Y_G = Y_0 + (Z_G - Z_0) \frac{r_{12}(x - x_0) + r_{22}(y - y_0) + r_{32}c}{r_{13}(x - x_0) + r_{23}(y - y_0) + r_{33}c} \quad (4.24b)$$

In order to simplify these equations, some parameters with small influence on the results can be eliminated. For *pitch* (ω) and *roll* (ϕ) nought values can be assumed for both mean and standard deviation, since in aerial blocks they are subjected to narrow tolerances (usually $\pm 3^\circ$). The rotation matrix \mathbf{R} results then as follows:

$$\mathbf{R} = \begin{bmatrix} \cos \kappa & -\sin \kappa & 0 \\ \sin \kappa & \cos \kappa & 0 \\ 0 & 0 & 1 \end{bmatrix} \quad (4.25)$$

By substituting \mathbf{R} into the eq.s (4.24) and by referring the image coordinates (x,y) to the P.P. ($\bar{x} = x - x_0$, $\bar{y} = y - y_0$), the collinearity equations become:

$$X_G = X_0 + \frac{Z_G - Z_0}{c} (\bar{x} \cos \kappa + \bar{y} \sin \kappa) \quad (4.26a)$$

$$Y_G = Y_0 - \frac{Z_G - Z_0}{c} (\bar{x} \sin \kappa - \bar{y} \cos \kappa) \quad (4.26b)$$

These equations can be solved in a straightforward manner if the ground model is a horizontal plane, because in this case $Z_G = \text{constant}$. If a more accurate DTM is available, also the elevation of point P_G depends on the planimetric position ($Z_G = f(X_G, Y_G)$) and then an iterative computation should be adopted.

The covariance matrix \mathbf{C}_G of point P_G is built up by the covariance matrix of X_G and Y_G as well as the variance of the DTM. Furthermore, X_G and Y_G are also function of the DTM's elevation Z_G and then in the covariance matrix \mathbf{C}_G also the covariances between these parameters should be considered. The covariance matrix of P_G results as:

$$\mathbf{C}_G = \begin{bmatrix} \mathbf{C}_{X_G Y_G} & \sigma_{X_G Z_G} \\ \sigma_{X_G Z_G} & \sigma_{Y_G Z_G} \\ \sigma_{X_G Z_G} & \sigma_{Y_G Z_G} & \sigma_{Z_G}^2 \end{bmatrix} \quad (4.27)$$

Except for the variance $\sigma_{Z_G}^2$ which is a priori known (or guessed), the other elements of \mathbf{C}_G must be determined. The covariance matrix of the planimetric coordinates of P_G could be derived by the covariance propagation:

$$\mathbf{C}_{x_G y_G} = \mathbf{J} \mathbf{C} \mathbf{J}^T \quad (4.28)$$

The matrix \mathbf{C} contains the variance of the stochastic parameters in eq.s (4.26), considered as mutually independent:

$$\mathbf{C} = \text{diag}(\sigma_{X_0}^2, \sigma_{Y_0}^2, \sigma_{Z_0}^2, \sigma_{\kappa}^2, \sigma_{Z_G}^2) \quad (4.29)$$

while the *jacobian matrix* is defined:

$$\mathbf{J} = \begin{bmatrix} \frac{\partial X_G}{\partial X_0} & \frac{\partial X_G}{\partial Y_0} & \frac{\partial X_G}{\partial Z_0} & \frac{\partial X_G}{\partial \kappa} & \frac{\partial X_G}{\partial Z_G} \\ \frac{\partial Y_G}{\partial X_0} & \frac{\partial Y_G}{\partial Y_0} & \frac{\partial Y_G}{\partial Z_0} & \frac{\partial Y_G}{\partial \kappa} & \frac{\partial Y_G}{\partial Z_G} \end{bmatrix} = \begin{bmatrix} 1 & 0 & -\frac{\bar{x} \cos \kappa + \bar{y} \sin \kappa}{c} & -(Z_G - Z_0) \frac{\bar{x} \sin \kappa - \bar{y} \cos \kappa}{c} & \frac{\bar{x} \cos \kappa + \bar{y} \sin \kappa}{c} \\ 0 & 1 & \frac{\bar{x} \sin \kappa - \bar{y} \cos \kappa}{c} & -(Z_G - Z_0) \frac{\bar{x} \cos \kappa + \bar{y} \sin \kappa}{c} & -\frac{\bar{x} \sin \kappa - \bar{y} \cos \kappa}{c} \end{bmatrix} \quad (4.30)$$

Covariances $\sigma_{x_G z_G}$ and $\sigma_{y_G z_G}$ are given by:

$$\sigma_{x_G z_G} = \frac{\partial X_G}{\partial Z_G} = \frac{\bar{x} \cos \kappa + \bar{y} \sin \kappa}{c} \quad (4.31a)$$

$$\sigma_{y_G z_G} = \frac{\partial Y_G}{\partial Z_G} = -\frac{\bar{x} \sin \kappa - \bar{y} \cos \kappa}{c} \quad (4.31b)$$

Once the coordinates and the covariance matrix of point P_G have been calculated, the position of point P' in the second image can be evaluated. The mean values of its image coordinates are derived from the inverse form of collinearity equations (4.26) (in the following, the parameters concerning the second image are marked with a prime):

$$x' = x'_0 + c' \frac{(X_G - X'_0) \cos \kappa' + (Y_G - Y'_0) \sin \kappa'}{(Z_G - Z'_0)} \quad (4.32a)$$

$$y' = y'_0 + c' \frac{-(X_G - X'_0) \sin \kappa' + (Y_G - Y'_0) \cos \kappa'}{(Z_G - Z'_0)} \quad (4.32b)$$

The covariance matrix \mathbf{C}' of point P' is derived by using the covariance propagation:

$$\mathbf{C}' = \mathbf{J}' \mathbf{C}_2 \mathbf{J}'^T \quad (4.33)$$

whereby the covariance matrix \mathbf{C}_2 is set up by the variances of EO parameters of the second image and by the covariance matrix \mathbf{C}_G :

$$\mathbf{C}_2 = \begin{bmatrix} \sigma_{X'_0}^2 & 0 & 0 & 0 & 0 & 0 & 0 \\ 0 & \sigma_{Y'_0}^2 & 0 & 0 & 0 & 0 & 0 \\ 0 & 0 & \sigma_{Z'_0}^2 & 0 & 0 & 0 & 0 \\ 0 & 0 & 0 & \sigma_{\kappa'}^2 & 0 & 0 & 0 \\ 0 & 0 & 0 & 0 & & & \\ 0 & 0 & 0 & 0 & & \mathbf{C}_G & \\ 0 & 0 & 0 & 0 & & & \end{bmatrix} \quad (4.34)$$

The *jacobian matrix* in this case is:

$$J' = \begin{bmatrix} \frac{\partial x'}{\partial X'_0} & \frac{\partial x'}{\partial Y'_0} & \frac{\partial x'}{\partial Z'_0} & \frac{\partial x'}{\partial \kappa'} & \frac{\partial x'}{\partial X_G} & \frac{\partial x'}{\partial Y_G} & \frac{\partial x'}{\partial Z_G} \\ \frac{\partial y'}{\partial X'_0} & \frac{\partial y'}{\partial Y'_0} & \frac{\partial y'}{\partial Z'_0} & \frac{\partial y'}{\partial \kappa'} & \frac{\partial y'}{\partial X_G} & \frac{\partial y'}{\partial Y_G} & \frac{\partial y'}{\partial Z_G} \end{bmatrix} = \quad (4.35)$$

$$= \begin{bmatrix} -A & -B & \frac{C}{(Z_G - Z'_0)^2} & \frac{D}{Z_G - Z'_0} & A & B & -\frac{C}{(Z_G - Z'_0)^2} \\ B & -A & \frac{D}{(Z_G - Z'_0)^2} & \frac{-C}{Z_G - Z'_0} & -B & A & -\frac{D}{(Z_G - Z'_0)^2} \end{bmatrix}$$

$$A = \frac{c' \cos \kappa'}{Z_G - Z'_0} \quad B = \frac{c' \sin \kappa'}{Z_G - Z'_0} \quad (4.36a-b)$$

$$C = c'[(X_G - X'_0) \cos \kappa' + (Y_G - Y'_0) \sin \kappa'] \quad (4.37)$$

$$D = c'[-(X_G - X'_0) \sin \kappa' + (Y_G - Y'_0) \cos \kappa'] \quad (4.38)$$

In this way is possible to define the error ellipse of the homologous point [INGHILLERI 1974; SANSÒ 1993]. Here we adopted a probability of 95%, corresponding to an ellipse having axes two times the standard deviations along the main directions. If the model is correct and the parameter uncertainties were properly given, the homologous point lies inside the ellipse and may be discriminated in a list of interest points extracted within the ellipse by matching algorithms. Since this operation is repeated many thousand times during an AAT of a photogrammetric block, in order to speed up the process we box the ellipse by a rectangle. Looking for points inside a rectangle is faster and simpler; optimal algorithms to perform this search can be found in computer graphics literature [e.g. HARRINGTON 1995].

4.2.2 Influence of EO parameter uncertainty on the search window shape

How does the uncertainty of each parameter affect size and orientation of the search window? Let us assume flat terrain and two nadir images (this simplification allows to better understand the influence of each single parameter). Figure 4.7 shows how the search area changes as a consequence of the uncertainty of each group of parameters. Six points in the “Von Grüber” positions are projected from the first image to the second and the rectangular shape of the resulting search window is depicted. The photographs of this ideal example have a mean scale of 1:10000 and were acquired with an aerial camera with standard objective ($c=150$ cm). For each

case, three levels of magnitude for the uncertainty of EO have been considered, resulting in search windows depicted in different colors.

First we consider only the uncertainty of the planimetric coordinates (X_0, Y_0) of the perspective center of both images. This shifts the search area on the second image irrespective of the position of the initial point P.

The influence of the height of the photo center (Z_0) is the sum of two effects: the first stretches the search window along a direction which is parallel to the ray PO on the first image; the second effect is similar, but parallel to the ray P'O' on the second image. In addition, the farther is the point from the P.P., the larger is the variation of the search window's size.

Likewise, the variations of the angle κ stretch the search window along directions which are orthogonal respectively to the ray PO and to the ray P'O'. Again, points farthest from the P.P. result in a major size of the search area.

Finally, the uncertainty of DTM does not result in a proper search area, but rather in a segment on the epipolar line.

4.3 Outlier rejection in relative orientation

The most effective outlier rejection strategy used in TRIADIGIT to discard mis-matched tie points is by computing a robust relative orientation between each pair of overlapping images. For the method to be successful, the geometric distribution of the points in the overlap area is important. Every "Von Grüber" zone should have a fair number of points (in theory at least one, in practice more, because the redundancy is strictly necessary). Possible degenerate configurations might cause the failure of the rejection: an a priori check on number and geometry of the tie-points should be performed.

In the definition of the procedure for outlier rejection through relative orientation, three main requirements have been kept into account:

1. No need for approximate relative orientation parameters.
2. Robustness against also large fraction of outliers in the data set (30-40% and even more).
3. Complete automation of the procedure, without any decision to be interactively taken.

Many papers can be found in literature about this subject, either in the field of photogrammetry, either in that of computer vision and image processing. Reviews of existing algorithms are reported in [HEIPKE 1997; TORR AND MURRAY 1997].

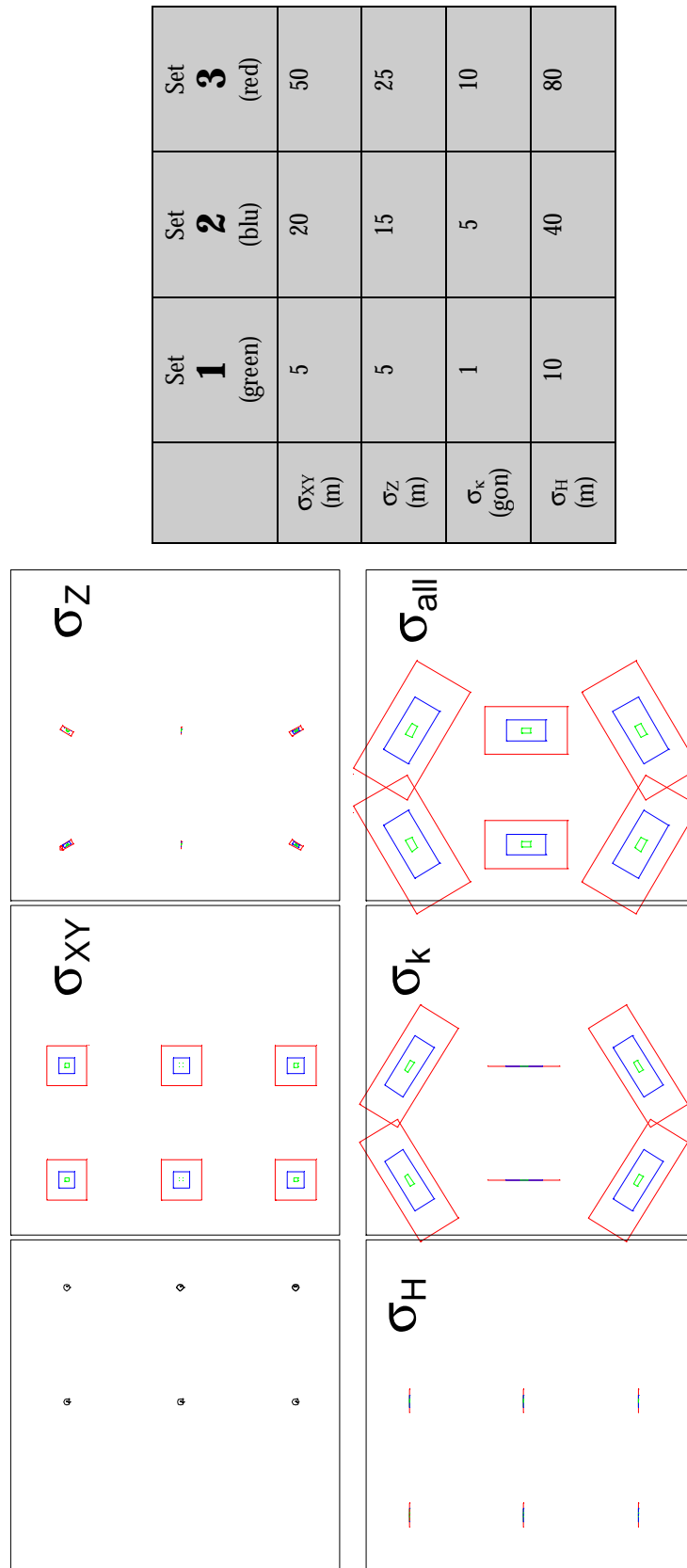


Fig. 4.7 – Definition of the search window according to different exterior parameter uncertainties. The 6 yellow points in the left-most image of the top row represent the starting points (primary points); in the other images are depicted the resulting search window depending on the parameters indicated. The 3 colors represent different sets (see the table on the right) of uncertainty, from the lowest (green) to the largest (red). Images are assumed at a scale 1:10000.

In the sequel the procedure applied to compute the relative orientation in TRIADIGIT is presented. This task is not performed in order to improve the EO of the block, but only to discard outliers from the data set of tie-points. Therefore, no geometric parameters of relative orientation are explicitly derived. First we introduce the algorithm of “Longuet-Higgins” that is used for computing relative orientation through the so called *fundamental matrix*. To solve for the elements of the fundamental matrix *Orthogonal Least Squares* are proposed instead of classical l.s., while the use of *Least Median Squares* estimator allows to compute a fully robust solution which is adopted to discriminate for outliers in the data set.

4.3.1 The “Longuet-Higgins” algorithm

Traditional formulation of the relative orientation leads to the solution of a system of non-linear equations. Disregarding the mathematical method to solve this system, it must however perform iterations which should start from good approximations for the unknowns. If as many as eight corresponding points are measured, the relative orientation can be computed by a direct method, which is based on the solution of a system of linear equations set up by using the image coordinates of the homologous points. Even though more points than the traditional 6 “Von Grüber” points are required, this method, first proposed by LONGUET-HIGGINS (1981)¹, presents the advantage that does not require approximations for the relative orientation parameters and thus it may work out any spatial configuration of the image pair. The straightforward solution consists of the set of unknown coefficients of the linear system, from which the geometric parameters (base and rotations, according to the considered model) can be derived.

After [LONGUET-HIGGINS 1981], in the following years many other papers came up giving further developments and extensions of this algorithm. In particular, many efforts have been made in order to introduce into the problem the interior orientation parameters. In case they are already known, they may be used to improve the solution, otherwise a joint solution for orientation and calibration parameters may be performed. Outlines of these methods are reported by [LUONG *et al.* 1993; TORR AND MURRAY 1997; PAN 1996]. The description of the algorithm of “Longuet-Higgins” proposed below keeps into account also some aspects that were re-formulated afterwards by other authors.

First of all, the geometric parameters used to describe the problem are presented. We consider a 3D object coordinate system with orthogonal axes XYZ (see Fig. 4.8). A pair of stereo images is positioned in this reference frame, which we refer to as “left” and “right”. The 2D image coordinate system xy will be local to the left image, while symbols relating to the right image will be marked with a prime. Let x_0 and y_0 denote the P.P. coordinates in the left image and c the principal (left) distance, and accordingly for the right image. Suppose an object point P is projected to both images respectively in p and p' . Let us define the following vectors:

$$\mathbf{p} = [x \quad y \quad 1]^T \quad (4.39)$$

is the *uncalibrated image coordinate vector*, expressed in dummy coordinates;

$$\tilde{\mathbf{p}} = [x - x_0 \quad y - y_0 \quad -c]^T = \mathbf{K}\mathbf{p} \quad (4.40)$$

is the *calibrated image coordinate vector*, the matrix \mathbf{K} is set up by the interior orientation parameters:

¹ It is also known as “8 points” method, because it requires at least 8 corresponding points to be applied.

$$\mathbf{K} = \begin{bmatrix} 1 & 0 & -x_0 \\ 0 & 1 & -y_0 \\ 0 & 0 & -c \end{bmatrix} \quad (4.41)$$

These vectors refer to the 2D image reference frame of the left image and may be written for the right one as well. The 3D coordinates of point P are defined in the vector $\bar{\mathbf{p}}$ and considering the rotation matrix \mathbf{R} of the left image:

$$\bar{\mathbf{p}} = [\bar{x} \quad \bar{y} \quad \bar{z}]^T = \mathbf{R}\mathbf{p} \quad (4.42)$$

The perspective projection from P to p is given by the collinearity equations (4.24). It is well known that the mere knowledge of homologous points in the pair does not allow to solve for the collinearity equations, because you need to know a minimum number of GCPs to compensate for the rank deficiency. Therefore, the computation of relative orientation is performed through the *coplanarity equations*. We introduce the *baseline vector* \mathbf{B} :

$$\mathbf{B} = [B_x \quad B_y \quad B_z]^T = [X_0 - X_{0'} \quad Y_0 - Y_{0'} \quad Z_0 - Z_{0'}]^T \quad (4.43)$$

The magnitude of \mathbf{B} cannot be determined without control information, so \mathbf{b} is a positively scaled version of \mathbf{B} :

$$\mathbf{b} = [b_x \quad b_y \quad b_z]^T = \gamma \mathbf{B}^T \quad \gamma > 0 \quad (4.44)$$

Considering any point P in object space which is projected to both the images, we can observe that the point P itself, its projections p and p' as well as the baseline vector \mathbf{b} lie in the same plane. This coplanarity relation can be written as a cross-product of three vectors being equal to zero:

$$\bar{\mathbf{p}} \cdot (\mathbf{b} \times \bar{\mathbf{p}}') = 0 \quad (4.45)$$

This formulation may be developed in several analytical form [CRIPPA AND MUSSIO 1995; KRAUS 1997] which lead to the classic iterative solutions. THOMPSON (1959) first writes this equation in linear form by introducing a skew-symmetric matrix for image coordinates of one of the two photographs instead of the classical vector. Moreover, he reformulates the rotation matrix in the rational algebraic form introduced by [RODRIGUES 1840; CAYLEY 1843]. In PAN (1996) the coplanarity relation (4.45) is rewritten considering a skew-symmetric matrix of the baseline vector \mathbf{b} :

$$\mathbf{b}^* = \begin{bmatrix} 0 & -b_z & b_y \\ b_z & 0 & -b_x \\ -b_y & b_x & 0 \end{bmatrix} \quad (4.46)$$

According to this assumption, eq. (4.45) becomes the so called *explicit coplanarity equation*, whose name arises from the fact that every geometric parameters is explicitly shown for either the interior and exterior orientation:

$$\mathbf{p}^T \mathbf{K}^T \mathbf{R}^T \mathbf{b}^* \mathbf{R}' \mathbf{K}' \mathbf{p}' = 0 \quad (4.47)$$

Another form for (4.47) is the *implicit coplanarity equation*, which is explicit only with respect to the purely measured coordinates of image points:

$$\mathbf{p}^T \mathbf{F} \mathbf{p}' = 0 \quad (4.48)$$

FAUGERAS *et al.* (1992) called \mathbf{F} *fundamental matrix* in case the interior orientation parameters of both images are the same. The matrix \mathbf{F} can therefore be decomposed as:

$$\mathbf{F} = \mathbf{K}^T \mathbf{R}^T \mathbf{b}^* \mathbf{R}' \mathbf{K}' \quad (4.49)$$

This way to cope with the the problem is just that was adopted firstly by LONGUET-HIGGINS.

After having illustrated the way for establishing the relative orientation problem in linear form, now we deal with its solution. Many authors published solutions considering also interior orientation parameters as unknowns; some algorithms keep into account the estimation of a camera distortion model [e.g. FAUGERAS *et al.* 1992]. In aerial photogrammetry the use of metric cameras allows to bound the unknowns strictly to the external orientation parameters; in this case it's easy to write the coplanarity equation in the form (4.48) and then to estimate the *fundamental matrix*. This doesn't directly show any geometric parameters, but they can be derived according to the model adopted for the relative orientation; [HATTORY AND MYINT 1995] gives a solution based on the symmetric model, while [LONGUET-HIGGINS 1981; PAN 1996] describes the asymmetric one.

4.3.2 Estimation of the fundamental matrix by Orthogonal Least Squares

Let now have a look to the computation method to estimate the solution when applying the "Longuet-Higgins" algorithm such as proposed by TORR AND MURRAY (1997). As mentioned above, vectors \mathbf{p} and \mathbf{p}' contain the dummy coordinates of corresponding points. For each pair of homologous points one eq. (4.48) can be written. The least number of equations which set up the system must be 8, because the unknowns of the problem are just 8. In fact, although the fundamental matrix \mathbf{F} is a 3×3 matrix, the real degree of freedom is 7, because only the ratio of parameters is significant (eq. 4.48 is homogeneous) and because $\det \mathbf{F} = 0$. A further analysis of the properties of the fundamental matrix is given by [HUANG AND FAUGERAS 1989]. Ignoring for the moment the problem of enforcing the rank 2 constraint, this system appears as a linear regression which may be solved by a l.s approach. Linear here refers to linearity in the elements f_i of fundamental matrix, as can be seen by writing out eq. (4.48):

$$f_1 x'_1 x_i + f_2 x'_1 y_i + f_3 x'_1 \zeta + f_4 y'_1 x_i + f_5 y'_1 y_i + f_6 y'_1 \zeta + f_7 x_i \zeta + f_8 y_i \zeta + f_9 \zeta = 0 \quad (4.50)$$

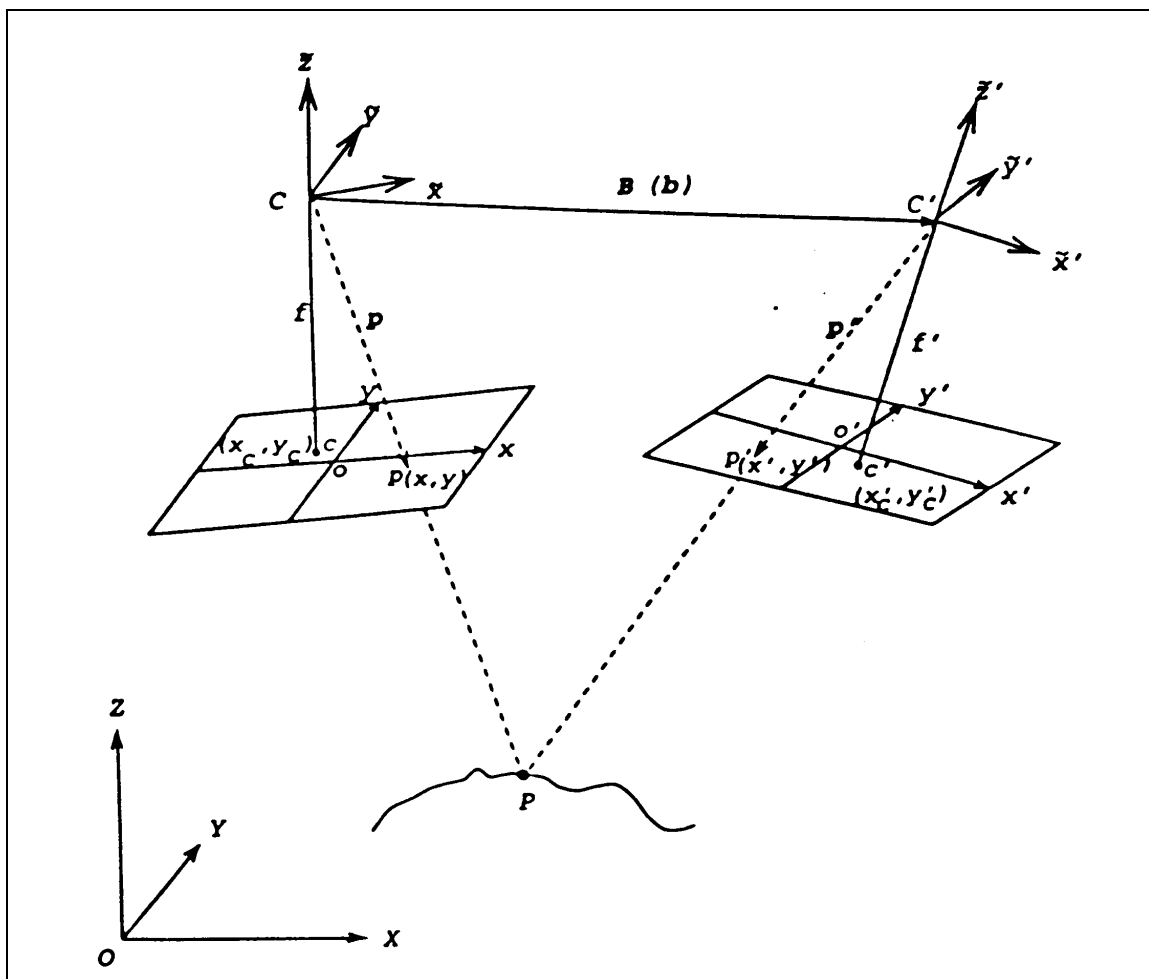


Fig. 4.8 – Analytical geometry of two stereo images [PAN 1996]

where the letter ζ indicates the dummy coordinate. Because errors exist in all the measured image coordinates (x, y, x', y') , *Orthogonal Least Squares* [PEARSON 1901; KENDALL AND STUART 1983] rather than ordinary l.s. should be used². Considering fitting a hyperplane $\mathbf{f}=(f_1, f_2, \dots, f_p)$ through a

² The difference between these methods can be easily understood by observing a simple bidimensional linear regression. In the figure 4.9 below the distances minimized in either cases are shown.

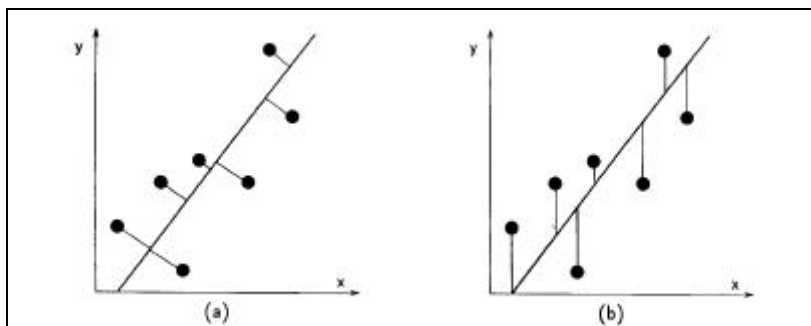


Fig. 4.9 – Distances minimized in orthogonal (a) and ordinary (b) l.s. for a linear regression

set of n points in \mathfrak{R}^p with coordinates $\mathbf{z}_i=(z_{i1},z_{i2},\dots,z_{i3})$, taking the centroid of the data as origin. Assuming that the noise is Gaussian and that the elements of \mathbf{z}_i have equal variance, the hyperplane \mathbf{f} with maximum likelihood is estimated by minimizing the sum of Euclidean distances from the points to the plane subject to $\mathbf{f}^T\mathbf{f}=1$.

This constraint ensures that the estimate will be invariant to conformal transformation of the inhomogeneous coordinates.

To reformulate this as an eigen-problem, let \mathbf{Z} be the $n \times p$ *design matrix* with rows \mathbf{z}_i :

$$\mathbf{Z} = \mathbf{W} \begin{bmatrix} x'_1x_1 & x'_1y_1 & x'_1\zeta & y'_1x_1 & y'_1y_1 & y'_1\zeta & x_1\zeta & y_1\zeta & \zeta \\ \vdots & \vdots & \vdots & \vdots & \vdots & \vdots & \vdots & \vdots & \vdots \\ x'_nx_n & x'_ny_n & x'_n\zeta & y'_nx_n & y'_ny_n & y'_n\zeta & x_n\zeta & y_n\zeta & \zeta \end{bmatrix} \quad (4.51)$$

where \mathbf{W} is a diagonal matrix of the weights given to each pair of homologous points, inversely proportional to the error variance. This is assumed to be homogeneous and can be omitted. Let $\mathbf{M}=\mathbf{Z}^T\mathbf{Z}$ be the $p \times p$ *moment matrix*, with eigenvalues, in increasing order, $\lambda_1, \lambda_2, \dots, \lambda_p$ and with $\mathbf{u}_1, \mathbf{u}_2, \dots, \mathbf{u}_p$ the corresponding eigenvectors forming an orthonormal system. The best fitting hyperplane is given by the eigenvector \mathbf{u}_1 corresponding to the minimum eigenvalue λ_1 of the moment matrix. It is evident that:

$$I_1 = \sum_{i=1}^n (\mathbf{u}_1^T \mathbf{z}_i)^2 = \sum_{i=1}^n r_i^2 \quad (4.52)$$

which is the sum of residuals r_i , in this case the *algebraic distances*, namely the perpendicular distances to the hyperplane.

The Orthogonal l.s. method produces a sub-optimal estimate of \mathbf{F} because the residuals that are minimized are not normally distributed. The algebraic distance, however, has not geometrical significance and does not, for example, measure the perpendicular distance of a feature to the quadric variety represented by \mathbf{F} in 4D image coordinate space (x, y, x', y') . On the contrary, the best fitting, maximum likelihood quadric curve is such that the sum of squares of the perpendicular *geometric distances* of points to the curve is a minimum [KANATANI 1994]. In [TORR AND MURRAY 1997] different solutions to this problem are analyzed and proposed; here we refer to that derived from [WENG *et al.* 1989]. Noting that the expression for the residuals for the fits to a conic and to the fundamental matrix were both bilinear in the measurements, they adapted the method of SAMPSON (1982) to the computation of the fundamental matrix. They estimate \mathbf{f} by computing:

$$\mathbf{f} = \min_{\mathbf{f}} \sum_{i=1}^n (w_{s_i} \mathbf{f}^T \mathbf{z}_i)^2 \quad (4.53)$$

where w_{s_i} is the optimal weight, the variance of the residual:

$$w_{s_i} = \frac{1}{\nabla r_i} = \frac{1}{\sqrt{(r_{xi}^2 + r_{yi}^2 + r_{x'i}^2 + r_{y'i}^2)}} \quad (4.54)$$

and where the partial derivatives at the denominator are:

$$\begin{aligned} r_x &= f_1x' + f_4y' + f_7\zeta & r_x &= f_1x + f_2y + f_3\zeta \\ r_y &= f_2x' + f_5y' + f_8\zeta & r_y &= f_4x + f_5y + f_6\zeta \end{aligned} \quad (4.55a-b-c-d)$$

This is a first order approximation to the standard deviation of the residual. Because calculation of the weights requires a value for the fundamental matrix and vice versa, an iterative method is called for. Here this aspects is not analyzed because, as it will be presented in the paragraphs 4.3.4 and 4.3.5, the weights w_{s_i} will not be used to estimate the fundamental matrix, but only to perform outlier rejection. Finally, by introducing the weights w_{s_i} the *distance of Sampson/Weng* may be defined as:

$$d_i = w_{s_i} r_i \quad (4.56)$$

and it can be minimized in the orthogonal l.s. instead of the algebraic distance.

4.3.3 Robust estimators for the fundamental matrix

The results given by l.s. methods may be largely affected by the presence of outliers in the data set. Using the relative orientation to discard wrong corresponding points found by image correlation algorithms, it is necessary to introduce a robust estimator in the procedure. Although considerable work appears in the statistical literature on the detection of outliers in the context of ordinary, non-orthogonal regressions³, little work has been done on outlier detection in orthogonal regression. Exceptions appear the work of SHAPIRO AND BRADY (1993) on hyperplane fitting and, in particular, that of TORR AND MURRAY (1997), which perform a full analysis of different methods and make comparison among them. TORR AND MURRAY consider three categories of robust estimators for the fundamental matrix:

1. *M-estimators* [MARONNA 1976; HÜBER 1981; HAMPEL *et al.* 1986]
2. *Case Delection Diagnostics* [CHATERJEE AND HADI 1988]
3. *Random Sampling Algorithms* [FISCHLER AND BOLLES 1981; ROUSSEEUW AND LEROY 1987]

From results of empirical tests the authors conclude that the most suitable robust estimator for the fundamental matrix is one out of the *Random Sampling Algorithms*, possibly followed by an *M-estimator*.

4.3.4 Random Sampling Algorithms

Random Sampling Algorithms concept is opposite to conventional smoothing techniques. Rather than using as much as data as possible to obtain an initial solution and then attempting to identify outliers, a small subset, made up of the minimum number of data necessary to compute the parameters is used, and this process is repeated enough times on different subsets to ensure that there is a fixed chance that one of the subsets will contain only good data points. The best solution is that which maximizes the number of points whose residuals are below a given

³ In [CHATERJEE AND HADI 1988] an exhaustive review of the main methods is presented.

threshold. Once outliers are removed, the set of points identified as inliers may be combined to give the final solution.

Ideally every possible subsample of the data would be considered, but this is usually computationally infeasible; therefore the number of subsamples is chosen sufficiently high to give a probability in exceed of a fixed value (e.g. $P=95\%$) that a good subsample is selected. ROUSSEEUW AND LEROY (1987) proposed the following expression for this probability (a slightly different one may be found in [FISCHLER AND BOLLES 1981]):

$$P = 1 - (1 - (1 - \epsilon)^p)^{m_s} \quad (4.57)$$

whereby ϵ is the fraction of outliers (to be guessed) and p the number of data in each subsample. The minimum number of trials necessary to find at least one good sample with probability P is given by inverting (4.57):

$$m_s > \frac{\log(1-P)}{\log(1-(1-\epsilon)^p)} \quad (4.58)$$

In Table 4.10 are reported the value of m_s corresponding to different fractions of outliers in the case of fundamental matrix estimation ($p=8$, $P=95\%$).

Generally it is better to take more samples than are needed because some of them may be degenerate [TORR *et. al.* 1995, 1996]; otherwise, any extracted sample should be checked against weak geometric configurations and, if necessary, discarded.

RANSAC [FISCHLER AND BOLLES 1981] has been the first algorithm implementing this technique. It performs well also with very high fraction of outliers (90%), if a sufficient number of subsample is selected [ROTH AND LEVINE 1993]. The drawback of *RANSAC* is that it requires a priori knowledge of the variance of data. On the contrary, *Least Median Squares* (LMS) [ROUSSEEUW AND LEROY 1987] may estimate the variance of the measurements as well, so that no a priori information is called for. For this reason, LMS has been implemented in TRIADIGIT for outlier rejection through the computation of fundamental matrix.

In LMS algorithm the selection of the best subsample is done on the basis of the least median of the weighted residuals (4.56):

$$\text{med}(d_i^2) = \min \quad (4.59)$$

The use of the median breaks down the number of gross errors which might be effectively coped with to $(n-p)/2+1$. For the fundamental matrix, if the number of corresponding points is high ($n \gg p=8$), the break down point is slightly less than 50% of outliers in the data set. On the other hand, a lower bound to the number of points should be adopted, otherwise the break down point sharply falls down. For example, considering $n=20$ the break down point becomes 26%.

parameters to estimate	fraction of outliers (ϵ)						
	5%	10%	20%	25%	30%	40%	50%
$p=8$	3	6	17	29	51	177	766

Table 4.10 – Number of subsamples to extract for the estimation of the fundamental matrix by LMS, given a probability $P=95\%$

4.3.5 Outlier rejection

Before actually performing outlier rejection, a robust estimate of the standard deviation σ_0 of the errors is required, as outliers are typically discriminated from inliers using:

$$i \in \begin{cases} \text{set of inliers} & \text{if } d_i \leq 1.96\sigma_0 \\ \text{set of outliers} & \text{otherwise} \end{cases} \quad (4.60)$$

where d_i is the Sampson/Weng distance (4.56).

The standard deviation σ_0 is related to the characteristics of the images (resolution, texture, etc.), the feature detector and the matching technique. If there are no outliers in the data, σ_0 can be estimated directly as the standard deviation of the residuals of a non-linear l.s. minimization. If there are outliers and they are in minority, a first estimate of σ_0 can be derived from the median squared error of the chosen parameter fit, multiplied by a finite-sample correction factor for the case of normal errors [ROUSSEEUW AND LEROY 1987]:

$$\sigma_0 = 1.4826 \left(1 + \frac{5}{n-p} \right) \sqrt{\text{med } d_i^2} \quad (4.61)$$

where n is the number of data and p the number of parameters.

This preliminary estimate of σ_0 is then used to determine a weight w_i for the i th observation, namely:

$$w_i = \begin{cases} 1 & \text{if } |d_i| \leq 2.5\sigma_0 \\ 0 & \text{otherwise} \end{cases} \quad (4.62)$$

By means of these weights, the final estimate σ_0^* is calculated:

$$\sigma_0^* = \sqrt{\left(\sum_{i=1}^n w_i d_i^2 \right) / \left(\sum_{i=1}^n w_i - p \right)} \quad (4.63)$$

The advantage of this formula for σ_0^* is that outliers do not influence its estimate any more. Finally, by using σ_0^* in the test (4.60), all data can be divided into inliers and outliers.

In Figure 4.11 the whole procedure to perform outlier rejection in relative orientation is summarized.

Robust Outlier Rejection in Relative Orientation

1. Determination of the number m_s of subsamples to extract by (4.58).
2. Repeat for each subsample j :
 - Random extraction of 8 points to estimate \mathbf{F}_j through (4.52).
 - Calculate the distance of Sampson/Weng d_i (4.56) for each feature given \mathbf{F}_j .
 - Calculate $d_j^2 = \text{med } d_i^2$.
3. Select the best solution \mathbf{F}_k so that $d_k^2 = \min d_j^2$.
4. Calculate the distance of Sampson/Weng d_i (4.56) for each feature given the solution \mathbf{F}_k .
5. First estimate of σ_0 through the formula (4.61).
6. Re-weight the observations by (4.62).
7. Final estimate of σ_0^* through the formula (4.63).
8. Outlier rejection using σ_0^* in the test (4.60).

Figure 4.11 – Scheme of the LMS estimation of the fundamental matrix

Chapter 5

Experimental Results

5.1 Description of the tests

As already mentioned in Chapter 1, TRIADIGIT has been built and partly tested under way. After the last changes, a new series of tests has been performed, to check the technical performances of the system (see 1.7.1), with particular emphasis to the block stability and the accuracy of tie points. Thus, only small blocks have been considered, resulting in manageable data volumes and not involving too much computation time.

After a description of the data set, the chapter will deal with the analysis of the results obtained by TRIADIGIT. Two points will be analysed: the theoretical accuracy of tie points extracted by TRIA_DIGIT, by looking at the outcome of the bundle block adjustment, and an independent check of their accuracy obtained by comparing the results of AAT to those of interactive aerotriangulation.

5.1.1 Test data sets

The guidelines for the selection of the blocks to be tested has been the same used by the organizers of OEEPE-ISPRS test on performance of tie point extraction [HEIPKE AND EDER 1998]. We remind them:

- The need for a representative test data set covering different standard applications in photogrammetry, i.e. different scene contents, topography, cameras, scales, film material, and overlap configurations.
- Large scale blocks have been preferred, because in these cases potential matching problems due to occlusions and relief displacement are more pronounced.
- Small blocks resulting in manageable data volumes.
- A fair chance for success for AAT, excluding blocks with imagery at different scales, with large rotations and non-topographic images.



Fig. 5.1 – Area covered by the block “Lucera”

- Use of aerial images derived from photographs on first quality films and digitalized by photogrammetric scanners only.

According to these guidelines, two blocks have been selected within the material delivered in occasion of the OEEPE-ISPRS test (block “Echallens”) and that available at Dept. IIAR (block “Lucera”). Table 5.3 shows some general information about the data sets, which are described in more detail in the following.

- Lucera: this block was flown in December 1991 over the area surrounding Lucera (Southern Italy), a small town on the top of a hill (see Fig. 5.1). Apart from this urban area, the rest of the block covers a flat country with different crops and small industrial settlements. The black and white images present a good texture and the 60% side overlap offers many areas where multi-ray are likely to be found. The flight was commissioned by a consortium made up of different italian research institutes in order to carry out a test on AT; a set of natural GCPs is available, but unfortunately after an accurate check only 8 of them have been retained to be reliable for use. The diapositives have been scanned directly by a scanner LH DSW300 of *Istituto Geografico Militare Italiano* (IGMI), Florence. Due to the fact that the flight dates some years ago, small deformations affect the films, as some measurements at the analytical plotter have shown accordingly.
- Echallens: this scene near Lausanne (Switzerland) is rather flat and shows mainly open terrain. The black and white images are rich in texture, the overlap configuration corresponds to the standard values of aerial photogrammetry. The negatives were scanned directly and had not been converted to positives. This block can be considered as a sort of basic test for an AAT system.

In Figure 5.2 is reported a whole image and a patch showing the texture for each block.

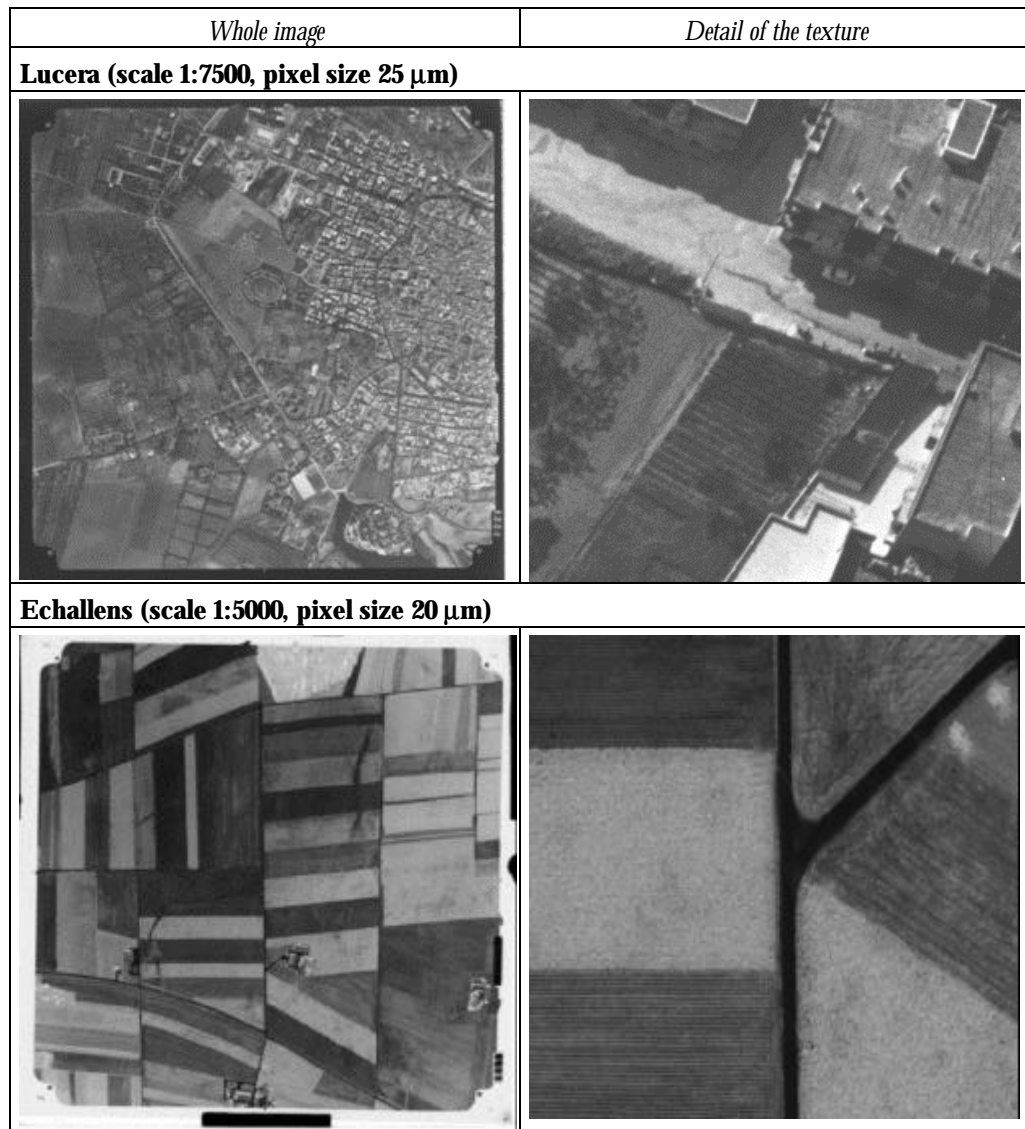


Fig. 5.2 – Examples of images and details of the texture from the blocks used for the tests

Project name	Lucera	Echallens
<i>Scene content</i>	Country, small town	open, partly forest
<i>Scene topography</i>	flat, partly hilly	flat
<i>Average image scale</i>	1:7500	1:5000
<i>Average flight height (m)</i>	2300	850
<i>Camera</i>	Wild RC10	Wild RC10
<i>Focal length (mm)</i>	150	150
<i>Flight date</i>	December 1991	September 1982
<i>Film material</i>	B/W	B/W
<i>No. of images</i>	6 × 3	3 × 3
<i>Overlap</i>	l=60%,q=60%	l=60%, q=30%
<i>Scanner used</i>	LH DSW 300	LH DSW 200
<i>Pixel size (mm)</i>	25	20
<i>Posit./negat. images</i>	positive	negative
<i>Scanned material</i>	positive, original	negative, original
<i>Scanned channel</i>	pan	pan
<i>Scan date</i>	November 1998	January 1996
<i>Source</i>	DIAR	EPFL, Lausanne
<i>No. of GCPs</i>	8	not available
<i>Kind of GCPs</i>	natural	—

Table 5.3 - Description of the test data sets

5.2 AAT of the blocks

In this paragraph we report about setup, running and outcomes of AAT of the blocks described at 5.1.1 by TRIADIGIT. Before starting the procedure for tie point extraction, the interior orientation of every image has been computed by the program ORINT. The results are reported in Table 5.4. Besides, image pyramids have been generated up to the level 5, at resolutions varying from 620 μm for “Echallens” to 800 μm for “Lucera”.

5.2.1 AAT setup

Under the term AAT setup we collect different aspects, which can be summarized in the following three items:

1. Definition of the approximate exterior orientation of the block and its uncertainty, either to start AAT or to exploit the block structure for the extraction of interest points.
2. Selection of an appropriate ground model; in most cases, a horizontal plane at the mean elevation of the block area is enough; moreover, its uncertainty has to be provided.
3. Setup of program control parameters.

These topics will be analyzed in more detail in the sequel, showing the problems and the solutions adopted for each block.

5.2.1.1 Approximate exterior orientation

Two cases must be distinguished: the block “Echallens”, delivered in the occasion of the OEEPE-ISPRS test, was already provided with approximate values of the exterior orientation parameters, accurate to about 50 m for the projection centers and 2° for the three attitude angles. Besides, the overlaps were given as well. These values have been directly used.

The second case concerns the block “Lucera”, for which every image has been roughly georeferenced in a map at the scale 1:25000, obtaining approximate values for X_0 and Y_0 with an accuracy of about 100 m, and values for angles k with an accuracy of about 3°. For the elevation Z_0 the instrumental flight heights registered on each photograph have been used (accuracy about 50 m), as the angles ω and ϕ have been put equal to zero. This demonstrated that the derivation of the approximate exterior parameters without GPS on board is not critical, because the procedure converged despite the low accuracy.

The knowledge of the rough exterior orientation allows to determine the overlaps of the images so that the initial interest points are extracted in those areas where they are more likely to become multi-ray tie points. The number of interest points, either primary and secondary, found in each block is depicted in Table 5.5.

5.2.1.2 Ground model

For both blocks a horizontal plane has been adopted as ground model. For block “Lucera”, the average height and the maximum variation in elevation have been derived from an existing map. For block “Echallens”, the average height of the ground was given, while the variation has been guessed according to the kind of topography.

5.2.1.3 Program control parameters

The system TRIADIGIT requires two kinds of control parameters. The first collects the characteristics of the imagery (number, names, resolution, kind of camera, etc.); their selection is obvious and so we do not comment on that. The second control the algorithms and the strategy for AAT, resulting in the success (or in the failure) of tie point extraction; these are depicted in Table 5.4. Information about the rough EO, the ground model and their uncertainties, whose setup has been illustrated in the previous paragraphs, are also included.

We tried to find some standard values for the control parameters, in order to decouple their selection from the block characteristics. For example, we found that a 6 levels image pyramids may be used with image resolutions in the range 20÷30 μm .

Another critical point is the size of the window for l.s. matching. After many trials, we have concluded that the best results may be obtained by increasing by two pixels the size of the window at each level of the image pyramids, starting from a size of 9 pixels.

Project name	Lucera	Echallens
Original resolution (mm)	25	20
# of image pyramid levels	5	5
Lower resolution (mm)	800	640
Average ground height (m)	190	570
Max elevation difference (m)	50	35
Uncertainty of X_0 - Y_0 (m)	50	100
Uncertainty of Z_0 (m)	30	100
Uncertainty of k (gon)	3	2

<i>Size of LSM window [pel]</i>	9+2 at each level	9+2 at each level
<i>Min. correlation for LSM</i>	0.7	0.7
<i>Type of ground control</i>	8 GCPs	7 EO parameters

Table 5.4 – Setup of AAT control parameters

Project name	Lucera	Echallens
<i>Average s_0 of inner orientation [pel]</i>	0.27	0.53
<i>Average no. of primary pts per image (initial level)</i>	180	330
<i>Average no. of secondary pts per image (initial level)</i>	770	1060
<i>Average no. of primary pts per image (second level)</i>	720	970
<i>Average no. of secondary pts per image (second level)</i>	3200	4640

Table 5.5 – Outcomes of preliminary tasks (automatic inner orientation by program ORINT and extraction of interest points)

5.2.2 AAT strategy

By AAT strategy we mean the setup of the tie point extraction workflow, i.e. the number of image pyramid levels involved in the refinement of initial EO parameters (stage 1, see par. 2.4.1), how many times intermediate bundle adjustments are computed and the backprojection of tie points is performed, to increase the multi-ray points.

For both blocks we followed this strategy:

1. Improvement of approximate EO involving only the initial level (level 5) of the image pyramids.
2. Tie point densification at level 4: after the bundle adjustment, all the tie points found are backprojected from the ground to the images.
3. In the remaining levels (3-0), tie points are traced along the image pyramids; an intermediate bundle adjustment followed by the backprojection of tie points is executed after level 2.
4. After level 0 the final bundle adjustment is computed.

This solution still recover many multi-ray points which have been lost, avoiding to compute the bundle adjustment at the end of each level.

5.2.3 AAT outcomes

AAT results for the blocks are evaluated on four criteria:

1. number of tie points found at each stage of AAT;
2. outlier rejection;
3. tie point distribution in the last level;
4. outcomes of the final bundle adjustment.

5.2.3.1 Intermediate results

Tie point extraction for blocks “Lucera” and “Echallens” is summarized in Tables 5.6 and 5.7, according to the workflow presented in 5.2.2. In each table, the first entry reports the number of tie points found at the end of the initial pyramid level, with the aim to improve the approximate EO. The small set of tie points found is due to the fact that at the beginning few interest points have been extracted, and to the roughness of EO. The next level (here level 4) gives raise to a large increase of tie points, many of them multi-rays. In the remaining levels, their number decreases during the image coordinate refinement by l.s. matching, as more details appear in higher resolution images. This effect is bounded by the backprojection of tie points from the ground to the images.

5.2.3.2 Outlier rejection

Another aspect shown by the above mentioned Tables is outlier rejection. We report the number of tie point discarded (in image space) by the internal procedure (robust relative orientation or parallax analysis), by data snooping in the bundle adjustment and the total.

As you can see, the internal procedure is highly effective in rejecting even large fractions of gross errors; peaks of about 40% of blunders are reached in some cases. This fact allows to obtain a data set containing a low fraction of outliers to be processed by l.s. bundle adjustment.

5.2.3.3 Tie point distribution

The geometric distribution of tie points over the block and the abundance of manifold points is the key for an accurate and stable aerotriangulation. We reported in Table 5.8 the number of tie points found, and that of multi-ray points.

For the block “Lucera” a consistent set of points has been found, as you can see in Figure 5.12; in Figure 5.13 only the multi-ray points have been drawn. In theory, the 60% side overlap entails also some areas where 8-ray and 9-ray points might be found, which TRIA_DIGIT could not find. This may be due to the fact that in not all the images a sufficient correlation during l.s. matching has been achieved.

Block “Echallens” is covered by a consistent set of conjugate points (see Fig. 5.14 and 5.15), this could be expected due to the flat terrain, which represents an ideal condition for AAT.

Level	Pixel size [mm]	Total # of tie pts found (image space)	# of tie points discarded			# of multi-ray tie points per level in object space								
			Total (%)	By data snooping (%)	By internal procedure (%)	total	2	3	4	5	6	7	8	9
5	800	6664	1254(19)	216(4)	1038(16)	2042	1123	540	246	82	44	6	1	0
4	400	25964	5632(22)	613(3)	5019(19)	7203	3835	1782	900	461	176	37	12	0
2	100	15288	2800(18)	1371(10)	1429(9)	4801	2939	1145	472	185	58	2	0	0

0	25	9212	1630(17)	221(3)	1409(15)	2838	1679	669	284	157	47	2	0	0
----------	----	------	----------	--------	----------	------	------	-----	-----	-----	----	---	---	---

Table 5.6 – Block “Lucera”: tie point found and outlier rejection results at each level of the image pyramids

Level	Pixel size [mm]	Total # of tie pts found (image space)	# of tie points discarded			# of multi-ray tie points per level in object space					
			Total (%)	By data snooping (%)	By internal procedure (%)	total	2	3	4	5	6
5	640	7087	3155(44)	347(8)	2808(40)	1525	992	259	228	17	29
4	320	19893	4260(21)	540(3)	3720(23)	5677	3174	1224	954	153	172
2	80	9682	1218(13)	183(2)	1035(11)	3226	1939	749	409	71	58
0	20	4705	621(13)	86(2)	535(13)	1587	1041	335	164	27	20

Table 5.7 – Block “Echallens”: tie point found and outlier rejection results at each level of the image pyramids

Project name	Av. # of rays per points	# of multi-ray points in object space								
		Total	2	3	4	5	6	7	8	9
Lucera	2.7	2838	1679	669	284	157	47	2	0	0
Echallens	2.5	1607	1041	335	164	27	20	—	—	—

Table 5.8 – Multi-ray tie points at the end of AAT

5.2.3.4 Outcomes of bundle adjustment

We report in Table 5.9 the results of bundle adjustment in terms of sigma nought and the accuracy of tie points in object space, which are representative of the block accuracy.

As far as σ_0 is concerned, for block “Lucera” we expected a lower value, because the potential accuracy of l.s. matching is better than 0.4 [pel] and the tie point set is consistent and well distributed. The reason of this result is likely to arise from the bundle adjustment, which should use a robust method; indeed, the internal blunder detection procedure copes effectively with gross errors, but does not the same with small outliers. For the block “Echallens” the result is satisfying, but also in this case it might be further improved by adopting a robust bundle adjustment.

The theoretical accuracy of object coordinates obtained for both blocks are sufficiently accurate according to image scales (1:7500 and 1:5000 respectively).

Project name	s_0 of bundle adjustment		Ratio observations/ unknowns	Theoretical accuracy		
	[pel]	[mm]		s_x [cm]	s_y [cm]	s_z [cm]
Lucera	0.40	10.7	1.75	7.2	8.3	19.6
Echallens	0.27	5.4	1.67	5.8	5.9	9.6

Table 5.9 – Results of bundle adjustment: sigma nought and theoretical accuracy of tie point object coordinates

Project name	Photo centers theoretical accuracy			Attitude angles theoretical accuracy		
	X_0 [cm]	Y_0 [cm]	Z_0 [cm]	w [mgon]	f [mgon]	k [mgon]
Lucera	9.8	12.1	9.2	5.6	4.9	1.7
Echallens	4.7	6.1	3.0	5.7	4.3	3.2

Table 5.10 – Results of bundle adjustment: theoretical accuracy of photo centers and attitude angles

Project name	# correct tie points per image (av.)	<i>Blunders in the final bundle adj.</i>	
		#	%
Lucera	421	221	2.8
Echallens	453	86	2.1

Table 5.11 – Results of bundle adjustment: data snooping

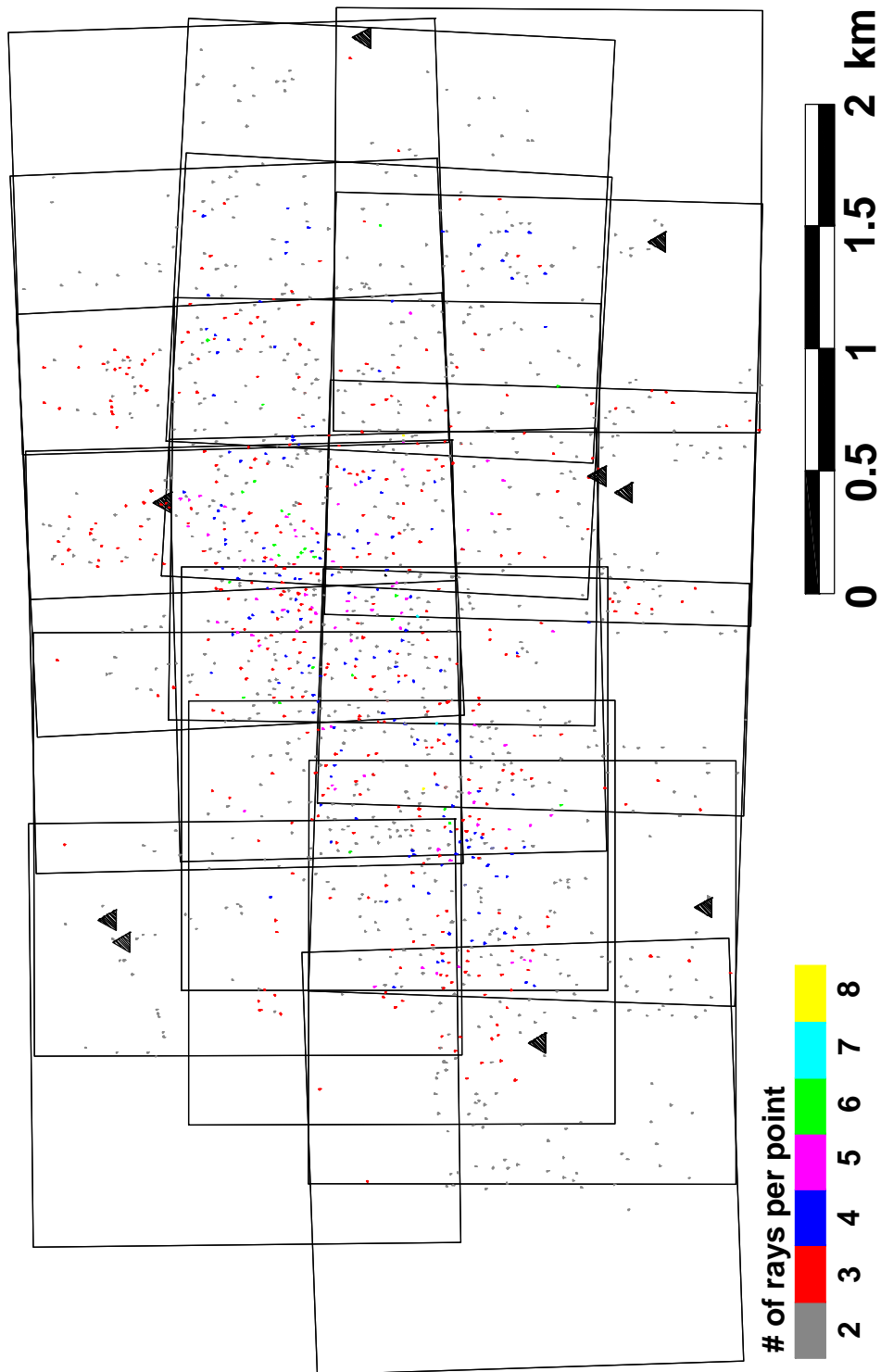


Fig. 5.12 – Block “Lucera”: distribution of all tie points found in object space

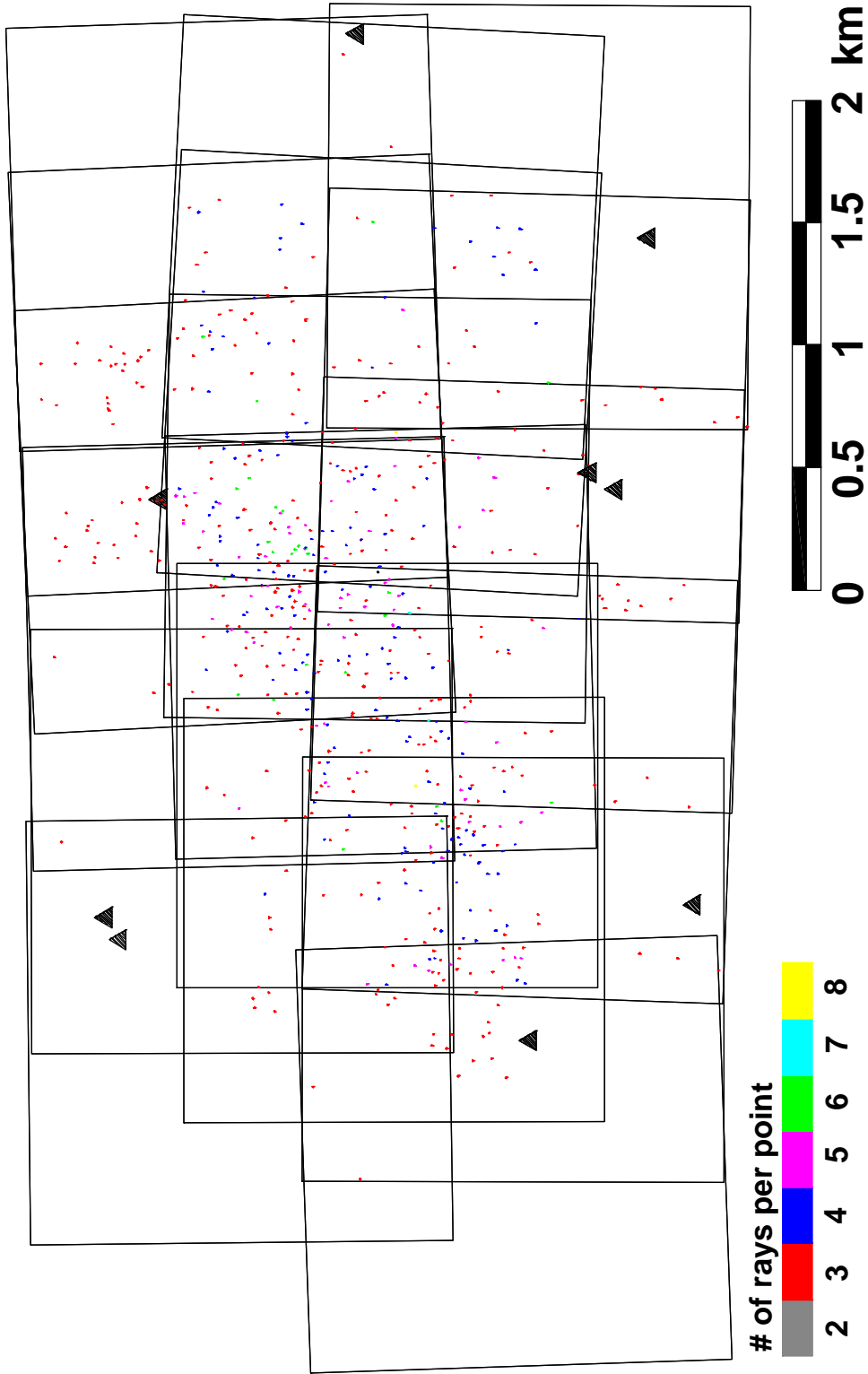


Fig. 5.13 – Block “Lucera”: distribution of manifold tie points (more than 2 rays per point) in object space

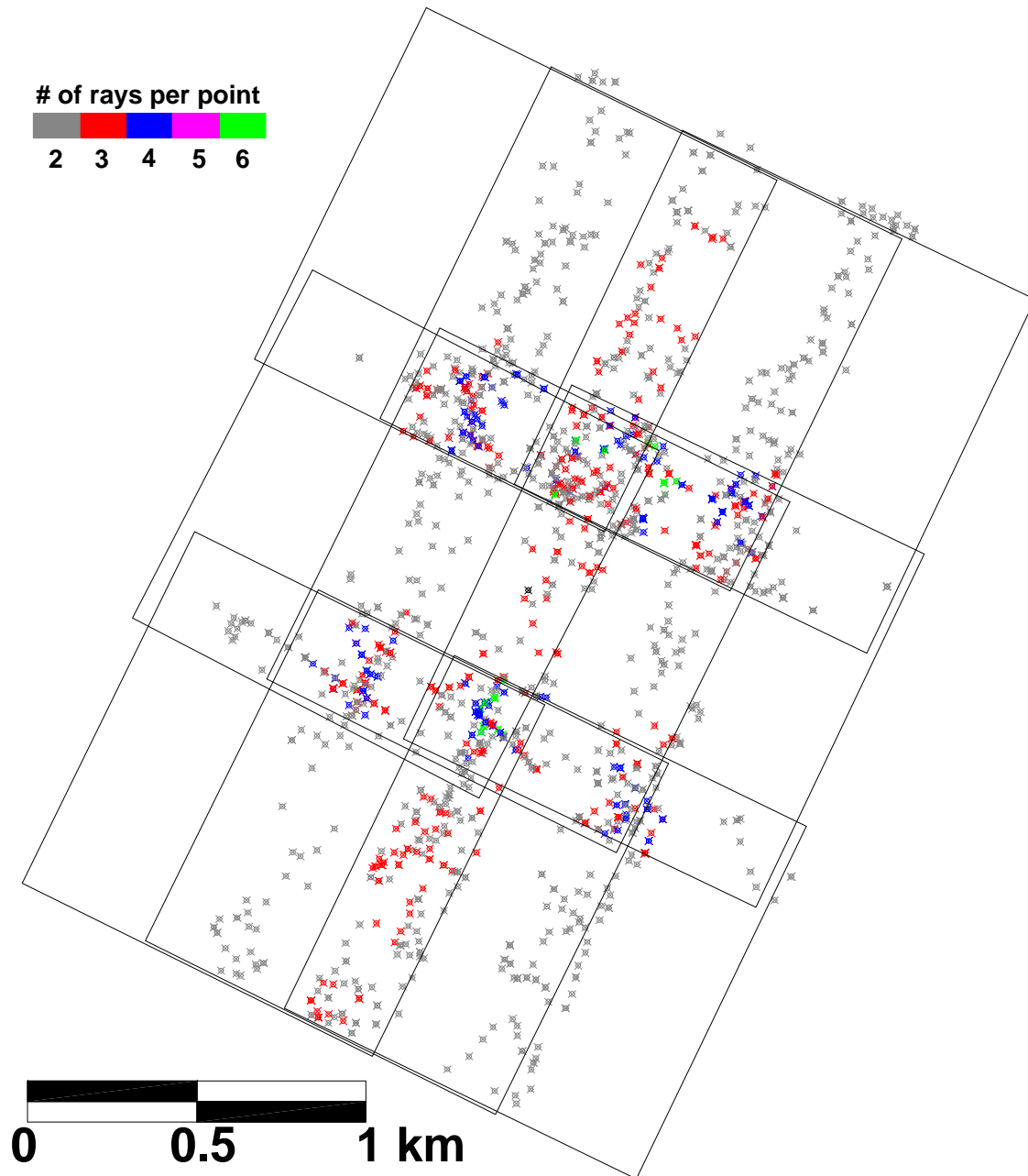


Fig. 5.14 – Block "Echallens": distribution of all tie points found in object space

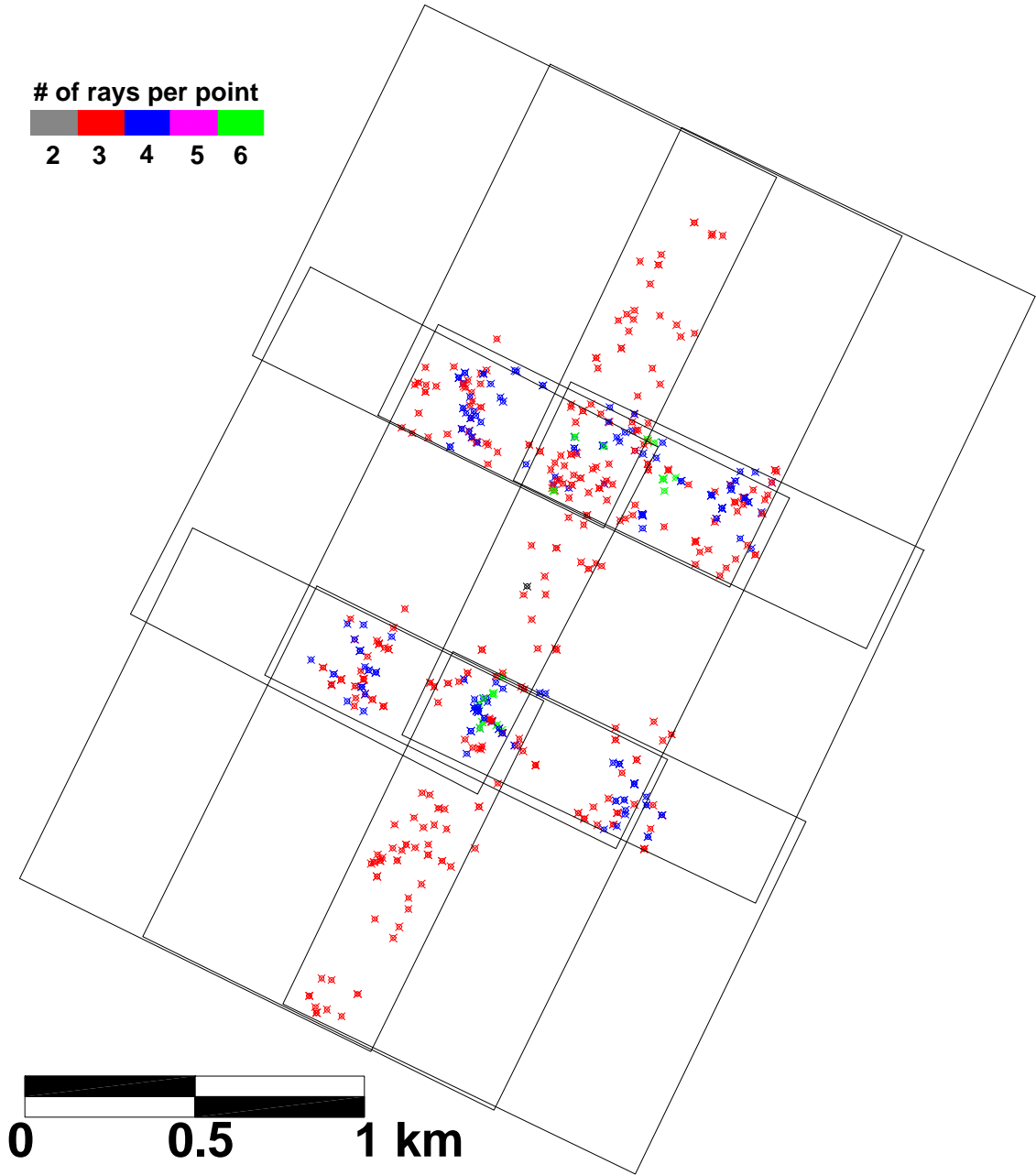


Fig. 5.15 – Block “Echallens”: distribution of manifold tie points (more than 2 rays per point) in object space

5.3 Independent accuracy check

Though standard deviations of the tie points and external reliability may highlight weakness in the block, deformations cannot be traced without an external check. We therefore performed an independent test, adopting the same procedure applied during the OEEPE-ISPRS test [HEIPKE AND EDER 1998].

The block “Lucera” has been used for this test. A set of 41 well distributed tie points has been interactively measured by means of the program APPBLOCK. The same interior orientation parameters were applied, so both sets of image coordinates (“automatic” and “manual”) are homogeneous. The “manual” block has been adjusted by using the same constraints (8 GCPs) and the object coordinates of tie points have been computed.

Then the image and object coordinates of tie points belonging to the “manual” block have been inserted as *check points* in the adjustment of the block made up by the “automatic” measurements. The discrepancies between these two data sets are reported in Table 5.16, while in Figure 5.17 the residuals in planimetry and in height are depicted.

The RMS computed in this way may be assumed as the accuracy of “automatic” measurements. The planimetric values are rather similar for both directions (13.0 and 10.4 cm respectively in X and Y), while the difference in height is greater (37.8 cm). Comparing these figures with those in Table 5.9, we see that the RMS are, as usual, larger than the theoretical accuracies. The difference is of less than 5 cm in X-Y, while in elevation it is significantly larger. The discrepancies in height might be due also to the weakness in elevation of the “manual” block, which should be strengthened by introducing more tie points.

	<i>Mean [cm]</i>	<i>Standard deviation [cm]</i>	<i>RMS [cm]</i>
X	6.7	11.1	13.0
Y	1.7	10.3	10.4
Z	-18.9	32.8	37.8

Fig. 5.16 – Discrepancies between coordinates of check points computed by “manual” and “automatic” measurements (Block “Lucera”)

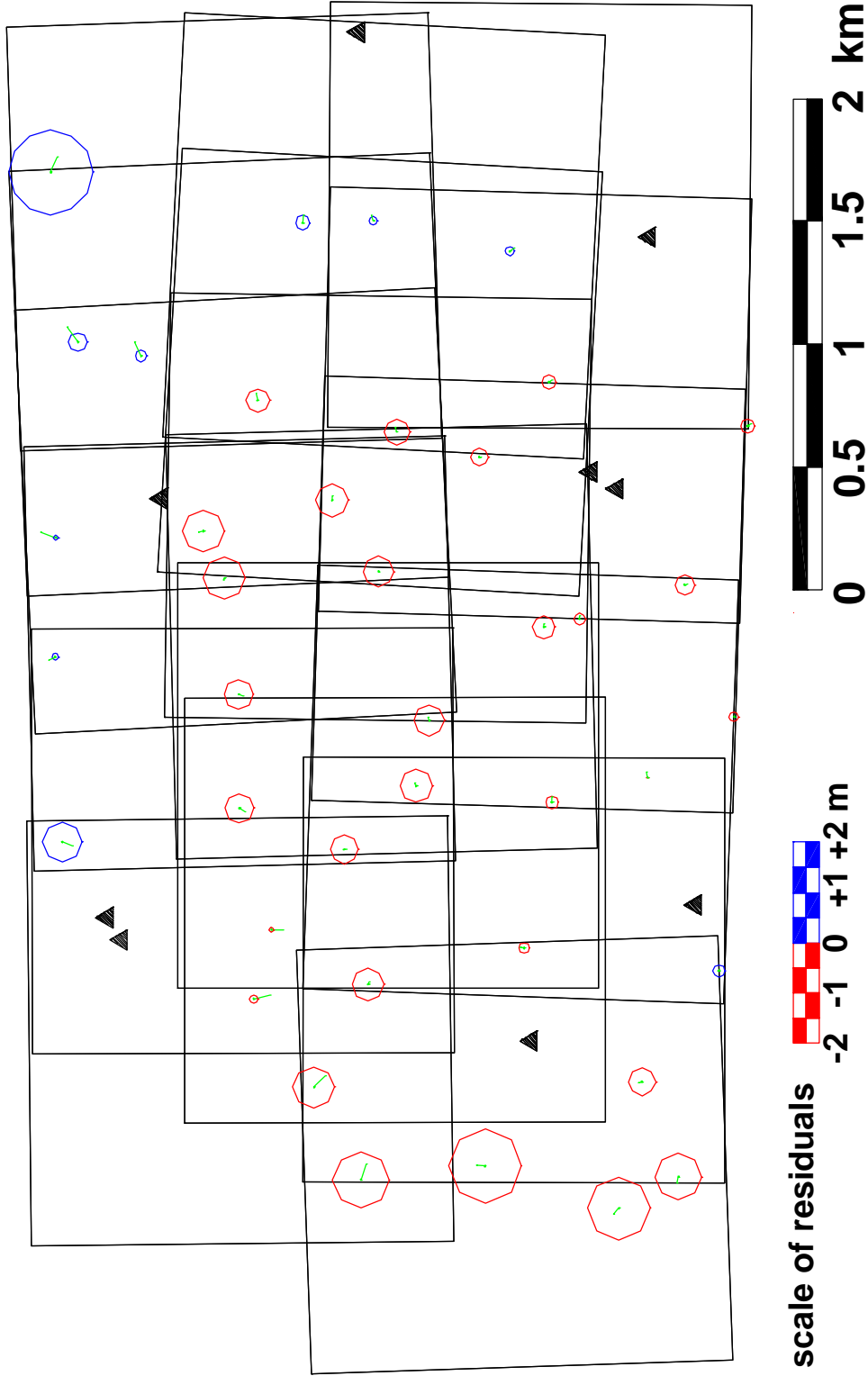


Fig. 5.17 – Block "Lucera": discrepancies between ground coordinates of tie points determined by AAT and by interactive measurements (height residuals are represented by a circle)

Chapter 6

Conclusions

6.1 TRIADIGIT system performance: status and prospects

The experimental tests of TRIADIGIT AAT system presented in Chapter 5 were carried out in order to investigate the performance obtainable in term of outer orientation parameters accuracy and of block stability. We draw from these outcomes pointing out what is already achieved as well as the problems that are still open in the different modules.

6.1.1 Tie point extraction

Test results show that in blocks flown over flat or hilly areas (e.g. blocks “Lucera” and “Echallens”) a consistent set of tie points may be automatically computed even by starting from a rough exterior orientation (perspective centers uncertainty of ± 50 m with an image scale in the range 1:5000÷7500) and by using a simple horizontal plane as ground model. Some other tests carried out on block flown over hilly and/or forest areas with standard overlap, resulted in a weak link between strips. We retain that in such situations a true (though raw) DEM is mandatory to define the approximate positions for the homologous points. To this aim, we would like to integrate into TRIA_DIGIT the computation of a DTM at the end of the top image pyramid level, to be used to reduce the search window size and to densify tie points wherever they are scarce. This DTM is indeed a by-product of AAT and may be refined separately later.

The goal of AT, that is the accurate determination of the exterior orientation parameters of all images, depends on the number of tie points, but also on their distribution: a great deal of multi-ray points in the multi-overlap areas of the block is required. To this aim we perform the backprojection of tie points found from the ground to all the images where they may appear, effectively increasing the number of rays per point.

As far as matching techniques are concerned, different aspects may be addressed. The empirical accuracy of l.s. matching algorithm was found to be about 0.3÷0.5 pixels, a range in agreement with the conclusions of the OEEPE-ISPRS test (see 1.6.2). A procedure for testing the determinability of the shape parameters of l.s. matching was implemented, allowing to fix those parameters which can be estimated with low accuracy. Redefinition of

the point at each level of image pyramids contributes to improve the quality of the measured points.

Currently the procedure for tie point extraction is too time-consuming and improvements are badly needed. Besides the optimization of the software code, the use of l.s. matching only for final point refinement while using simple cross correlation through the image pyramids should give the same results in accuracy and speed up AAT. Another important aspect of the tie point extraction is the internal procedure for outlier rejection. It is based on the computation of a robust relative orientation by a Least Median Squares approach between all the pairs of images with a sufficient overlap. The method copes effectively with blocks having large side overlaps, where relative orientations may be computed also between images belonging to different strips. In case of strips with small side overlaps, currently a simple test on the x-y parallaxes is executed, but a more complex geometric transformation would be better (e.g. an affine). Barring blocks in critical areas, the method implemented allows to discard most of the outliers in the data set. The amount of remaining errors is about 2÷3% of the image points, a percentage which does not prevent the correct convergency of l.s. bundle adjustment.

So far, only small blocks (max. 18 photographs) were used for the experimental tests; besides, the structure of these blocks was quite regular, without any cross strip or images at different scales. Actually, the behaviour of TRIA_DIGIT under these conditions is unknown and should be tested.

6.1.2 Interior Orientation

The series of tests performed show that the strategy adopted for the determination of the interior orientation works fully satisfactorily. The accuracy and the reliability of localization and measurement, at least for cameras with eight fiducials, is more than enough for practical applications. The identification of symbols is corrected in both cases of digits and bars. We want to add also the possibility to identify the pose of images when fiducial marks have no symbols, e.g. by exploiting the asymmetry of the photograph border.

Although the future will be of digital cameras, it is foreseeable that for more than a decade analogue cameras will remain the main tool for photogrammetric data acquisition. This will keep the interest in automatic interior orientation procedures high.

6.1.3 Ground Control Point Measurement

The measurement of ground control points was implemented interactively. The operator is assisted in the localization of areas where to look for the GCPs, while a subpixel resampling allows a precise mensuration by a pointing device.

An improvement of the measurement accuracy will soon come from the implementation of the refinement by l.s. matching of manually measured image coordinates: after a GCP has been located and measured manually in one image, it will only need to be approximately located (to a few pixels accuracy) to start the measurement by l.s. matching. A longer term

goal may be the automation of the search and measurement of a GCP all over the block, given its position in one image. This second task is more complex, especially in case of natural points, which very often cannot be easily distinguished from the background. An approach integrating relational and area-based matching could be devised to perform their localization and mensuration.

6.1.4 Miscellanea

As it was pointed out in chapter 2, the implementation of TRIADIGIT somehow disregarded the operational issues, concentrating on the algorithmic aspects. The time has come for the programs to become more user-friendly, so that also other users may work with them, adding up the experience in practical applications.

A further improvement is required in the computation of bundle adjustment, by introducing a robust solution method (a release of CALGE with such capabilities is under testing) and completing the reliability analysis (currently only local redundancies are provided), which is the only way to check the sensitivity of the block to outliers.

6.2 What future for Automatic Aerotriangulation?

One of the hottest topic in photogrammetry today is the *direct orientation* of sensors by *Inertial Navigation Systems* (INS), whose performance has much improved while cost kept coming down. Many believe they will substitute for AT very soon. We don't share such a view and we argue that AT will not become obsolete in future.

In principle, if the exterior orientation is obtained directly with sufficient accuracy and if there are not errors in the calibration of the multi-sensor system (GPS, INS and imaging sensor), the practise of AT is redundant. Outcomes of several experimental tests (see e.g. [COLOMINA 1999; CRAMER 1999] among others) have shown that the accuracy obtainable by direct methods are in the same order of that coming from indirect methods (AT). Moreover it is faster, requires less GCPs and enables more freedom in choosing the block configuration. Compared to AAT, direct orientation does not suffer from image matching problems in difficult areas such as forests, steep slopes, poor textured lands.

The weak point of INS/GPS is its intrinsic low reliability: direct georeferencing strictly depends on the precise time alignment between the sensor components; a proper and stable calibration of the system is mandatory, because an error in the interior orientation elements will deteriorate the accuracy of object point determination. On the contrary, the indirect exterior orientation is less influenced by calibration errors, which can be compensated for in the bundle adjustment.

Therefore, the integration of the INS/GPS technology in a combined AAT provides the most flexible approach. This combination allows the control of the whole process by increasing the reliability of the system and gives the possibility to self-calibrate camera parameters. An automatic procedure for tie point extraction such as that implemented in TRIADIGIT may take advantage from the knowledge of precise values for initial orientation parameters coming from INS/GPS, strongly reducing the percentage of mismatches while

increasing the success rate of tie point search. Besides, precise approximations may contribute to the convergency of the bundle block adjustment as well.

We therefore believe that AT will continue to be one of the main task in the photogrammetric process and that automatic AT will replace analytical AT also in operational environments: the first commercial digital aerial cameras are coming up in summer 2000 [FRICKER *et al.* 1999; HINZ 1999], paving the way to an “all-digital photogrammetry”.

References

- ACKERMANN, F. (1984): High Precision Digital Image Correlation. *PhW*.
- ACKERMANN, F. (1995): *Automation of Aerial Triangulation*. 2nd CDP.
- ACKERMANN, F. (1996): Experimental tests on fast ambiguity solutions for airborne kinematic GPS positioning. *IAPRS*, 31 (6/3):1-6.
- ACKERMANN, F. (1997): Geo-Kodierung ohne Paßpunkte. *Geo-Informationssysteme*, 10(2): 28-32.
- ACKERMANN, F., HAHN, M. (1991): Image Pyramids for Digital Photogrammetry. In: EBNER, H., FRITSCH, D., HEIPKE, C. (Ed.s), *Digital Photogrammetric Systems*, Wichmann-Verlag: 43-58.
- ACKERMANN, F., KRZYSZEK, P. (1997): Complete automation of digital aerial triangulation. *PhRe*, 15: 645-656.
- AGOURIS, P., SCHENK, T. (1996): Automated Aerotriangulation Using Multiple Image Multipoint Matching. *PE&RS*, 62(6): 703-710.
- AUTOMETRIC, INC. (1999): *SoftPlotterTM Functional Specification*. Autometric, Inc., Springfield (VA USA).
- BAARDA, W. (1968): A Testing Procedure for Use in Geodetic Networks. *NGCPG*, 2(5), Delft (Holland).
- BALTSAVIAS, E.P. (1991): *Geometrically Constrained Multiphoto Matching*. Mitteilungen No. 49, Institute of Geodesy and Photogrammetry, ETH, Zurich.
- BALTSAVIAS, E.P. (1999): On the performance of photogrammetric scanners. *PhW*: 155-173.
- BARRODALE, I., ROBERTS, F. (1973): An Improved Algorithm for Discrete l_1 Linear Approximation. *SIAM, JNA*, No. 10.
- BRAND, R., HEIPKE, C. (1998): A system for automatic aerial triangulation. *IAPRS*, 32(2): 27-31.
- BURT, P.J., ADELSON, E.H. (1983): The Laplacian Pyramid as a Compact Image Code. *IEEE TrComm*, 31(4): 532-540.
- CAYLEY A. (1843). *Cambridge Mathematical Journal*, Vol. 3, and reprinted in his *Collected Papers*, 1(1889): 28 ff.
- CHATERJEE, S., HADI, A.S. (1988): *Sensitivity Analysis in Linear Regression*. John Wiley, New York.
- CHRISTMAS, W., KITTLER, J., PETROU, M. (1995): Structural matching in computer vision using probabilistic relaxation. *IEEE PAMI*, 17(8):749-764.

- COLOMINA, I. (1999): GPS, INS and Aerial Triangulation: what is the best way for the operational determination of photogrammetric Image Orientation? *IAPRS*, 32(3-2W5): 121-130.
- CRAMER, M. (1999): Direct Geocoding – is Aerial Triangulation Obsolete? *PhW*: 59-70.
- CRIPPA B., MUSSIO L. (1995). *Gli algoritmi della fotogrammetria analitica*. Politecnico di Milano, Dip. I.I.A.R.
- CSURKA, G., ZELLER, C., ZHANG, Z.Y., FAUGERAS, O.D. (1997): Characterizing the Uncertainty of the Fundamental Matrix. *CVIU*, 68(1): 18-36.
- DAL POZ, A.P. (1996): Relational Matching Applied to Automatic Extraction of Ground Control in Digital Images. *IAPRS*, 31 (B3): 131-134.
- DE VENECIA, K., MILLER, S., PACEY, R, WALKER, S. (1997): Experiences with a commercial package for automated aerial triangulation. Proc. of ASPRS/ACSM Annual Convention, Part 1: 548-557.
- DÖRSTEL, C. (1999): Perspectives for aerial triangulation offered by Z/I Imaging. *PrPhW99*: 205-210.
- DOWMAN, I.J., MORGADO, A., VOHRA, V. (1996): Automatic registration of images with maps using polygonal features. *IAPRS*, 31(B3): 139-145.
- DREWNIOK, C., ROHR, K. (1997): Exterior orientation – an automatic approach based on fitting analytic landmark models. *ISPRS JPRS*, 52: 132-145.
- EBNER, H., HOHLOF, T. (1994): Utilisation of ground control for image orientation without point identification in image space. *IAPRS*, 30(3/1): 206-211.
- EBNER, H., STRUNZ, G. (1988): Combined Point Determination Using Digital Terrain Models as Control Information. *IAPRS*, 27(B11/3): 578-587.
- FAUGERAS, O.D., LUONG, Q.T., MAYBANK, S.J. (1992): Camera self-calibration: Theory and experiments. Proc. ECCV '92: 321-334.
- FISCHLER, M.A., BOLLES, R.C. (1981): Random Sample Consensus: A Paradigm for Model Fitting with Applications to Image Analysis and Automated Cartography. *CommACM*, 24: 381-395.
- FORLANI, G. (1986): Sperimentazione del nuovo programma CALGE dell'ITM. Bollettino SIFET No. 2: 63-72.
- FORLANI, G., GIUSSANI, A., SCAIONI, M., VASSENA, G. (1996). Target detection and epipolar geometry for image orientation in close-range photogrammetry. *IAPRS*, 31(B5): 518-523.
- FORLANI, G., PINTO, L., TREBESCHI, A. (1995): Measuring Ground Control Points by L.S. Matching. In BINAGHI, E., BRIVIO, P.A., RAMPINI, A. (Ed.s), *Soft Computing in Remote Sensing Data Analysis*. World Scientific.
- FORLANI, G., PINTO, L., SCAIONI, M. (1998): The TRIADIGIT program for automatic aerial triangulation. *IAPRS*, 32(2): 67-73.
- FORLANI, G., PINTO, L., SCAIONI, M. (1999): A Procedure for Automatic Inner Orientation. *IAPRS*, 32(2W5): 131-135.
- FÖRSTNER, W. (1982): On the Geometric Precision of Digital Correlation. *IAPRS*, 24(3): 176-189.
- FÖRSTNER, W. (1984): Quality Assessment of Object Location and Point Transfer Using Digital Image Correlation Techniques. *IAPRS*, 25(A3/a): 197-219.
- FÖRSTNER, W. (1985): The Reliability of Block Triangulation. *PE&RS*, 51(6): 1137-1149.

- FÖRSTNER, W. (1986): A Feature Based Correspondence Algorithm for Image Matching. *IAPRS*, 26(3/3): 150-166.
- FÖRSTNER, W. (1988): Model Based Detection and Location of Houses as Topographic Control Points in Digital Images. *IAPRS*, 27(B11/3): 505-517.
- FÖRSTNER, W. (1995): Matching Strategies for Point Transfer. *PhW*: 173-183.
- FRICKER, P., SANDAU, R., WALKER, S. (1999): Digital photogrammetric cameras: possibilities and problems. *PhW*: 71-82.
- FRITSCH, D. (1995): Introduction into Digital Aerotriangulation. *PhW*: 165-171.
- FUCHS, C., HEUEL, S. (1998). *Feature Extraction*. 3rd CDP (chapter 4)..
- GRÜN, A. (1985): Data Processing Methods for Amateur Photographs. *PhRe*, 11(65): 567-579.
- GÜLCH, E. (1994): Using feature extraction to prepare the automated measurement of control points in digital aerial triangulation. *IAPRS*, 30 (3/1): 333-340.
- GÜLCH, E. (1995a): From Control Points to Control Structures for Absolute Orientation and Aerial Triangulation in Digital Photogrammetry. *ZPF*, 63(3): 130-136.
- GÜLCH, E. (1995b): Automatic Control Point Measurement. *PhW*: 185-196.
- GÜLCH, E. (1996): Deformable models as a photogrammetric tool – Potential and problems. *IAPRS*, 31(B3): 279-284.
- HÄDEN, I. (1994): Identification and Localization of Point-Like Features for Digital Aerial Triangulation. OEEPE Workshop on Digital Methods in Aerial Triangulation, Espoo.
- HAHN, M. (1994): *Bildsequenzanalyse für die passive Navigation*. PhD Thesis, Institut für Photogrammetrie, Universität Stuttgart, Stuttgart.
- HAHN, M. (1997): Automatic Ground Control Point Measurement. *PhW*: 115-126.
- HAHN, M., KIEFNER, M., QUEDNAU, A., HINZ, E. (1996): Semi-Automatic Measurement of Signalized Ground Control Points at Digital Photogrammetric Workstations. *IAPRS*, 31(B3): 291-296.
- HAMPEL, J.P., RONCHETTI, E.M., ROUSSEEUW, P.J., STAHEL, W.A. (1986): *Robust Statistics: An Approach Based on Influence Functions*. John Wiley, New York.
- HANNAH, M.J. (1974): *Computer Matching of Areas in Stereo Images*. PhD Thesis, Stanford University, Stanford CA.
- HARALICK, M., SHAPIRO, L.G. (1993): *Computer and Robot Vision*. Vol. II, Addison-Wesley.
- HÄRING, S. (1995). *Automatisierung der Inneren Orientierung*. Semester Thesis, Institute of Geodesy and Photogrammetry, ETH, Zurich.
- HARRINGTON, S. (1983): *Computer Graphics. A programming Approach*. McGraw-Hill, Japan.
- HARTFIEL, P. (1997): Higher performance with automated aerial triangulation. *PhW*: 109-113.
- HATTORY, S., MYINT, Y. (1995): Automatic Estimation of Initial Approximations of Parameters for Bundle Adjustment. *PE&RS*, 61(7): 909-915.
- HEIKKINEN, J. (1994): Linear Feature Based Approach to Map Revision. OEEPE Workshop on Digital Methods in Aerial Triangulation, Espoo.
- HEIPKE, C. (1997): Automation of Interior, Relative and Absolute Orientation. *ISPRS JPRS*, 52: 1-19.
- HEIPKE C., EDER K. (1998). Performance of tie-point extraction in automatic aerial triangulation. OEEPE Official Publication n.35: 125-185.

- HEIPKE, C., MAYR, W., WIEDEMANN, C., EBNER, H. (1997): Automatic Aerotriangulation with Frame and Three-Line Imagery. In: MCKEOWN, D.M.JR., MCGLONE, J.C., JAMET, O. (Ed.s), *Integrating Photogrammetric Techniques with Scene analysis and Machine vision III.*, Proc. of SPIE, Vol. 3072: 286-294.
- HELAVA, U. (1987): The Digital Comparator Correlator System (DCCS). *Proc. of the Intercommission conference on Fast Processing of Photogrammetric Data*, Interlaken (Switzerland): 404-418.
- HILD, H., FRITSCH, D. (1998): Integration of vector data and satellite imagery for geocoding. *IAPRS*, 32(4): 246-251.
- HINZ, A. (1999): The Z/I Imaging Digital Aerial Camera System. *PhW*: 109-115.
- HÖHLE, J. (1998): Automatic Orientation of Aerial Images by Means of Existing Orthoimages and Height Data. *IAPRS*, 32 (2): 121-126.
- HOLM, M., PARMES, E., ANDERSSON, K., VUORELA, A. (1995): A Nationwide Automatic Satellite Image Registration System. *SPIE Proc.* (2486): 156-167.
- HONKAVAARA, E., HØGHOLEN, A. (1996): Automatic tie point extraction in aerial triangulation. *IAPRS*, 31 (B3): 337-342.
- HOUGH, P. (1962): *Methods and Means for Recognizing Complex Pattern*. U.S. Patent 3069654.
- HUANG, T.S., FAUGERAS, O.D. (1989): Some properties of the E-matrix in two view motion estimation. *IEEE PAMI*, 11: 1310-1312.
- HUBER, P.J. (1981): *Robust Statistics*. John Wiley, New York.
- ILLINGWORTH, J., KITTLER, J. (1988): A Survey of the Hough Transform. *CVGIP*, 44: 87-116.
- INGHILLERI, G. (1974): *Topografia Generale*. UTET, Torino.
- JAAKOLA, J., SARJAKOSKI, T. (1996): *Experimental Test on Digital Aerial Triangulation*. OEEPE Official Publication No. 31.
- JACOBSEN, K., WEGMANN, H. (1998): Experiences with Automatic Aerotriangulation. In *Proc. of ASPRS Annual Convention*, Tampa.
- JÄHNE B. (1989). *Digitale Bildverarbeitung*. Springer-Verlag, New York.
- KANATANI, K. (1994): Statistical bias of conic fitting and renormalization. *IEEE PAMI*, 16(3): 320-326.
- KENDALL, M., STUART, A. (1983): *The Advanced Theory of Statistics*. Charles Griffin and Co., London.
- KERSTEN, T., HÄRING, S. (1997a): Efficient automated digital aerial triangulation through customization of a commercial photogrammetric system. *IAPRS*, 32(3-2W3): 72-79.
- KERSTEN, T., HÄRING, S. (1997b). *Automatic Interior Orientation of Digital Aerial Images*. *PE&RS*, 63(8): 1007-1011.
- KERSTEN, T., HÄRING, S., O'SULLIVAN, W. (1998): Digital aerial triangulation in alpine regions – a challenge. *IAPRS*, 32(2): 149-156.
- KERSTEN, T., O'SULLIVAN, W. (1996): Experiences with the Helava automated triangulation system. *IAPRS*, 31(B3): 591-596.
- KNABENSCHUH, M. (1995): *Generation and Use of Digital Orthophotos*. 2nd CDP, (Paper No. 8).
- KÖHLER, (1998): Digitale Photogrammetrie – Konzept und Umsetzung beim Hessischen Landesvermessungsamt. *ZfV*, (123) 9: 301-306.

- KRAUS, K. (1993). *Photogrammetry - Vol. 1*. Dümmler Verlag, Bonn. Trad. italiana (1994) a cura di S. Dequal, Levrotto & Bella, Torino.
- KRAUS, K. (1997). *Photogrammetry - Vol. 2*. Dümmler Verlag, Bonn.
- LANG, F., FÖRSTNER, W. (1998): *Matching Techniques*. 3rd CDP, (chapter 5).
- LIM, J.S. (1990): *Two-Dimensional Signal and Image Processing*. Prentice Hall, USA.
- LONGUET-HIGGINS, H.C. (1981): A computer algorithm for reconstructing a scene from two projections. *Nature*, 293: 133-135.
- LUE, Y. (1996): Towards a higher level of automation for SoftPlotter™. *IAPRS*, 31(B3): 478-483.
- LUE, Y. (1997): One step to a higher level of automation for softcopy photogrammetry Automatic Interior Orientation. *ISPRS JPRS*, 52: 103-109.
- LUHMANN, T., ALTROGGE, G. (1986): Interest-operator for image matching. *IAPRS*, 26(3/2): 459-474.
- LUONG, Q.T., DERICHE, R., FAUGERAS, O.D., PAPADOPOULOU, T. (1993): On Determining the Fundamental Matrix: Analysis of Different Methods and Experimental Results. Tech. Rep. INRIA-1894, France.
- LUONG, Q.T., FAUGERAS, O.D. (1996): The Fundamental Matrix: Theory, Algorithms and Stability Analysis. *IJCV*, 17(1): 43-75.
- MALMSTRÖM, H. (1986): *Measuring ground control for satellite image rectification*. Schriftenreihe des Instituts für Photogrammetrie der Universität Stuttgart, Stuttgart.
- MARONNA, R.A. (1976): Robust M-estimators of multivariate location and scatter. *Ann. Stat.*, 4: 51-67.
- MILLER, S.B., PADERES, F.C., WALKER, A.S. (1996): Automation in Digital Photogrammetric Systems. *IAPRS*, 31(B2): 250-255.
- PAN, H.P. (1996). A direct Closed-Form Solution to General Relative Orientation. Tech. Report, Cooperative Research Centre for Sensor Signal and Information Processing, Adelaide, Australia.
- PEARSON, K. (1901): On lines and planes of closest fit to systems of points in space. *Philos. Mag. Ser.*, 6(2): 559 ff.
- PEDERSEN, B.M. (1996): Automated Measurement of Ground Control Objects in Large Scale Aerial Photographs. *IAPRS*, 31(B3): 633-637.
- PRATT, W.K. (1991): *Digital Image Processing*. Wiley Interscience, USA.
- RODRIGUES, O. (1840): *Journal de Mathématiques*, 5:404 ff.
- ROTH, G., LEVINE, M.D. (1993): Extracting Geometric Primitives. *CVGIP*, 58(1):1-22.
- ROUSSEUW, P.J., LEROY, A.M. (1987): *Robust Regression and Outliers Detection*. John Wiley, New York.
- SAMPSON, P.D. (1982): Fitting conic sections to 'very scattered' data: An iterative refinement of the Bookstein algorithm. *CGIP*, 18: 97-108.
- SANSÒ, F. (1993): *Il trattamento statistico dei dati*. CLUP Editore, Milano.
- SCHENK, T. (1995): Zur Automatischen Aerotriangulation. *ZPF*, 63: 137-144.
- SCHENK, T. (1997): Towards Automatic Aerial Triangulation. *ISPRS JPRS*, 52(3): 110-121.
- SCHENK, A., LI, J.C., TOTH, C. (1991): Towards an Autonomous System for Orienting Digital Stereopairs. *PE&RS*, 57(8): 1057-1064.

- SCHICKLER, W. (1993): Towards Automation in Photogrammetry – An Example: Automatic Exterior Orientation. *GIM*, 7(4): 32-35.
- SCHICKLER, W. (1996): Feature Matching for Outer Orientation of Single Images Using 3-D Wireframe Controlpoints. *IAPRS*, 29 (B3/III): 591-598.
- SCHICKLER, W., POTH, Z (1996): The automatic interior orientation and its daily use. *IAPRS*, 31(B3): 746-751.
- SESTER, M., FÖRSTNER, W. (1989): Object location based on uncertain models. In: BURKHARDT, H., HÖHNE, K.H., NEUMANN, B. (Ed.s), *Mustererkennung 1989*, Springer, Berlin.
- SHAPIRO, L.S., BRADY, J.M. (1993): Rejecting outliers and estimating errors in an orthogonal regression framework. Dept. of Engineering Sciences, University of Oxford, Tech. Report OUEL 1974/93, and to appear on *PTRS*.
- SKALLOUD, J. (1999): *Optimizing georeferencing of airborne survey systems by INS/DGPS*. PhD Thesis, Dept. Of Geomatics Eng., The University of Calgary, Calgary.
- SKALLOUD J., SCHWARZ K.P. (1998). Accurate orientation for airborn mapping system. *IAPRS*, 32(2): 283-290.
- STRACKBEIN, H., HENZE, M. (1995): *Automatische innere Orientierung* Tech. Rep., Landesvermessungsamt Nordrhein-Westfalen, Bonn.
- TANG, L., BRAUN, J., DEBITSCH, R. (1997): Automatic aerotriangulation – concept, realization and results. *ISPRS JPRS*, 52: 122-131.
- TANG, L., HEIPKE, C. (1996): Automatic Relative Orientation of Aerial Images. *PE&RS*, 62(1): 47-55.
- THOMPSON, E.H. (1959): A rational algebraic formulation of the problem of relative orientation. *PhRe*, 3(14): 152-159.
- TORR, P.H.S., MAYBANK, S., ZISSERMAN, A. (1996): Robust Detection of degenerate Configurations for the Fundamental Matrix. *OUEL Report 2090-96*, Dept of Eng. Science, University of Oxford.
- TORR, P.H.S., MURRAY, D.W. (1997): The Development and Comparison of Robust Methods for Estimating the Fundamental Matrix. *IJCV*, 24(3): 271-300.
- TORR, P.H.S., ZISSERMAN, A., MAYBANK, S. (1995): Robust Detection of degeneracy. *Proc. 5th ICCV*, Boston MA: 1037-1044.
- TOTH, C.K., KRUPNIK, A. (1996): Concept, Implementation, and Results of an Automatic Aerotriangulation System. *PE&RS*, 62(6): 711-717.
- TSINGAS, V. (1991): Automatische Aerotriangulation. *PhW*: 253-268.
- TSINGAS, V. (1994): A graph-theoretical approach for multiple feature matching and its application on digital point transfer. *IAPRS* 30 (3/2): 865-871.
- TSINGAS, V. (1995): Operational Use and Empirical Results of Automatic Aerial Triangulation. *PhW*: 207-214.
- VOSSelman, G, HAALA, N. (1992): Erkennung topographischer Paspunkte durch relationale Zuordnung. *ZPF*, 6: 170-176.
- WALLIS, R. (1976). An approach to the space variant restoration and enhancement of images. Proc. of Symposium on Current Mathematical Problems in Image Science, Naval Postgraduate School, Monterey CA.

- WANG, Y. (1996): Structural Matching and Its Applications for Photogrammetric Automation. *IAPRS*, 31(B3): 918-923.
- WENG, J., HUANG, T.S., AHUJA, N. (1989): Motion and structure from two perspective views: Algorithms, error analysis, and error estimation. *IEEE PAMI*, 11: 451-476.
- WOLFF, K. (1998): *Automatic Orientation Procedures*. 3rd CDP, (chapter 7).

Abbreviations used in references

<i>CGIP</i>	Computer Graphics and Image Processing
<i>CommACM</i>	Communication of the Association for Computing Machinery
<i>CDP</i>	Course on Digital Photogrammetry, Institute for Photogrammetry, Bonn University
<i>CVGIP</i>	Computer Vision, Graphics, and Image Processing
<i>CVIU</i>	Computer Vision and Image Understanding
<i>EECV</i>	European Conference on Computer Vision
<i>GIM</i>	Geodetical Info Magazine
<i>IAPRS</i>	International Archives of Photogrammetry and Remote Sensing
<i>ICCV</i>	International Conference of Computer Vision
<i>IEEE PAMI</i>	IEEE Transactions on Pattern Analysis and Machine Intelligence
<i>IEEE Tcomm</i>	IEEE Transactions on Communications
<i>IJCV</i>	International Journal of Computer Vision
<i>ISPRS JPRS</i>	ISPRS Journal of Photogrammetry and Remote Sensing
<i>JNA</i>	Journal of Numerical Analysis
<i>NGCPG</i>	Netherlands Geodetic Commission – Publications on Geodesy
<i>PE</i>	Photogrammetric Engineering
<i>PE&RS</i>	Photogrammetric Engineering and Remote Sensing
<i>PhRe</i>	Photogrammetric Record
<i>PhW</i>	Proceedings of Photogrammetric Week, Stuttgart 1993-95-97: FRITSCH, D., HOBBIE, D. (Ed.s), Wichmann, Heidelberg, Germany 1999: FRITSCH, D., SPILLER, R. (Ed.s), Wichmann, Heidelberg, Germany
<i>PTRS</i>	Philosophical Transactions of the Royal Society
<i>ZFV</i>	Zeitschrift für Vermessungswesen. Konrad Wittwer Verlag, Stuttgart
<i>ZPF</i>	Zeitschrift für Photogrammetrie und Fernerkundung. Herbert Wichmann Verlag, Karlsruhe

Aknowledgements

My gratitude is firstly extended to Prof. Gianfranco Forlani, my Tutor, for his many useful advices and criticisms. I very much enjoyed the long discussions with him, which were the most serious test for the results of my work and always gave rise to new improvements. Nevertheless, I remember with great pleasure the first period of my PhD course, when the implementation of the program for automatic aerial triangulation was at the beginning and I, Prof. Gianfranco Forlani and Ing. Livio Pinto spent all our day in a fruitful (and amusing too) working group.

I've already introduced Ing. Livio Pinto, my Co-Tutor, who accompanied and shared my research and continuously proposed new goals and challenges. In many critical moments, an afternoon spent with him yielded the solution to problems for which I had been working for days. Thanks Livio and Gianfra, for your friendship and the familiar climate of our working team too.

I am grateful to Prof. Luigi Mussio for coordinating the Doctorate and for many useful advices he gave me.

I would like to express my gratitude to Prof. Heinrich Ebner, who during his visit at Dept. IIAR appreciated and encouraged my activities. Thanks also to Dr. Konrad Eder, for his precious comments to our result obtained at OEEPE-ISPRS test, which helped us to focus the aspects to improve.

I am indebted to Ing. Fabio Remondino, who carried out his Degree Thesis in our Department working on automatic aerial triangulation. I found his collaboration very fruitful.

My thanks to EPFL, Lausanne, for providing the imagery set "Echallens" used in the experimental tests. Thanks goes also to *Istituto Geografico Militare Italiano*, in particular to Ing. Antonio Arrighi, for the digitalization of the photogrammetric block "Lucera".

A cordial thank to all the people working and studing at the Surveying Section of Dept. IIAR, *Politecnico di Milano*.

My aknowledgements also extend to my parents and my friends who have been close to me during my studies.

Milan, December 1999

Marco Scaioni